ARO-URI Center for

OPTO-ELECTRONIC SYSTEMS RESEARCH

TECHNICAL REPORT

STOCHASTIC AND DETERMINISTIC

FLUCTUATIONS IN

STIMULATED BRILLOUIN SCATTERING

AD-A230 988

Alexander L. Gaeta

October 1990

DTIC
ELECTE
JAN 15 1991
S E D

The Institute of Optics
University of Rochester

REPORT DOCUMENTATION PAGE

ORT SECURITY CLASSIFICATION	1b. RESTRICTIVE MARKINGS
Unclassified	

URITY CLASSIFICATION AUTHORITY	3. DISTRIBUTION/AVAILABILITY OF REPORT
	Approved for public release;
:LASSIFICATION/DOWNGRADING SCHEDULE	distribution unlimited.

ORMING ORGANIZATION REPORT NUMBER(S)	5. MONITORING ORGANIZATION REPORT NUMBER(S)
	ARO $24626./76$ $PH-UIR$

ME OF PERFORMING ORGANIZATION	6b OFFICE SYMBOL (If applicable)	7a. NAME OF MONITORING ORGANIZATION
versity of Rochester		U. S. Army Research Office

)RESS (City, State, and ZIP Code)	7b. ADDRESS (City, State, and ZIP Code)
Institute of Optics	P. O. Box 12211
hester, New York 14627	Research Triangle Park, NC 27709-2211

ME OF FUNDING/SPONSORING ;ANIZATION	8b. OFFICE SYMBOL (If applicable)	9. PROCUREMENT INSTRUMENT IDENTIFICATION NUMBER
S. Army Research Office		$DAAL03-86-K-0173$

)RESS (City, State, and ZIP Code)	10. SOURCE OF FUNDING NUMBERS			
O. Box 12211	PROGRAM ELEMENT NO	PROJECT NO.	TASK NO.	WORK UNIT ACCESSION NO
earch Triangle Park, NC 27709-2211				

.E (Include Security Classification)
Stochastic and Deterministic Fluctuations in Stimulated Brillouin Scattering

SONAL AUTHOR(S)
Alexander L. Gaeta

PE OF REPORT Technical	13b. TIME COVERED FROM _____ TO _____	14. DATE OF REPORT (Year, Month, Day) October 1990	5. PAGE COUNT 121

PLEMENTARY NOTAT!ON
The view, opinions and/or findings contained in this report are those he author(s) and should not be construed as an official Department of the Army position, cy or decision unless so designated by other documentation

COSATI CODES			18. SUBJECT TERMS (Continue on reverse if necessary and identify by block number)
LD	GROUP	SUB-GROUP	Deterministic chaos; stimulated brillouin scattering

TRACT (Continue on reverse if necessary and identify by block number)

Please see Abstract on pp. ix-x.

TRIBUTION/AVAILABILITY OF ABSTRACT	21. ABSTRACT SECURITY CLASSIFICATION
NCLASSIFIED/UNLIMITED ☐ SAME AS RPT. ☐ DTIC USERS	Unclassified

ME OF RESPONSIBLE INDIVIDUAL	22b. TELEPHONE (Include Area Code)	22c OFFICE SYMBOL
Robert Boyd	/16-275-2329	

STOCHASTIC AND DETERMINISTIC FLUCTUATIONS IN STIMULATED BRILLOUIN SCATTERING

by

Alexander L. Gaeta

Submitted in Partial Fulfillment

of the

Requirements for the Degree

DOCTOR OF PHILOSOPHY

Supervised by Professor Robert W. Boyd

The Institute of Optics

University of Rochester

Rochester, New York

1990

Curriculum Vitae

Alexander Luis Gaeta ██████████████████████ ████████████. He was raised in Buffalo, New York. He attended the University of Rochester where he received a Bachelor of Science Degree in Optics. While at the University of Rochester, he earned All-American Honors in tennis and received the Louis A. Alexander Award for athletic excellence.

In September of 1983, the author began his graduate studies at the Institute of Optics at the University and earned a Master of Science degree in Optics in February of 1985. His thesis work has been conducted under the supervision of Professor Robert W. Boyd. While at the University of Rochester, he held a University Research Initiative Fellowship. He is also a member of the Optical Society of America.

Publications

M. T. Gruneisen, A. L. Gaeta, and R. W. Boyd, "Exact Theory of Pump-Wave Propagation and Its Effect on Degenerate Four-Wave Mixing in Saturable Absorbing Media," J. Opt. Soc. Am. B **2**, 1117 (1985).

A. L. Gaeta, M. T. Gruneisen, and R. W. Boyd, "Theory of Degenerate Four-Wave Mixing in Saturable Media with the Inclusion of Pump Propagation Effects," IEEE J. Quantum Electron. **QE-22**, 1095 (1986).

A. L. Gaeta, R. W. Boyd, P. W. Milonni, and J. R. Ackerhalt, "Instabilities in the Propagation of Arbitrarily Polarized Counterpropagating Waves in a Nonlinear Kerr Medium," Optical Bistability III, edited by H. M. Gibbs, P. Mandel, N. Peyghambarian, and S. D. Smith, Springer-Verlag, Berlin pp. 302-305 (1986).

R. W. Boyd, A. L. Gaeta, D. J. Gauthier, M. S. Malcuit, and P. Narum, "Instabilities in Four-Wave Mixing," SPIE **667**, 156 Optical Chaos (1986).

A. L. Gaeta, R. W. Boyd, J. R. Ackerhalt, and P. W. Milonni, "Instabilities and Chaos in the Polarizations of Counterpropagating Light Fields," Phys. Rev. Lett. **58**, 2432 (1987).

P. Narum, A. L. Gaeta, M. D. Skeldon, and R. W. Boyd, "Instabilities of Laser Beams Counterpropagating through a Brillouin-Active Medium," J. Opt. Soc. Am. B **5**, 623 (1988).

A. L. Gaeta and R. W. Boyd, "Quantum Noise in Phase Conjugation," Phys. Rev. Lett. **60**, 2618 (1988).

A. L. Gaeta, M. D. Skeldon, R. W. Boyd and P. Narum, "Observation of Instabilities of Laser Beams Counterpropagating through a Brillouin medium," J. Opt. Soc. Am. B **6**, 1709 (1989).

M. T. Gruneisen, K. R. MacDonald, A. L. Gaeta, R. W. Boyd, and D. Harter, "Energy Transfer in an Atomic Vapor," Phys. Rev. A **40**, 3464 (1989).

R. W. Boyd, A. L. Gaeta, D. J. Gauthier, and M. S. Malcuit, "Bistability and Chaotic Instabilities of Laser Beams Counterpropagating Through Sodium Vapor," Laser Spectroscopy IX, edited by M. S. Feld, J. E. Thomas, and Aram Mooradian, Academic Press, Boston pp. 164-166 (1989).

A. L. Gaeta and R. W. Boyd, "Quantum Statistics of Optical Phase Conjugation," to be published in Coherence and Quantum Optics VI, edited by J. H. Eberly, L. Mandel, and E. Wolf, Plenum, New York (1990).

D. J. Gauthier, M. S. Malcuit, A. L. Gaeta, and R. W. Boyd, "Polarization Bistability of Counterpropagating Beams," Phys. Rev. Lett. **64**, 1721(1990)

G. G. Luther, C. J. McKinstrie, and A. L. Gaeta, "The transverse instability of counterpropagating waves," to be published in <u>Nonlinear Dynamics on Optical Systems</u>, edited by N. B. Abraham, E. Garmire, and P. Mandel (1990).

M. T. Gruneisen, K. R. MacDonald, A. L. Gaeta, R. W. Boyd, and D. Harter, "Laser Beam Combining in Potassium Vapor," to be published in IEEE J. Quantum Electron. (1990).

M. Kauranen, J. J. Maki, A. L. Gaeta, and R. W. Boyd, "Observation of Two-Beam Excited Conical Emission," to be published (1990).

A. L. Gaeta and R. W. Boyd, "Stochastic Fluctuations in Stimulated Brillouin Scattering," to be published (1990).

A. L. Gaeta and R. W. Boyd, "Stimulated Brillouin Scattering in the Presence of Feedback," to be published (1990).

Patents

"System for Combining Laser Beams by Transfering Energy therebetween in Atomic Vapor," R. W. Boyd, A. L. Gaeta, M. T. Gruneisen, K. R. MacDonald, #4,918,699, April 17 1990.

vii

Acknowledgements

Abstract

The dynamical behavior of stimulated Brillouin scattering (SBS) under a variety of conditions is investigated both theoretically and experimentally. Under conditions of a single continuous-wave laser field, the initiation of the SBS process is treated by including the thermal fluctuations of the material density which lead to spontaneous Brillouin scattering. Predictions are made for the threshold of SBS, for the output Stokes spectrum, and for the temporal behavior of the Stokes light. The spectrum of the output Stokes light is predicted to exhibit gain-narrowing as the input laser intensity is increased. Under certain conditions, the Stokes output intensity is expected to exhibit nearly 100% fluctuations even far above the threshold for SBS. Experiments performed in a single-mode optical fiber verify many of the predictions of the theory.

Due to the high gain that can be achieved for the Stokes wave, a small amount of feedback from both interfaces of the interaction region is found to dramatically modify the characteristics of the output Stokes light. The system is found to undergo a transition from stochastic to deterministic behavior. Theoretical analysis demonstrates that the threshold for Brillouin oscillation can be much lower than the threshold for single-beam SBS, and the spectrum is shown to be nearly monochromatic. The temporal behavior of the Stokes light above threshold is found to exhibit both stable and periodic output.

Experiments utilizing a single-mode optical fiber with feedback from the endfaces confirmed many of the theoretical predictions.

Stimulated Brillouin scattering in the presence of two counterpropagating laser beams is studied. Under these conditions, the laser beams become temporally unstable to the growth of Stokes and anti-Stokes light. For the case when the input intensities of the two waves are comparable, the threshold for instability can be significantly lower than the threshold for usual single-beam SBS and, for the case of a broad Brillouin line, the system can show a period-doubling route to chaos. This Brillouin instability was observed experimentally using carbon disulfide as the Brillouin-active material.

Table of Contents

List of Figures

Tables

Chapter 1
Introduction

Predicting the temporal evolution of natural phenomena is an innate desire in all of us. However, nature has posed certain obstacles which limit one's ability to know precisely the manner in which a system evolves. There exist various mechanisms due to which a system can fluctuate in time, and these fluctuations can be classified into two distinct types: stochastic and deterministic. A stochastic system is one whose behavior is inherently "noisy" in the usual sense; the global behavior of the system may be described only through the use of statistical methods. Thus, for a stochastic system one may speak only in terms of the *likelihood* of a variable assuming a range of values at a particular time. A deterministic system is one whose dynamics are well defined in the sense that equations can be formulated which completely describe the evolution of all the variables in the system; by specifying the initial conditions of the system, the temporal evolution is then known for all time. Nevertheless, under certain conditions, a deterministic system can display extremely complicated behavior reminiscent of a stochastic system in which the ability to make long-time predictions is lost.

The origin of the randomness associated with a stochastic system is the existence of many (essentially infinite in number) degrees of

freedom. The global behavior of the ensemble is determined through statistical methods, since treating the dynamical behavior of each degree of freedom would be intractable. In many systems there exist only a few degrees of freedom of interest which are coupled to a large ensemble (i.e., a reservoir) of variables that behave similarly to one another. This coupling leads to a translation of the stochastic behavior of the ensemble to the principal variables. One of the most studied and most important examples of a stochastic process is that of Brownian motion in which a particle immersed in a liquid undergoes irregular movements due to collisions with the molecules of the liquid. Einstein[1] first addressed this problem by assuming that the action of the liquid molecules on the particle can be described as a random sequence of kicks which could be treated as a delta-correlated fluctuating force. He was then able to relate the mean-square displacement of the particle to the temperature of the liquid and the frictional force experienced by the particle. This model is an example of one which obeys the fluctuation-dissipation theorem: the presence of fluctuations leads to dissipation and vice-versa.[2]

A deterministic system can show three types of temporal behavior: steady-state, quasi-periodic, and chaotic. When a system displays the first two types of behavior, predicting the future evolution of the system is trivial. However, a system that possesses nonlinearity and as few as three degrees of freedom can show deterministic chaos. A system is defined to be chaotic, if one of the Lyapunov exponents associated with the attractor of the system is positive.[3] A positive Lyapunov exponent implies that the trajectories for two arbitrarily close initial conditions

become entirely distinct and uncorrelated after a period of time (i.e., the inverse of the value of the positive Lyapunov exponent). Since in practice it is impossible to know the initial conditions of a system to infinite accuracy, the ability to make long-term predictions is lost. This type of behavior was first quantitatively treated by Lorenz[4] in 1963. By using a simple theoretical model of fluid flow in the atmosphere, he showed that the resulting equations displayed a temporal evolution that was aperiodic and that small changes in the initial conditions led to entirely distinct trajectories. Lorenz concluded that this type of behavior suggests that long-term predictions of the weather may be impossible.

Optics has lent itself well to theoretical and experimental studies of stochastic and deterministic behavior. In Section 1.1, examples are discussed of a system that displays classically stochastic behavior. Examples of chaotic systems in optics are reviewed in Section 1.2, in which particular attention is devoted to nonlinear optical systems. In Section 1.3, the field of stimulated Brillouin scattering is reviewed, and reasons are given to explain why it provides an ideal system with which to study both stochastic and deterministic behavior in nonlinear optics.

1.1 Stochastic Behavior in Optics

Perhaps the simplest and most fundamental stochastic system in optics is the light that is emitted by a source composed of a large number of identical dipoles oscillating at a frequency ω_o.[5] The dipoles are assumed to undergo collisions with one another such that the effect of each collision between the dipoles is assumed to impart a phase shift

onto the field emitted by each of the participating dipoles; during the period of time between collisions each dipole is assumed to oscillate sinusoidally. Since each collision occurs with a different geometry, the phase shifts imparted onto the emitted field by all the collisions are assumed to be uniformly distributed between 0 and 2π. The temporal nature of the collisions can be described statistically in such a way that the probability that the dipole does not experience a collision during a time between t and $t + dt$ is given by

$$p(t)dt = \frac{1}{\tau_o}e^{-t/\tau_o}\,dt \tag{1.1}$$

where τ_o is the mean period of between collisions for the dipole. The total complex field amplitude can be expressed as a sum of the fields from each dipole

$$E_T(t) = E_o \sum_i^N e^{i\phi_i(t)} \tag{1.2}$$

where ϕ_i is the phase associated with the field from each dipole and E_o is the dipole-field amplitude (all the dipoles are assumed to emit a field polarized along the same direction). For simplicity the dipole amplitude will be taken to be equal to unity. By assuming that the phases from each dipole are not correlated with each other and are uniformly distributed between 0 and 2π, the sum in Eq. (1.2) can be performed at a time t which leads to a particular value for $E_T(t)$. If the the total field is then calculated after a time τ, which is short in comparison to the mean
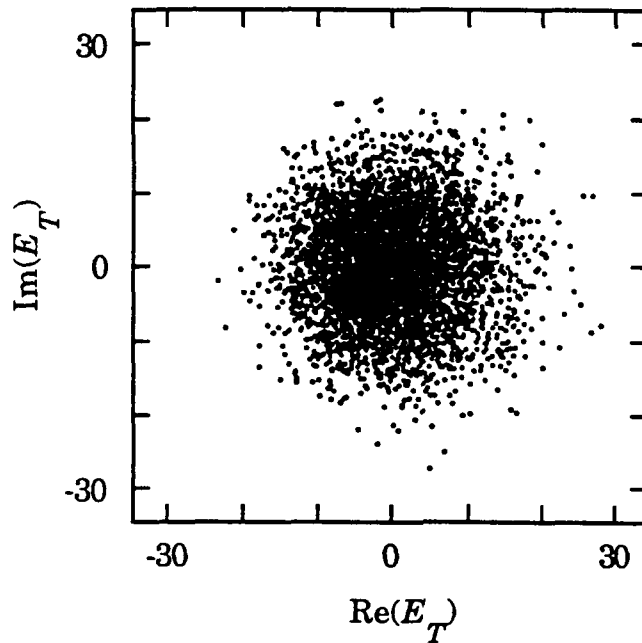
Fig. 1.1 Plot of 5000 realizations of the total field E_T emitted by a collection (N = 100) of dipoles.

period between collisions τ_o, then the phases ϕ_i will not have changed their values and the resulting value for the total field will be the same as at time t. However, if τ is longer than τ_o then the resulting value for $E_T(t+\tau)$ will be a new realization. If a large number of these realizations are performed then a distribution of values for the total field is created. Figure 1.1 is a plot of the distribution of values for $E_T(t)$ on the complex plane for the case of N = 100. The distribution is centered at $E_T(t)$ = 0 and appears to be symmetric about the origin with a width approximately equal to 10. In fact, this model possesses the same statistical properties as the Gaussian random process associated with the two-dimensional model of Brownian motion.[1] The probability density for the total field in the limit of large N is then given by

$$P[E_T(t)] = \frac{1}{\pi N}\, e^{-|E_T|^2/N} \; .$$

(1.3)

This distribution confirms the observations made previously concerning Fig. 1.1. An important point to consider is that as long as the time interval over which the field E_T has been sampled is much longer than the mean period of between collisions τ_o, the time averages will be equal to the ensemble averages of similarly prepared systems taken at the same time. This statement is simply an assertion that the field emitted by the dipoles is an ergodic process for times long compared to τ_o. The origin of this ergodicity can be attributed to the form of the probability density of the period between collisions for the dipole (Eq. 1.1), which tends to zero for long times.

Since a photodetector makes a direct measurement of the intensity of the field, it is useful to calculate the probability density $P[I(t)]$ for the intensity $I_T = |E_T|^2$. This quantity can be easily derived from Eq. (1.3) and is given by

$$P[I_T(t)] = \frac{1}{N}\, e^{-I_T/N} \; .$$

(1.4)

The expectation value of the intensity is then simply given by $< I_T > = N$. A measure of the fluctuations in the intensity relative to the expectation value of the intensity is given by the normalized standard deviation ΔI

$$\Delta I = \frac{\sqrt{< I^2 > - < I >^2}}{< I >} = 1 \; .$$

(1.5)

Thus, one sees that the fluctuations in the field intensity are, on the average, as large as its average value. Experimental realization of an optical system analogous to a collection of dipoles has been made by Arecchi et al.[6]

The example discussed here is an example of a stochastic system in which the statistical uncertainty of an ensemble of variables (i.e., the dipoles undergoing collisions) is translated to the dynamical variable of interest (i.e., the total electric field of the dipoles). Although the ability to predict the actual temporal evolution of the field is lost, by making measurements of its statistical properties, information can be gained about the physical properties of the dipole collisions.

1.2 Deterministic Fluctuations in Optics

Since an electromagneti field varies in both space and time, two types of instabilities exist which can lead to a change in the dynamics of an optical system. A convective instability is said to occur if perturbations to the system grow exponentially in space; an absolute instability is said to occur if perturbations to the system grow exponentially in time. The study of these instabilities is important in order to study a system's transitions between static, periodic, and chaotic evolution. Examples of convective instabilities in optics are gain processes such as single-beam stimulated Raman scattering, single-beam stimulated Brillouin scattering, and stimulated emission from a collection of inverted two-level atoms. Examples of absolute instabilities

in optics are threshold for a laser and self-oscillation in phase conjugation. In this Section, we will focus the discussion on absolute instabilities that lead to changes in the temporal evolution of a system. In some cases these absolute instabilities are based partly on the presence of an existing convective instability.

The optical device that has been studied most extensively is the laser, and it has been found to display many of the dynamic instabilities that can occur in nonlinear systems: periodic oscillations, self-pulsing, and deterministic chaos.[7] Its universal behavior was demonstrated by Haken,[8] who showed that the equations describing a single-mode laser were isomorphic to the Lorenz equations. Thus, the study of chaotic dynamics entered the field of optics. Since then, nearly every type of laser has been shown both experimentally and theoretically to exhibit temporally unstable behavior, including chaos.[9]

The instabilities that occur in lasers have also been shown to exist in nonlinear optical devices.[7,10] Ikeda et al.[11] demonstrated that the
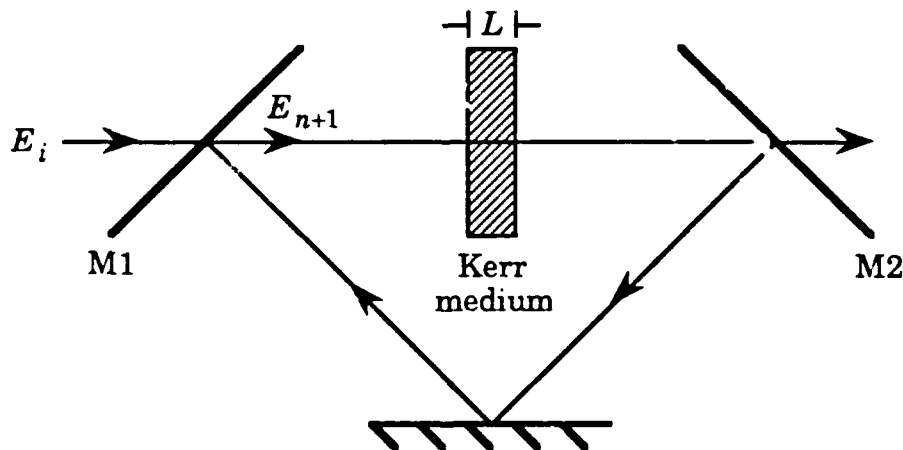
Fig. 1.2 The geometry of a ring cavity with a Kerr medium.

field transmitted through a ring cavity that contains a material with an intensity-dependent refractive index (see Fig. 1.2) could display self-pulsing and chaos. In the limit in which the transit time of the cavity is much longer than the response time of the nonlinear index, the temporal evolution of the field at mirror M1 can be reduced to the following mapping in which each iteration represents one transit time of the cavity:

$$E_{n+1} = \sqrt{1-R}\, E_i + R E_n \exp\!\left[i|E_n|^2\right] \qquad (1.14)$$

where E_i is the incident field amplitude, R is the reflectivity of the input (M1) and output (M2) mirrors; all the fields are normalized by $(n_2 kL)^{1/2}$, where k is the wavevector magnitude, n_2 is the nonlinear coefficient, and L is the length of the nonlinear material. The stationary solutions to this mapping can be multivalued for sufficiently large values of the transmitted incident field. However, most of these solutions are unstable and the mapping displays a period-doubling route to chaos as the incident field amplitude is increased. An example of the evolution of the field in the chaotic regime is shown in Fig. 1.3, which shows a phase-space plot of the field [i.e., $\mathrm{Im}(E_n)$ versus $\mathrm{Re}(E_n)$] for 5000 iterations of Eq. (1.14) with $R = 0.5$ and $|E_i|^2 = 15$. This chaotic phase-space trajectory is termed a strange attractor.[3] Although the structure of the attractor remains the same for different initial conditions, the sequences of values

of E_n become entirely distinct for any nonzero deviation between the two initial points. This deterministic structure strongly contrasts with the stochastic phase-space trajectory shown in Fig. 1.1, yet in both cases long-time predictions for the field are impossible.

In all the previously discussed optical systems in which complicated deterministic behavior occurred, a nonlinearity exists that is coupled to an external feedback mechanism provided by a cavity. Silberberg and Bar-Joseph[12] demonstrated that instabilities and chaos could occur in a nonlinear optical system in which no external feedback exists. The system they considered is conceptually very simple: two scalar waves with the same optical frequency counterpropagating in a medium with an intensity-dependent refractive index (i.e., a Kerr
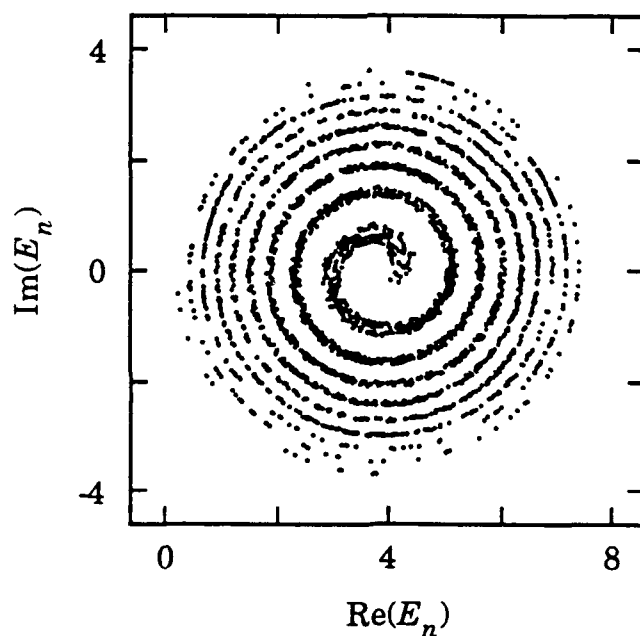
Fig. 1.3 A plot of E_n on the complex plane for the Ikeda mapping in the chaotic regime for a series of 5000 points for the case $R = 0.5$ and $|E_i|^2 = 15$.

medium) which has a finite response time τ. At low input intensities, the two fields pass through the medium experiencing only a nonlinear phase shift. However, above a certain threshold intensity, the output intensities begin to fluctuate periodically in time, and at higher intensities, the temporal evolution of the output intensity becomes chaotic. A gain-feedback argument can be used to explain the origin of this instability. Gain at the sidemodes to the input frequency of the two fields exists due to the sluggish response of the medium (e.g., stimulated Rayleigh-wing scattering). These sidemodes then experience distributed feedback as a result of the index grating created by the interference of the two input fields. An important criterion for the instability to have a low threshold is that the sidemodes that experience gain are also modes of the index grating; this mode-matching leads to the requirement that the response time of the material be approximately equal to the transit time through the medium. A similar treatment [13] was also performed for the case in which the material is composed of a collection of two-level atoms, and temporal behavior similar to the behavior that occurs in a Kerr medium is predicted.[14] Khitrova et al.[15] have observed a related instability in sodium vapor.

Gaeta et al.[16] extended the treatment of Silberberg and Bar-Joseph to include the vector nature of the field and found that the polarizations of the counterpropagating fields could become temporally unstable for threshold input intensities much less than those required for the scalar instability. They assumed that the tensor medium was an isotropic Kerr medium and that the input fields were polarized parallel to one another.

In some cases, both the intensities and the polarizations of the output fields could show instabilities and chaos, whereas in other cases only the polarization of the fields exhibit complicated temporal behavior. Since the instability is related to parametric four-wave mixing between the different polarization components, no restriction is placed on the response time of the material. Gauthier et al.[17] observed related polarization instabilities and chaos in sodium vapor.

1.3 Stimulated Brillouin Scattering

This Thesis deals with the temporal nature of stimulated Brillouin scattering (SBS) under various conditions. As will be shown, SBS provides a fertile nonlinear optical system with which studies of both stochastic and deterministic fluctuations can be performed. The following discussion is a brief review of the previous work on SBS.

Stimulated Brillouin scattering is the coupling of a laser and a Stokes field through an acoustic wave. Although first observed by Chiao et al. in 1964,[18] the majority of the research on SBS has been performed in the Soviet Union.[19] The prime reason for this intense study was the realization by Zel'dovich et al.[20] in 1972 that the strong Stokes light generated in the backward direction possessed certain spatial properties of the incident laser light which could lead to self-pumped phase conjugation. Thus, SBS provides a technique for performing aberration correction of high energy laser pulses without the need of external pump beams which are normally required for phase conjugation by four-wave mixing.[21] The simplicity and efficiency with which SBS can be

performed has made it attractive for performing phase conjugation: one simply focuses the laser beam into a Brillouin-active medium and as much as 90% of the laser light can be converted into Stokes light. Another important feature is that in many materials SBS is the dominant optical nonlinearity as long as the incident laser pulses are longer than the phonon lifetime (~1 ns) of the material.[22]

The theoretical foundation for most of the work that has dealt with SBS has been the steady-state coupled intensity equations for the Stokes field and the laser field,

$$\frac{dI_l}{dz} = -g_o I_l I_s \qquad (1.15a)$$

and

$$\frac{dI_s}{dz} = -g_o I_l I_s , \qquad (1.15b)$$

where I_l and I_s are the laser and Stokes intensity, respectively, g_o is the SBS gain factor, and the laser and the Stokes field are assumed to travel in the +z and the -z directions, respectively. In the limit in which the Stokes intensity does not grow sufficiently large to deplete the laser intensity, the Stokes intensity is seen to experience exponential gain in which the total single-pass gain G is equal to $g_o I_l L$. Equation (1.15) can been used to model SBS for the case in which the Stokes output is initiated from spontaneous Brillouin scattering. A very small nonfluctuating Stokes seed is injected at $z = L$, which can then be

amplified to intensities comparable to the input laser intensity. The magnitude of the injected Stokes seed can be estimated by determining the intensity of the spontaneously scattered light (e.g., $10^{-12}I_l$) that is generated near $z = L$.[19] This model has been useful for making predictions for the expected intensity of the Stokes signal at $z = 0$ for a particular value of the input laser intensity.

Several workers have included the temporal nature of the SBS process by including the time dependence in the propagation of the intensities in Eq. (1.7) or by including the differential equation for the acoustic wave. For the case in which the laser field is turned-on and maintained at a steady input value, the system reaches a steady-state via relaxation oscillations associated with the turn-on of the laser intensity. Attempts to treat rigorously the temporal nature of initiation of the SBS process have only been made recently.[23,24] Due to the stochastic nature of the density fluctuations which lead to the spontaneous scattering. it is expected that the amplified Stokes light could also exhibit these stochastic fluctuations. These issues are addressed theoretically and experimentally in Chapters 2 and 3, respectively.

Due to the extremely high values of the single-pass gain that are attainable in SBS, a small amount of feedback can lead to Brillouin oscillation in which the characteristics of the Stokes output is entirely different from the output associated with usual SBS. This Brillouin oscillation has been demonstrated experimentally by several workers[25] in a ring-configuration. As will be shown in Chapter 4, the behavior of the SBS process under conditions of Brillouin oscillation is of a

deterministic nature and, in a fashion analogous to that of the laser, can show both steady-state behavior as well as temporal instabilities.

As discussed in Section 1.2, instabilities due to counterpropagating waves have been demonstrated for a wide variety of nonlinear materials. Zel'dovich and Shkunov[26] first showed that for an extremely short Brillouin-active medium, counterpropagating laser beams could be temporally unstable. In Chapter 5, a more general theoretical treatment of counterpropagating beams in a Brillouin-active medium is given in which temporal instabilities and chaotic behavior are predicted. Experimental results are also presented in which these temporal instabilities are observed.

1. See for example, *Noise and Stochastic Processes,* edited by N. Wax (Dover, New York, 1954).
2. See, for example, H. Haken, *Synergetics,* (Springer-Verlag, New York, 1983) Chapter 6.
3. H. G. Schuster, *Deterministic Chaos,* (Physik-Verlag, Weinheim, 1984) Chapter 2.
4. E. N. Lorenz, "Deterministic nonperiodic flow," J. Atmospheric Sci. **20**, 130 (1963).
5. R. Loudon, *The Quantum Theory of Light* (Clarendon Press, Oxford, 1983) Chapter 3.
6. F. T. Arecchi, E. Gatti, and A. Sona, Phys. Lett. **20**, 27 (1966).
7. See for example, *Optical Instabilities,* edited by R. W. Boyd, M. G. Raymer, and L. M. Narducci
8. H. Haken, "Analogy between higher instabilities in fluids and lasers," Phys. Lett. **53A**, 77 (1975).
9. Special issue on Instabilities in J. Opt. Soc. Am. B **2**, (1988).
10. P. W. Milonni, J. R. Ackerhalt, and M. -L. Shih, *Chaos in Laser-Matter Interactions,* (World Scientific, Singapore, 1987).

11. K. Ikeda, H. Daido, and O. Akimoto, "Optical turbulence: chaotic behavior of transmitted light from a ring cavity," Phys. Rev. Lett. **45**, 709 (1980).

12. Y. Silberberg and I. Bar-Joseph, "Instabilities, self-oscillation, and chaos in a simple nonlinear optical interaction," Phys. Rev. Lett. **48**, 1541 (1982).

13. I. Bar-Joseph and Y. Silberberg, "Instability of counterpropagating beams in a two-level-atomic medium," Phys. Rev. A **36**, 1731 (1987).

14. D. J. Gauthier, "Instabilities of laser beams propagating through nonlinear optical media," Ph. D. Thesis, University of Rochester, Rochester, New York (1989).

15. G. Khitrova, J. F. Valley, and H. M. Gibbs, "Gain feedback approach to instabilities in sodium vapor," Phys. Rev. Lett. **60**, 1126 (1988).

16. A. L. Gaeta, R. W. Boyd, J. R. Ackerhalt, and P. W. Milonni, "Instabilities and chaos in the polarizations of counterpropagating light fields," Phys. Rev. Lett. **58**, 2432 (1987).

17. D. J. Gauthier, M. S. Malcuit, and R. W. Boyd, "Polarization instabilities of counterpropagating laser beams in sodium vapor," Phys. Rev. Lett. **61**, 1827 (1988).

18. R. Y. Chiao, C. H. Townes, and B. P. Stoicheff, "Stimulated Brillouin scattering and coherent generation of intense acoustic waves," Phys. Rev. Lett. **12**, 592 (1964).

19. B. Ya Zel'dovich, N. F. Pilipetsky, V. Shkunov, *Principles of Phase Conjugation* (Springer-Verlag, Berlin, 1985)

20. B. Ya. Zel'dovich, V. I. Popovichev, V. V. Ragulsky, and F. S. Faizullov, "On the relation between wavefronts of reflected and excited radiation in stimulated Brillouin scattering," JETP Lett. **15**, 109 (1972).

21. A. Yariv and D. M .Pepper, "Amplified reflection, phase conjugation, and oscillation in degenerate four-wave mixing," Opt. Lett. **1**, 16 (1977).

22. W. Kaiser and M. Maier, "Stimulated Rayleigh, Brillouin and Raman spectroscopy," in *Laser Handbook*, edited by F. T. Arecchi and E. O. Schulz-Dubois (North-Holland, Amsterdam, 1972) p. 1077-1149.

23. S. M. Wandzura, "Stimulated scattering does not have a steady-state," paper MC3 in Conference on Lasers and Electro-Optics Technical Digest (1988).

24. E. M. Dianov, A. Ya. Karasik, A. V. Lutchnokov, A. N. Pilipetski, "Saturation effects at backward stimulated scattering in the single-mode interaction," Opt. and Quantum Electron. **21**, 381 (1989).

25. K. O. Hill, B. S. Kawasaki, and D. C. Johnson, "cw Brillouin laser," Appl. Phys. Lett. **28**, 608 (1976); D. R. Ponikvar and S. Ezekiel, "Stabilized single-frequency stimulated Brillouin fiber ring laser," Opt. Lett. **6**, 398 (1981); I. Bar-Joseph, A. Dienes, A. A. Friesem, E. Lichtman, R. G. Waarts, and H. H. Yaffe, "Spontaneous mode locking of single- and multi-mode pumped SBS fiber lasers," Opt. Commun. **59**, 296 (1986).

26. B. Ya. Zel'dovich and V. V. Shkunov, "Characteristics of stimulated scattering in opposite pump beams," Sov. J. Quantum Electron. **12**, 223 (1982).

Chapter 2
Theory of Stimulated Brillouin Scattering

Spontaneous Brillouin scattering occurs when light propagates in a material and is scattered due to density fluctuations within the material. If the incident light field is sufficiently strong, stimulated Brillouin scattering (SBS) occurs in which the density variations in the material are induced through the process of electrostriction. Under these conditions, the incident laser field, a Stokes field, and an acoustic field become strongly coupled through a parametric nonlinear optical process (see Fig. 2.1) in which the frequencies and the wave vectors of the three waves satisfy the conditions.[1]

$$\omega_l = \omega_s + \Omega \qquad (2.1a)$$

and

$$\mathbf{k}_l = \mathbf{k}_s + \mathbf{q} \; , \qquad (2.1b)$$

where ω_l ($\mathbf{k}_l$), ω_s ($\mathbf{k}_s$), and Ω ($\mathbf{q}$) are the frequencies (wavevectors) of the laser, Stokes, and acoustic waves, respectively. These relations [Eq. (2.1)]
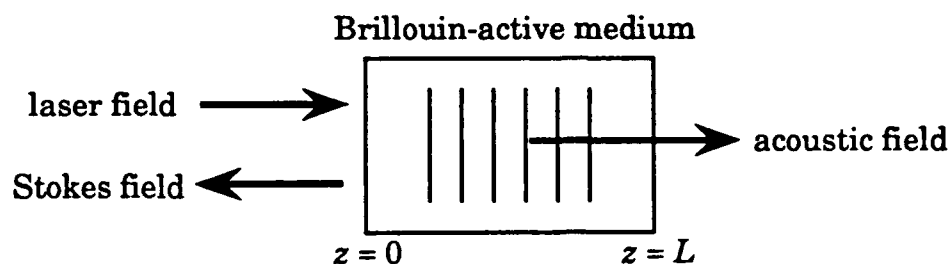
Fig. 2.1 Schematic illustration of the geometry for SBS in which the laser and Stokes fields are coupled through an acoustic field.

are equivalent to the requirements of energy and momentum conservation for efficient parametric coupling. Under conditions of strong excitation, nearly all the incident light can be converted into Stokes light. Although the SBS process can serve as an amplifier for a well-defined Stokes wave incident at $z = L$, SBS finds its greatest application for the case in which no Stokes wave is injected into the medium but grows spontaneously from noise (i.e., phase conjugation). The majority of the theoretical work that has been performed on SBS has neglected the spontaneous initiation of the SBS process and simply assumed that a small nonfluctuating Stokes seed is injected into the medium.[2,3] In order to determine the conditions under which this approximation is valid, the spontaneous intiation of SBS must be incorporated.

In order to treat the initiation and the statistical properties of the Stokes light generated through SBS, spontaneous Brillouin scattering must be accounted for in the theory. Zel'dovich[3] considered a localized model of the initiation of SBS in which he considered spontaneous

scattering only in the region near $z = L$ since the Stokes light in this region experiences the greatest gain. This model is useful in making reasonable predictions for the threshold of SBS. (Threshold being defined as the point at which the expected value of the output Stokes intensity reaches a particular fraction, i.e. 1%, of the input laser intensity.) Boyd et al.[4] performed a detailed calculation which includes a rigorous derivation for the amount of scattering that initiates the SBS process. Thus, they were able to make accurate predictions for the threshold for SBS and found that it depends upon the frequency of the incident laser field as well as upon the fundamental properties of the SBS medium. Wandzura,[5] Dainov et al.,[6] and Boyd et al.[4] included the distributed nature of the spontaneous scattering in the Brillouin medium and found through numerical simulations that the Stokes output intensity could have large temporal fluctuations even far above threshold for SBS.

In this Chapter, a theory that treats both spontaneous and stimulated Brillouin scattering is presented. In a procedure similar to Boyd et al.,[4] the equations for the laser, Stokes, and acoustic fields are derived with the inclusion of spontaneous scattering. In the limit in which the laser field is undepleted, an analytic solution for the Stokes field is found for which the output Stokes field exhibits large fluctuations and a gain narrowed optical spectrum. The effects of laser depletion are included by numerically integrating the full set of stochastic coupled nonlinear equations. The statistical properties of the Stokes output light are determined in the limit of a steady-state input laser field and they

are found to depend sensitively on the input laser intensity and ratio of the transit time through the medium to the phonon lifetime. Under certain conditions anomalous features appear in the the Stokes output intensity and are associated with relatively sharp phase discontinuities in the Stokes field. These features are similar to those predicted in theories of superfluorescence[7] and stimulated Raman scattering.[8,9]

2.1 Stochastic Initiation of Stimulated Brillouin Scattering

In accordance with Fig. 2.1, we assume that a single-mode laser propagates in the positive z direction and can be expressed as

$$\tilde{E}_l(z,t) = \frac{1}{2} E_l(z,t) e^{i(k_l z - \omega_l t)} + c.c. \quad , \tag{2.2}$$

where k_l is the laser wavevector magnitude. The Stokes wave generated by SBS is assumed to be counterpropagating to the laser field such that

$$\tilde{E}_s(z,t) = \frac{1}{2} E_s(z,t) e^{i(-k_s z - \omega_s t)} + c.c. \quad , \tag{2.3}$$

where k_s is the Stokes wavevector amplitude.

The acoustic wave equation describes the propagation of the variation of the density of the medium $\tilde{\rho}(z,t)$ from its mean value ρ_o. We assume that the acoustic wave is driven by two sources. The first source is present due to thermal fluctuations which give rise to spontaneous Brillouin scattering. The second source arises from the process of

electrostriction in the presence of the laser field and leads to SBS. The resulting equation of motion for the density[3]

$$\frac{\partial^2 \tilde{\rho}}{\partial t^2} - \Gamma \frac{\partial}{\partial t} \frac{\partial^2 \tilde{\rho}}{\partial z^2} - v^2 \frac{\partial^2 \tilde{\rho}}{\partial z^2} = \frac{-\gamma}{8\pi} \frac{\partial^2}{\partial z^2} \tilde{E}^2 + \tilde{f} \quad , \tag{2.4}$$

where $\Gamma = 4\eta/3\rho_0$ is a damping parameter, η characterizes the viscosity, v is the speed of sound in the medium, γ is the electrostrictive constant, $\tilde{E}(z,t) = \tilde{E}_l(z,t) + \tilde{E}_s(z,t)$ is the total optical field and $\tilde{f}(z,t)$ is a Langevin noise source. We assume that $\tilde{f}(z,t)$ is a Gaussian random variable with zero mean such that the ensemble average $<\tilde{f}(z,t)>$ is equal to zero. We also assume that $\tilde{f}(z,t)$ is delta correlated in the sense that

$$< \tilde{f}(z,t)\tilde{f}(z',t') > = \tilde{Q} \ \delta(z - z') \ \delta(t - t'). \tag{2.5}$$

In evaluating the electrostrictive driving term on the right-hand-side of Eq. (2.4), the terms that oscillate at zero frequency and at optical frequencies are neglected since they do not lead to excitation of acoustic waves inside the medium. The optical fields are also assumed to obey the slowly varying amplitude approximation (SVEA) in that $|\partial E_j / \partial z| << |k_j E_j|$ for j equal to l and s, in which case the electrostrictive driving term of Eq. (2.4) becomes

$$\frac{q^2 \gamma}{16\pi} \left(E_l E_s^* \ e^{i(qz - \Omega t)} + c.c. \right) \quad , \tag{2.6}$$

where $\Omega = \omega_l - \omega_s$ is the acoustic frequency and $q = k_l + k_s$ is the acoustic wavevector amplitude, which are related through the velocity of sound in the medium by the expression $\Omega = qv$. The form of Eq. (2.4) can now be simplified by introducing the complex representation

$$\tilde{\rho}(z,t) = \tfrac{1}{2}\rho(z,t)e^{i(qz-\Omega t)} + c.c. \ . \tag{2.7}$$

By substituting Eq. (2.7) into Eq. (2.4) and making the SVEA for the acoustic field, the equation for the acoustic amplitude becomes

$$\frac{\partial \rho}{\partial t} + \frac{\Gamma}{2}\rho + v\frac{\partial \rho}{\partial z} = \frac{i\gamma q^2}{16\pi\Omega}E_l E_s^* + f \ , \tag{2.8}$$

where $\Gamma = \Gamma q^2$ is the phonon (energy) decay rate and $f(z,t)$ is the complex amplitude of the Langevin noise source $\tilde{f}(z,t)$ which are related by

$$\tilde{f}(z,t) = -2i\Omega f(z,t)e^{i(qz-\Omega t)} + c.c. \ , \tag{2.9}$$

where $f(z,t)$ is also delta correlated such that

$$< f(z,t)f^*(z,t) >= Q\delta(z-z')\delta(t-t') \ , \tag{2.10}$$

where $Q = \tilde{Q}/4\Omega^2$. Equation (2.9) is valid under conditions in which the decay rate Γ of the acoustic field is much smaller than the Brillouin frequency Ω. In Appendix 2.1 the value of Q, which is a measure of the strength of the fluctuations in $f(z,t)$, is derived and is given by

$$Q = \frac{2k_B T \rho_o \Gamma}{v^2 A} \ ,$$

(2.11)

where k_B is Boltzman's constant, T is the temperature, and A is the cross-sectional area of the interaction region.

The driven wave equation that governs the propagation of plane-wave optical fields along the z axis through a Brillouin-active medium is given by

$$\frac{\partial^2 \tilde{E}}{\partial z^2} - \frac{n^2}{c^2}\frac{\partial^2 \tilde{E}}{\partial t^2} = \frac{4\pi}{c^2}\frac{\partial^2 \tilde{P}}{\partial t^2} \ ,$$

(2.12)

where n is the background refractive index and $\tilde{P}(z,t)$ is the additional material polarization arising from changes in the dielectric constant due to variations in the material density. This polarization can be expressed as

$$\tilde{P}(z,t) = \frac{\gamma}{4\pi\rho_o}\tilde{\rho}(z,t)\tilde{E}(z,t) \ .$$

(2.13)

In order to derive coupled-amplitude equations for the laser and Stokes field, the expression for the total optical field $\tilde{E} = \tilde{E}_l + \tilde{E}_s$ is substituted into both the wave equation [Eq. (2.12)] and into the expression for the polarization [Eq. (2.13)]. The complex representations for the laser field, the Stokes field, and the acoustic field [Eq. (2.2), (2.3), and (2.7), respectively] are then used to derive the following coupled-amplitude equations for the optical fields

$$\frac{\partial E_l}{\partial z} + \frac{n}{c}\frac{\partial E_l}{\partial t} = i\kappa\rho E_s \qquad (2.14a)$$

and

$$\frac{\partial E_s}{\partial z} - \frac{n}{c}\frac{\partial E_s}{\partial t} = -i\kappa\rho^* E_l \quad , \qquad (2.14b)$$

where $\kappa = \gamma\omega_l/4\rho_o nc$.

One last assumption is made regarding the spatial evolution of the acoustic field given by Eq. (2.8). For most materials the linear absorption $\Gamma/2v$ of hypersonic sound waves is sufficiently large that the acoustic wave is absorbed in a distance small compared to the distance over which the optical fields on the right-hand side of Eq. (2.8) have changed appreciably. The acoustic field is then assumed to be in a spatial steady-state such that $\partial\rho/\partial z = 0$, in which case the equation for the acoustic field becomes

$$\frac{\partial\rho}{\partial t} + \frac{\Gamma}{2}\rho = i\Lambda E_l E_s^* + f \quad , \qquad (2.15)$$

where $\Lambda = \gamma q^2/16\pi\,\Omega$. Equations (2.14) and (2.15) form the basis for the theoretical study of the initiation and of the statistical properties of SBS.

2.2 Limit of Undepleted Laser Field

In the limit in which the Stokes field E_s has not grown sufficiently large to deplete energy from the laser field E_l, the laser field can be taken

to be constant throughout the medium. In this case Eq. (2.14a) can be neglected and only Eqs. (2.14b) and (2.15) need be considered. The form of these equations is identical to the ones used in theories treating superfluorescence[10] and stimulated Raman scattering.[11] The solution to these equations is well known and, in the long-time limit in which no Stokes wave is injected at $z = L$, the relation for the Stokes waves at $z = 0$ is given by[4]

$$E_s(0,t) = i\kappa E_l \int_{-\infty}^{t} dt' \int_{L}^{0} dz'\, e^{-\frac{\Gamma}{2}(t-t')} f^*(z',t')\, I_0\left(\sqrt{G\Gamma z'(t'-t)/L}\right), \quad (2.16)$$

where I_0 is the zeroth-order modified Bessel function. The parameter $G = g_o I_l L$ is the single-pass logarithmic intensity gain experienced by the Stokes wave in the absence of pump depletion where $I_l = (nc/8\pi)\,|E_l(0)|^2$ is the steady-state input laser intensity and

$$g_o = \frac{\gamma^2 \omega_l^2}{\rho_o nc^3 v \Gamma} \quad (2.17)$$

is the SBS gain factor. The expectation value for intensity $I_s = (nc/8\pi)\,|E_s(0, t)|^2$ of the Stokes wave at $z = 0$ is then given by

$$< I_s > = \sigma I_l e^{G/2}\left[I_0(G/2) - I_1(G/2)\right], \quad (2.18)$$

where I_1 is the first-order modified Bessel function and where σ is given by

$$\sigma = \frac{g_0 L k_B T \omega_l \Gamma}{4 A \Omega} \ .$$

(2.19)

The contribution from the modified Bessel functions in Eq. (2.18) is due to the distributed nature of the noise in the medium. In the localized model of the intiation of SBS[3] in which a nonfluctuating noise seed is injected into the medium at $z = L$, the term in brackets containing the modified Bessel functions is replaced by the factor $e^{G/2}$. A detailed comparison between the two theories is made by Boyd *et al.*[4] In the limit of low gain ($G \ll 1$), Eq. (2.18) can be approximated by

$$< I_s > = \sigma I_l \ ,$$

(2.20)

which represents the spontaneous scattering of the laser light into the Stokes field. In the high gain limit ($G \gg 1$), large-argument expansions for the modified Bessel functions can be utilized[12] and the resulting expression for the Stokes intensity is

$$< I_s > = \sigma I_l \frac{e^G}{\sqrt{\pi} G^{3/2}} \ .$$

(2.21)

The Stokes intensity is seen to be reduced by a factor of $\sqrt{\pi} \, G^{3/2}$ from the usual single pass exponential gain factor e^G which is obtained by considering a localized noise source near $z = L$.

The fluctuations in the Stokes intensity can be estimated by calculating the second-order moment of the Stokes intensity $<I_s^2>$ from Eq. (2.16) which leads to

$$< I_s^2 > = 2 < I_s >^2 \ . \tag{2.22}$$

A measure of the fluctuations in the Stokes intensity is given by the normalized standard deviation ΔI_s

$$\Delta I_s = \frac{\sqrt{< I_s^2 > - < I_s >^2}}{< I_s >} \ , \tag{2.23}$$

which in the case of no pump depletion is equal to unity. This result can be simply understood by the fact that in the absence of pump depletion, the Brillouin medium is serving as a linear amplifier for thermal (or quantum) noise which also has 100% fluctuations. Thus, the fluctuations in the Stokes light are simply a macroscopic manifestation of the thermal (or quantum) noise which is initiating the SBS process.

Although the relative fluctuations of the Stokes field are as large as those of the Langevin noise source which initiates SBS, the spectra of the fluctuations for the two quantities are expected to be different. As a result of the delta-correlated property of the noise source f, its corresponding spectrum is broadband. However, the resulting fluctuations which drive the Stokes field will be spectrally filtered since ρ experiences damping which limits its ability to respond to fluctuations that occur in a time short compared to $2/\Gamma$. The spectrum of the Stokes field can be easily determined by taking the temporal Fourier transform of Eqs. (2.14b) and (2.15) and solving the resulting linear differential equations [or alternatively, by taking the Fourier transform of the two-

time correlation of the Stokes field using Eq. (2.16)]. The homogeneous solution may be neglected since no Stokes field is assumed to be injected at $z = L$. The resulting solution for the Fourier transform of the Stokes field $F_s(\delta)$ at $z = 0$ is

$$F_s(\delta) = \frac{-\kappa E_l}{\delta + i\Gamma/2} \int_0^L dz\, f_\delta^*(z') e^{\left(-in\delta/c + gI_l\right)z} \qquad (2.24)$$

where $\delta = \omega - \omega_s$ is the frequency detuning from the Stokes frequency, $h(z)$ is the Fourier transform of $f(z,t)$ and $g = \pounds g_0$ where $\pounds = (1 - i2\delta/\Gamma)^{-1}$. The normalized power spectrum $S(\delta)$ is

$$S(\delta) = \frac{< F_s(\delta)F_s^*(\delta) >}{< F_s(0)F_s^*(0) >} = \frac{e^{|\pounds|^2 G} - 1}{e^G - 1} . \qquad (2.25)$$

In the limit in which the gain is small $(G \ll 1)$, $S(\delta)$ reduces to a Lorentzian lineshape

$$S(\delta) = \frac{1}{1 + 4\delta^2/\Gamma^2} , \qquad (2.26)$$

with a full-width at half maximum (FWHM) equal to Γ. This result [Eq. 2.26)] is expected since spontaneous Brillouin scattering is the dominant contribution to the Stokes field in the limit of small Stokes gain. In the limit in which the gain is large $(G \gg 1)$, $S(\delta)$ has the form of a Gaussian lineshape

$$S(\delta) = e^{-4G\delta^2/\Gamma^2} , \qquad (2.27)$$
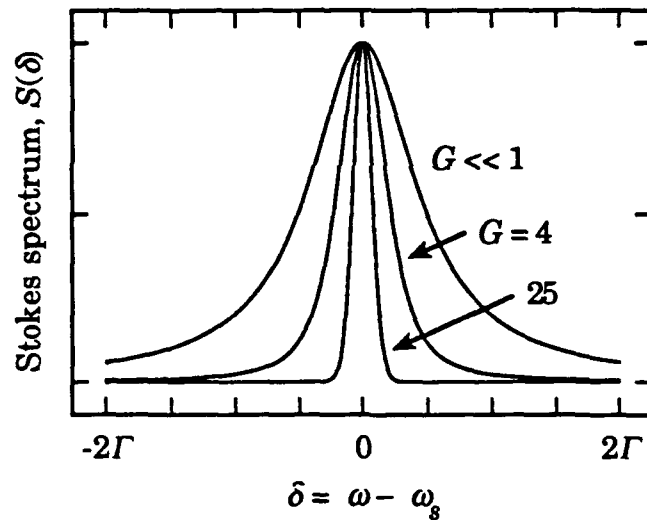
Fig. 2.2 Spectrum of the Stokes light in the limit of the undepleted laser field plotted for three different values of the single-pass gain G.

with a FWHM equal to $\Gamma/\sqrt{G/\ln 2}$. This effect of the narrowing of the spectrum by the factor of $\sqrt{G/\ln 2}$ is the well known effect of gain narrowing[13] that occurs in several types of amplifiers. Figure (2.2) shows a plot of the power spectrum $S(\delta)$ [Eq. (2.25)] for several different values of the single-pass gain G.

2.3 Numerical Simulations of SBS

In order to determine the statistical properties of the Stokes light in the regime in which the laser field is depleted, the full stochastic nonlinear differential equations [Eqs. (2.14) and (2.15)] must be numerically integrated. All the numerical simulations shown here were performed on a single computing element of an Alliant FX-8 mini-supercomputer. The Stokes field and the laser field are integrated using

the method of characteristics. The input laser field at $z = 0$ is assumed to be smoothly ramped on and kept at the steady-state value chosen for the particular case. The value of the Stokes field at $z = L$ is taken to be equal to zero. The noise source f is assumed to be a complex Gaussian random variable which is delta-correlated in both space and time. For each grid point in space and time, two uniformly random numbers were generated using a random number generator of Fortran and were then converted to a single complex Gaussian random number using the Box-Mueller method.[14]

There are three important parameters that determine the behavior of emitted Stokes light. First, the input intensity of the incident laser light (or correspondingly, the single-pass gain G) determines roughly the amount of SBS that occurs. Secondly, the ratio of the transit time of light through the medium $T_t = nL/c$ to the phonon lifetime Γ^{-1}, which is simply the product ΓT_t, is an estimate of the how rapidly the Stokes light is expected to fluctuate in comparison to the transit time through the medium. The reason why the quantity ΓT_t plays an important role is that the Stokes field and the laser field are counterpropagating. Thus, under conditions of laser depletion, the SBS process essentially possesses an extra degree of freedom that is not present in amplifiers (e.g., Raman) in which the pump wave and the amplified wave are copropagating. Thirdly, the strength of the fluctuations of the noise operator $f(z,t)$ which is quantified by σ [Eq. 2.19], determines the amount of laser light that is spontaneously scattered into the Stokes field initiating the SBS process. Although σ appears to be

proportional to the phonon damping rate Γ, it is actually independent of Γ since the gain factor g_o is inversely proportional to Γ.

For all the cases treated here, several of the parameters associated with the experiments performed in an optical fiber (see Chapter 3) will be used. That is, the following values are assumed: the photon energy is taken to be $\hbar\omega_l = 3.9 \times 10^{-19}$ J (i.e., the $\lambda_l = 514.5$ nm), $T = 300^\circ$K, the cross-sectional area $A = 1 \times 10^{-7}$ cm^2, $\Gamma/\Omega = 0.1$ and the gain factor $g_o = 2.5 \times 10^{-9}$ cm/W. In most single-mode SBS experiments performed in a focused geometry, the Fresnel number of the interaction is equal to unity, which fixes the ratio L/A to the value of $1/\lambda_l$ in the expression for σ [Eq. (2.19)]. However, in a single-mode optical fiber this restriction is lifted due to the guided nature of the light and L can be taken to be independent of A. Thus, the value of the quantity L/A can be much larger than the value for a focused geometry. Although the strength of the noise parameter for an optical fiber is used, it is expected that much of the ensuing analysis is general and can be applied to SBS in any medium.

Figures (2.3), (2.4), and (2.5) are plots of the output Stokes intensity for various values of G for the cases $\Gamma T_l = 1$, 10, and 100, respectively. The origin on the time axis is taken to be at an arbitrary time for which the effects of the turn-on of the laser field may be neglected. Since the Stokes light fluctuates on a time scale roughly equal to the phonon lifetime $1/\Gamma$, the temporal evolution of the Stokes intensity is displayed for an equal number of phonon lifetimes to allow for direct comparison between the three cases. On each plot the time averaged SBS reflectivity,

$R = <I_s>/I_l$, is listed. For the case of $G = 5$, the Stokes emission in each case appears very noisy, characteristic of amplified spontaneous Brillouin scattering. As expected, there is roughly a factor of ten increase in the Stokes output intensity for each ten-fold increase in ΓT_t, since in the undepleted-pump regime the amount of spontaneous scattering is proportional to the length L of the medium. For the case $G = 15$, the temporal evolution still appears similar in all cases. Large fluctuations persist with a time scale longer than for the case $G = 5$ due to the gain narrowing of the Stokes field. At larger input intensities and hence larger values of G, the temporal evolution for $\Gamma T_t = 1$ and 10 undergoes a qualitative change signified by reduced fluctuations and the appearance of "dispersive" looking features (which I will refer to as "phase-waves" and whose origin will be explained in the analysis that follows). For $\Gamma T_t = 100$ the output still appears noisy, with large fluctuations and with none of the "dispersive" looking features that appear for the other two values of ΓT_t. At still larger laser intensities ($G = 200$), the output intensity for $\Gamma T_t = 1$ is characterized by durations of steady output separated by phase waves. These phase waves are more pronounced for the case $\Gamma T_t = 10$ with peak intensities far exceeding the input laser intensity. Phase waves in the output intensity begin to appear among the random fluctuations for $\Gamma T_t = 100$. Note in all three cases the expected value for the SBS reflectivity is approximately the same due to the strong depletion of the laser light which leads to very weak dependence on the amount of noise that initiated the SBS process.
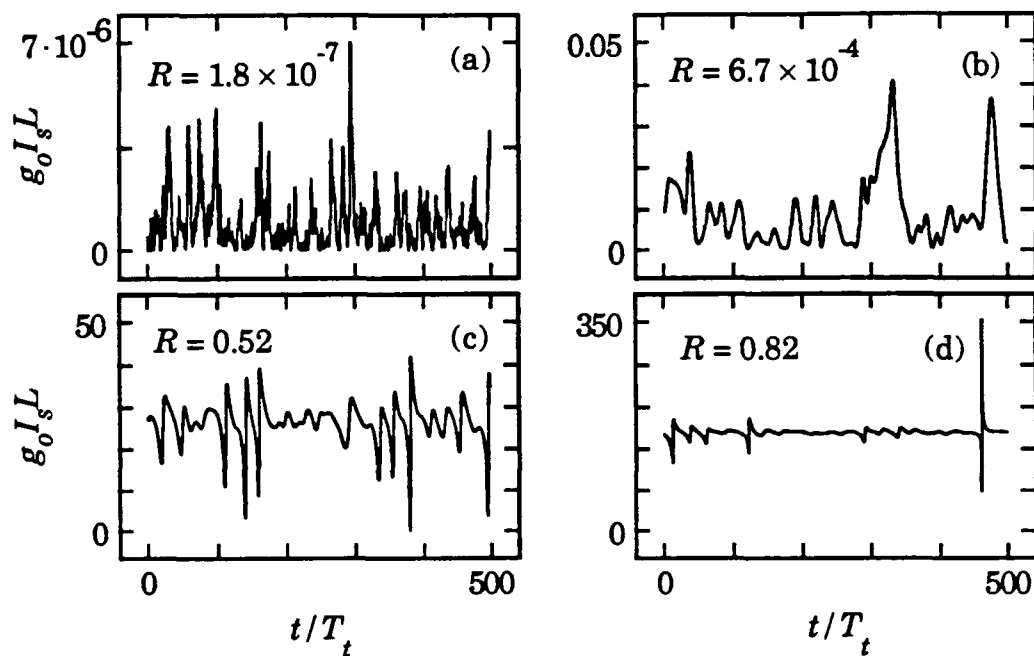
Fig. 2.3 Plots of Stokes output intensity, normalized by $1/g_oL$, as a function of time for the case $\Gamma T_t = 1$ and for single-pass gains of (a) $G = 5$, (b) $G = 15$, (c) $G = 50$, and (d) $G = 200$. The average SBS reflectivity, $R = <I_s>/I_l$, is listed for each case.
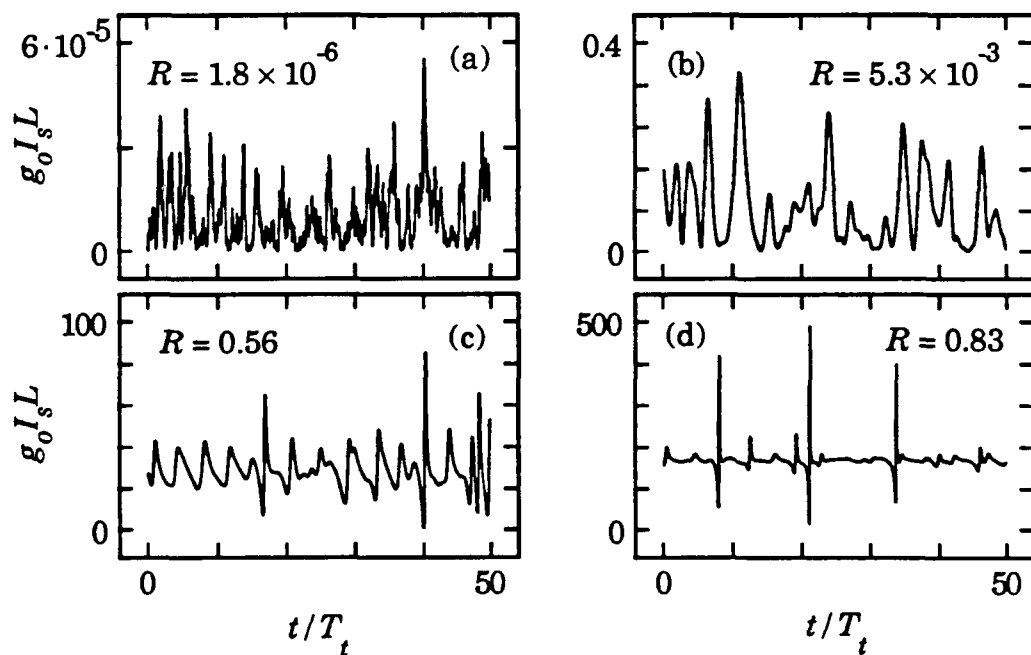
Fig. 2.4 Same as in Fig. 2.3, except $\Gamma T_t = 10$.
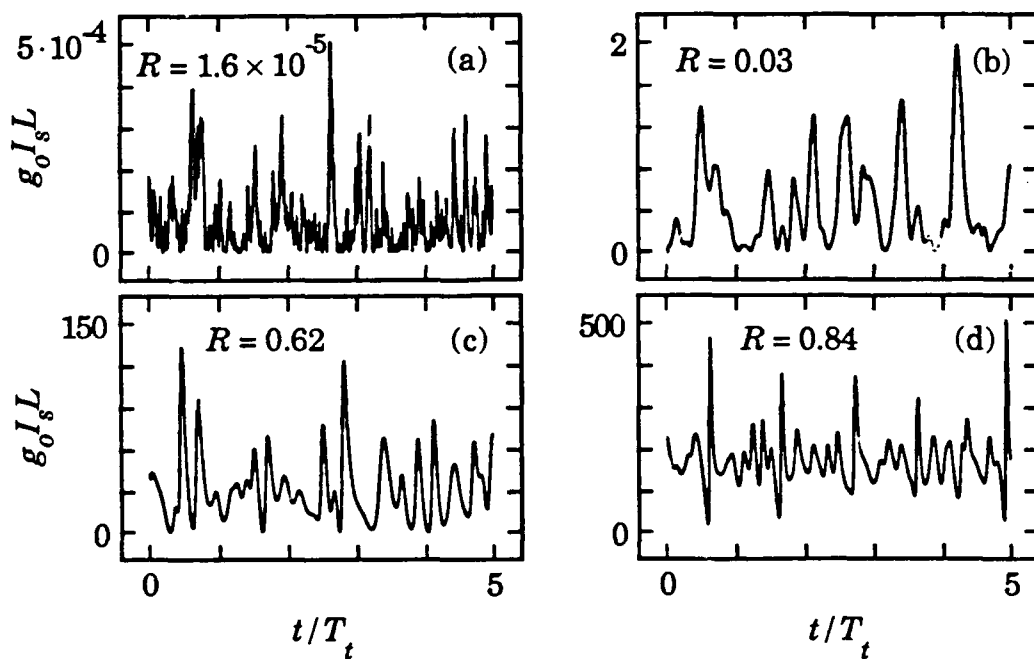
Fig. 2.5 Same as in Fig. 2.3, except $\Gamma T_t = 100$.
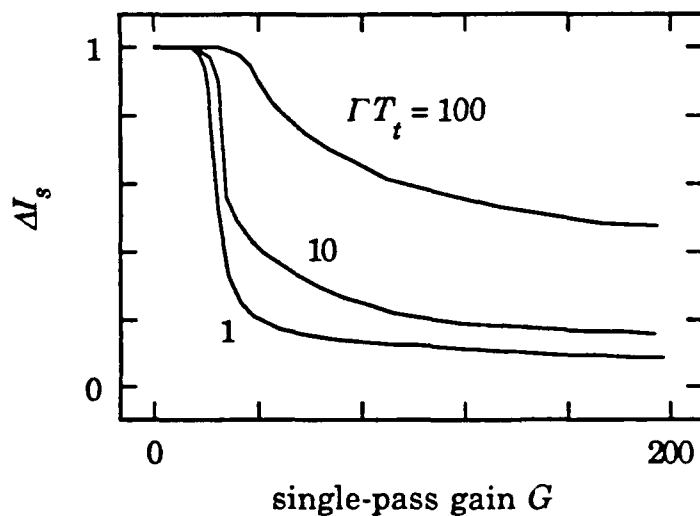
Fig. 2.6 Plot of the normalized standard deviation ΔI_s of the Stokes wave as a function ot the single-pass gain G.

Figure (2.6) shows a plot of the relative fluctuations ΔI_s [Eq. (2.23)] of the Stokes intensity as a function of the single-pass gain G for the three cases ΓT_t = 1, 10, and 100. As seen from the numerical simulations, the relative fluctuations decrease rapidly to zero with increasing values of G for smaller values of ΓT_t. However, large fluctuations persist for large values of ΓT_t even under conditions such that the Stokes field is strongly depleting the laser field. This behavior can be understood by noting that the region in which the laser is most strongly depleted is roughly within a gain length L/G of the front end of the Brillouin medium ($0 < z < L/G$), since this is where the Stokes field is largest. Figure 2.7 gives a schematic illustration of the SBS process in the regime of strong depletion and shows the expected value of the laser intensity distribution. If the Stokes seed generates an amplitude noise spike of temporal width $1/\Gamma$, then the full "pulse" can be better amplified in the pump depletion region ($z < L/G$) as long as the amount of energy contained within the spike is smaller than the energy contained within the laser field in the pump depletion region. If the peak intensity of the spike is roughly given by I_l, then the condition for amplification of the spike is simply that its length $c/n\Gamma$ be smaller than the length of the depletion region. Thus, the condition for observation of large fluctuations in the regime of strong pump depletion is given by the inequality $\Gamma T_t > G$. The rapid decay in the magnitude of the relative fluctuations for small values of ΓT_t explains why fluctuations are typically not observed in focused geometries with a Fresnel number equal to unity. The value of ΓT_t for CS_2 is approximately equal to $0.02L$
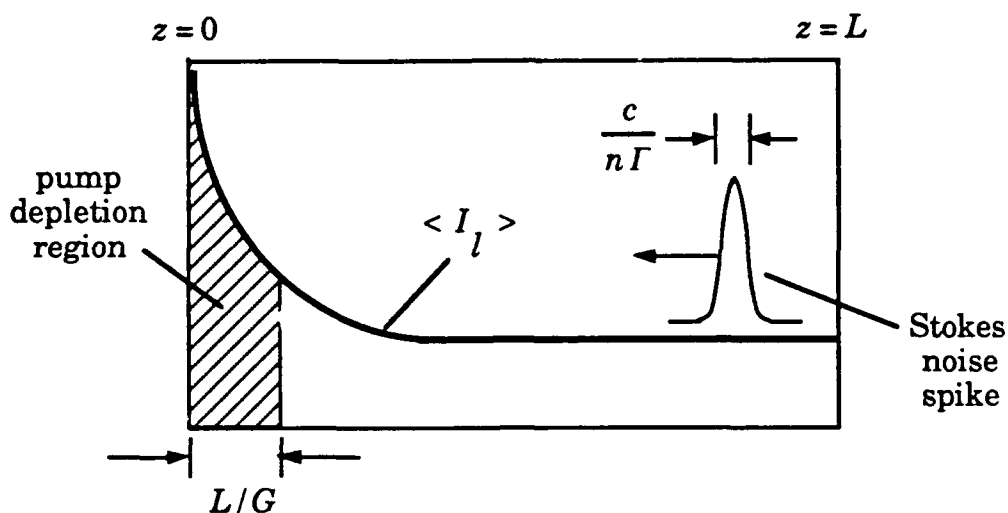
Fig. 2.7 Schematic drawing of the SBS interaction that illustrates how fluctuations of the Stokes light can persist under conditions of strong pump-wave depletion. The Stokes noise spike will be amplified if the energy in the spike at $z = 0$ is less than the energy that can be supplied by the pump wave in the depletion region.

at a laser frequency of 0.53 μm,[2] where L is the length of the interaction region in centimeters; in typical focused geometries, L is less than 10 cm which corresponds to a value of ΓT_t which is still considerably less than one.

Phase waves have been observed experimentally using a pulsed-laser input by Vasil'ev et al.,[15] Basov et al.[16] and by Dianov et al.[6] in a single-mode optical fiber. The origin of phase waves can be attributed to a phase fluctuation that occurs in the Stokes field near $z = L$. As this phase fluctuation propagates towards $z = 0$, the Stokes intensity experiences a sharp decrease followed by sharp spike which leads to its dispersive shape. Figure 2.8(a) is a plot of the phase of Stokes field at $z = 0$ as a function of time for the case $G = 200$ and $\Gamma T_t = 10$ and Fig. 2.8(b)
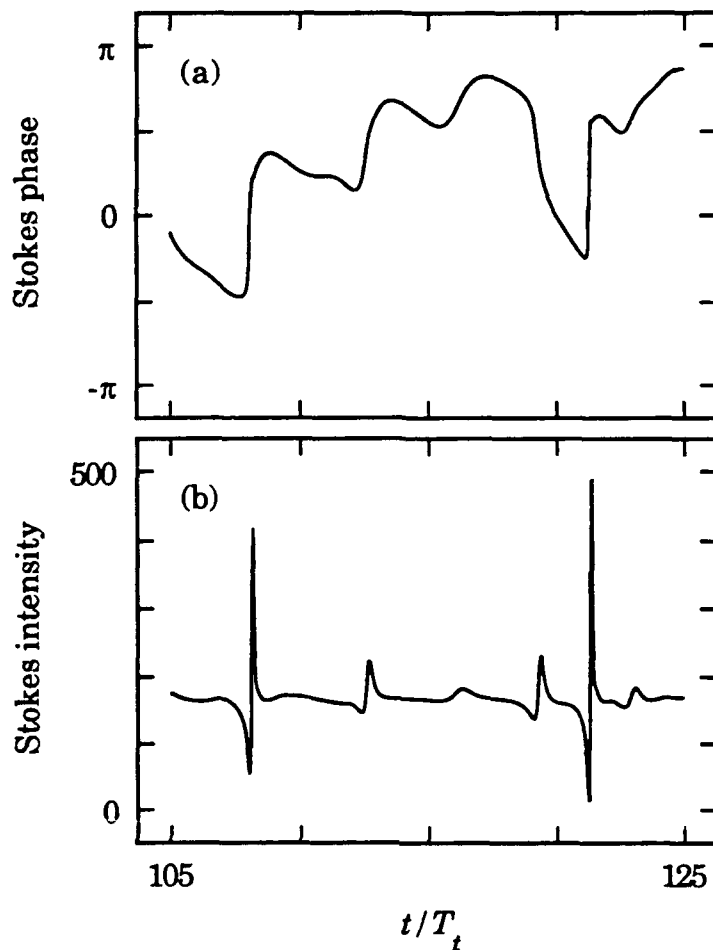
Fig. 2.8 Temporal evolution of (a) the phase of the Stokes field and (b) the intensity $(g_o I_s L)$ of the Stokes field for the case $G = 200$ and $\Gamma T_t = 10$. Sudden changes in phase are accompanied by dispersive-looking spikes in the Stokes intensity.

is the corresponding intensity. Whenever the phase of the Stokes field undergoes a relatively abrupt change, a dispersive looking feature appears in the intensity. Also note that the larger the change in phase, the larger the magnitude of the intensity spike. There are three requirements that must be satisfied for a strong phase wave to occur in SBS: 1) the phonon lifetime must be shorter than the transit time of light through the interaction region, 2) the single-pass gain G must be large

enough such that the pump beam is strongly depleted, and 3) the single-pass gain G must be larger than the ratio of the transit time to the phonon lifetime.

These points are best illustrated by considering the localized model for the initiation of SBS in which the interaction is separated into two regions such that in the region $L - l < z < L$ (where $l = L/G$ is the gain length) spontaneous Brillouin scattering dominates and provides the Stokes seed to be amplified in the remainder of the medium ($z < L - l \approx L$) for which SBS dominates. An expression for this spontaneous Stokes field is given by formally integrating the equation (2.15) for ρ in the long-time limit and neglecting the term which contributes to SBS and substituting this expression into the Eq. (2.14b) for the Stokes field. The solution for the Stokes field at $z = L - l$ is then given by

$$E_s(L-l,\tau) = -i\kappa E_l \int_{L-l}^{L} dz' \int_{-\infty}^{\tau} d\tau' \, f^*(z',\tau') \, e^{-\frac{\Gamma}{2}(\tau-\tau')} \, , \qquad (2.28)$$

where $\tau = t - nz/c$ is the local time variable. From this expression one can see that the spontaneous Stokes seed undergoes phase and amplitude fluctuations on a time scale comparable to its phonon lifetime. In order for phase waves to occur, the condition that the single-pass gain G be sufficiently large such that the Stokes field is depleting the pump field, stems from the need for the Stokes output to be relatively insensitive to the amplitude fluctuations of the Stokes seed. However, the additional condition $G > \Gamma T_t$ must also be imposed as explained above. If

the Stokes seed is now assumed to undergo nearly a π-phase change then, as it propagates towards $z = 0$, the phase change reverses the usual flow of energy from the laser to the Stokes field for a time $1/\Gamma$. The Stokes field that immediately follows this phase fluctuation experiences gain from a *repleted* pump field which leads subsequently to a sharp spike in the Stokes output. Thus, the condition that $\Gamma T_t > 1$ must be satisfied for the generation of the phase wave since an important feature of this process is that the phase of the density which initiates the Stokes seed must a have different phase than the phase of the density encountered by the phase wave as it propagates through the medium creating the reverse flow of energy to the laser field. However, in the limit which $\Gamma T_t < 1$ the density throughout the medium has a homogeneous phase distribution inhibiting the growth of the phase wave.

Appendix 2.1 Derivation of the value of Q

In order to determine the value of the parameter Q which characterizes the strength of the fluctuating noise source $f(z,t)$, we start with the acoustic wave equation (2.4) and assume that no optical fields are present in the medium. The equation of motion for the amplitude of the component of the density variation $\tilde{\rho}(z,t)$ which has a wavevector amplitude equal to q is given by

$$\frac{\partial^2 \tilde{\rho}_q}{\partial t^2} + \Gamma \frac{\partial \tilde{\rho}_q}{\partial t} + \Omega^2 \tilde{\rho}_q = \tilde{f}_q \ , \qquad (A2.1)$$

where

$$\tilde{\rho}_q(t) = \frac{1}{L}\int_L dz\,\tilde{\rho}(z,t)e^{-iqz} \quad , \tag{A2.2}$$

and

$$\tilde{f}_q(t) = \frac{1}{L}\int_L dz\,\tilde{f}(z,t)e^{-iqz} \quad , \tag{A2.3}$$

where the length of the medium has been assumed to be much greater than the acoustic wavelength $2\pi/q$. The complex representations are introduced such that

$$\tilde{\rho}_q(z,t) = \tfrac{1}{2}\rho_q(z,t)\,e^{-i\Omega t} + c.c. \tag{A2.4a}$$

and

$$\tilde{f}_q(z,t) = \tfrac{1}{2}f_q(z,t)\,e^{-i\Omega t} + c.c. \tag{A2.4b}$$

Equation (A2.4a) is substituted into Eq. (A2.1) and the SVEA is made which yields the following equation of motion for the complex amplitude $\tilde{\rho}_q(t)$

$$\frac{\partial\rho_q}{\partial t} + \frac{\Gamma}{2}\rho_q(t) = f_q(t) \quad . \tag{A2.5}$$

Formally integrating Eq. (A2.5) yields

$$\rho_q(t) = \rho_q(0)\, e^{-\frac{\Gamma}{2}t} + \int_0^t dt'\, f_q(t')\, e^{-\frac{\Gamma}{2}(t-t')} \ . \qquad (A2.6)$$

The energy density for an acoustic travelling plane wave is[17]

$$<u> = \frac{v^2}{\rho_o} < \tilde{\rho}_q^2 > = \frac{v^2}{2\rho_o} < \rho_q^2 > \ . \qquad (A2.7)$$

In the long-time limit ($t \gg 2/\Gamma$), the first term on the RHS of Eq. (A2.6) can be neglected in which case the total energy in mode q is given by

$$\begin{aligned}
E_q &= \int dV <u> \\
&= \frac{v^2}{2\rho_o} \int dV < \rho_q(t)\rho_q^*(t) > \\
&= \frac{v^2}{2\rho_o} \left(\frac{Q}{\Gamma L}\right) A L \\
&= \frac{v^2 Q A}{2\rho_o \Gamma} \qquad (A2.8)
\end{aligned}$$

where A is the cross-sectional area of the acoustic wave. According to the equipartition theorem a value of $k_B T$ is assigned to the energy in each mode in thermal equilibrium where k_B is Boltzman's constant. Equating Eq. (A2.8) with the value of $k_B T$ and solving for Q yields the following expression

$$Q = \frac{2k_B T \rho_o \Gamma}{v^2 A} \ . \qquad (A2.9)$$

This is the same result as that reached by Boyd *et al.*[4] A quantum mechanical treatment[18] of the phonon field yields a similar result in which case $k_B T$ is replaced by $(\bar{n} + 1)\hbar\Omega$ where $\bar{n} = (e^{\hbar\Omega/k_B T} - 1)^{-1}$ is the phonon occupation number. At room temperature $\hbar\Omega \ll k_B T$ in which case the classical result for Q is nearly equal to the quantum mechanical result.

1. R. Chiao, Ph. D Thesis, "Brillouin Scattering and Coherent Phonon Generation," Massachusetts Institute of Technology, Cambridge, Massachusetts (1965).

2. W. Kaiser and M. Maier, "Stimulated Rayleigh, Brillouin and Raman Spectroscopy," in *Laser Handbook*, edited by F. T. Arecchi and E. O. Schulz-Dubois (North Holland, Amsterdam, 1972).

3. B. Ya. Zel'dovich, N. F. Pilipetsky, and V. V. Shkunov, *Principles of Phase Conjugation* (Springer-Verlag, Berlin, 1985).

4. R. W. Boyd, K. Rzazewski, and P. Narum, "Noise initiation of stimulated Brillouin scattering," to be published (1990).

5. S. M. Wandzura, "Stimulated scattering does not have a staedy-state," paper MC3 in CLEO Technical digest, 1988.

6. E. M. Dianov, A. Ya. Karasik, A. V. Lutchnokov, A. N. Pilipetskii, "Saturation effects at backward-stimulated scattering in the single-mode interaction," Opt. and Quantum Electron. 21, 381 (1989).

7. F. A. Hopf, "Phase-wave fluctuations in superfluorescence," Phys. Rev. A 20, 2064 (1979).

8. K. Druhl, R. G. Wenzel, and J. L. Carlsten, "Observation of solitons in stimulated Raman scattering," Phys. Rev. Lett. 51, 1171 (1983).

9. J. C. Englund, C. M. Bowden, "Spontaneous generation of Raman solitons from quantum noise," Phys. Rev. Lett. 57, 2661 (1986).

10. D. Polder, M. F. H. Schuurmans, and Q. H. F. Vrehen, "Superfluorescence: Quantum-mechanical derivation of Maxwell-Bloch description with fluctuating field source," Phys. Rev. A 19, 1192 (1979).

11. M. G. Raymer and J. Mostowski, "Stimulated Raman scattering: Unified treatment of spontaneous initiation and spatial propagation," Phys. Rev. A **24**, 1980 (1983).

12. *Handbook of Mathematical Functions*, edited by M. Abramowitz and I. A. Stegun, (Dover, New York, 1972) pp. 377.

13. K. Rzazewski, M. Lewenstein, and M. G. Raymer, "Statistics of stimulated Stokes pulse energies in the steady-state regime," Opt. Commun. **43**, 451 (1982).

14. W. H. Press, B. P. Flannery, S. A. Teukolsky, and W. T. Vetterling, *Numerical Recipes*, (Cambridge, Cambridge, 1986) pp. 202.

15. M. V. Vasil'ev, A. L. Gyulameran, A. V. Mamaev, V. V. Ragul'skii, P. M. Semenov, and V. G. Sidorovich, "Recording of phase fluctuations stimulated scattered light," JETP Lett. **31**, 634 (1980).

16. N. G. Basov, I. G. Zubarev, A. B. Mironov, S. I. Mikhallov, and A. Yu. Okulov, "Phase fluctuations of the Stokes wave produced as a result of stimulated scattering of light," JETP Lett. **31**, 645 (1980).

17. L. D. Landau and E. M. Lifshitz, *Fluid Mechanics* (Pergamon, Oxford, 1959) Eq. 64.1..

18. K. Rzazewski, unpublished (1989).

Chapter 3
Experimental Study of Stimulated Brillouin Scattering in an Optical Fiber

In many materials, SBS is the dominant steady-state nonlinear optical process.[1] The first reported experimental observation of stimulated Brillouin scattering was by Chiao, *et al.*[2] in quartz. However, most studies of SBS have been performed in liquids and gases in a focused geometry with high energy laser pulses.[1] The first observation of SBS in an optical fiber was by Ippen and Stolen[3] with 600 ns laser pulses. Since then, absorption losses have been greatly reduced and optical fibers have lent themselves easily to the generation of SBS under continuous-wave (CW) excitation with milliwatt power levels.[4] Several workers have observed large fluctuations in the Stokes signal in single-mode fibers, these fluctuations were unexplained[5] or, as in the experiment of Ippen and Stolen,[3] were believed to be due to be relaxation oscillations. A possible explanation is that these observed fluctuations were the result of the spontaneous initiation of SBS discussed in Chapter 2. In a very recent experiment in a single-mode optical fiber with 1 μs and 200 ns laser pulses, Dianov *et al*[6] demonstrated that fluctuations can exist in the Stokes output and attributed them to the thermal

initiation of SBS. Although fluctuations in the Stokes signal have been observed in a focused geometry under pulsed conditions,[7] a single-mode fiber lends itself much more readily to the observation of fluctuations due to the large values of the product of the spontaneous Brillouin linewidth and the transit time ΓT_t that can be attained. For large values of ΓT_t, large fluctuations in the Stokes intensity should be observable far above the threshold for SBS (see Section 2.3).

In this Chapter, experimental studies of SBS in a single-mode fiber with CW excitation are described in which many of the theoretical predictions made in Chapter 2 regarding the statistical nature of the Stokes light are addressed. Section 3.1 describes the direct measurement of the gain factor g_o for the optical fibers used in the experiments. In Section 3.2 the threshold for SBS is characterized by measuring the Stokes output power as a function of the input laser power. In accordance with theoretical predictions, the value of the threshold single-pass gain is found to be considerably lower than the value which would be measured in a focused geometry. In Section 3.3, the temporal behavior of the Stokes output intensity is described. The Stokes intensity is found to be extremely noisy with nearly 100% fluctuations. In Section 3.4, the measurements of the spectrum of the Stokes light as a function of input intensity are described and the spectrum is found to exhibit gain narrowing.

Section 3.1 Measurement of the SBS Gain Factor

In order to obtain an accurate estimate of the single-pass gain G for the Stokes waves, the gain factor g_0 for the optical fiber was measured. A pump-probe experiment is performed in which the transmitted power of the probe beam through a known length of fiber was measured for a fixed value of the pump laser power. By measuring the total gain experienced by the probe beam, an accurate estimate of the gain factor can be made. The optical fibers used in the experiment were manufactured by Corning and are composed of silica with a 3 mol % GeO_2-doped core. The fibers are step-indexed with a core diameter equal to 3.6 μm. In all the experiments fiber couplers were used with 10× objectives to couple light into the fibers.

The experiment to measure the gain factor was performed with a 10-meter-long fiber since for this length the absorption losses within the fiber could be neglected. The experimental set-up is shown in Fig. 1.
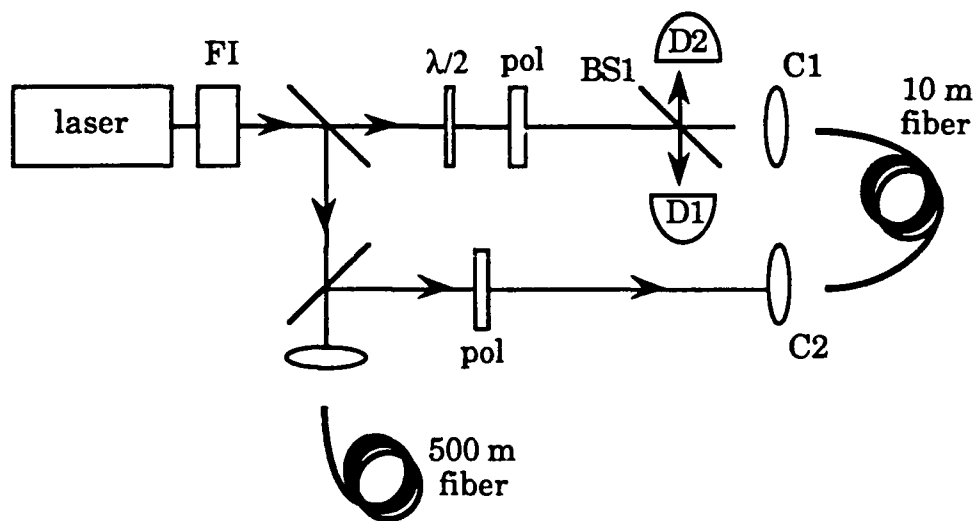
Fig. 3.1 Experimental set-up used to measure the SBS gain factor of the optical fiber.

Light from a Coherent Innova argon-ion laser operating in a single longitudinal mode at a wavelength of 514.5 nm is sent through a Faraday isolator in order to keep Stokes light from reflecting off the laser mirrors and back into the fiber. The light is then split into two beams by a 50/50 dielectric beamsplitter with each beam containing approximately 700 mW of optical power. One of the beams, which served as the pump beam, is passed through a half-wave plate and a polarizing beamsplitter to allow the pump power to the fiber to be varied. The pump beam is then launched by coupler C1 into the 10 meter-long fiber, and the power of the pump beam inside the fiber is estimated by measuring the power through the coupler (C2) at the opposite end of the fiber with a calibrated UDT power meter and calibrating this measurement with large area photodetector (D1) which monitors the input beam power via reflection from the pellicle beamsplitter (BS1). The transmitted pump beam is found to contain 80% of its power in one polarization direction. The Stokes probe beam is generated by launching the other beam into the 500 meter long fiber which generates a Stokes signal. Under conditions of normal SBS, the spectrum of the Stokes signal would be the gain-narrowed spontaneous Brillouin spectrum. However, the cleaved ends of the fiber can form a low-Q cavity due to the weak reflection (~ 4%) at each endface. In the presence of the very high gain, the fiber can serve as a Brillouin oscillator and the Stokes output spectrum becomes essentially as narrow as the linewidth of the laser (< 2 MHz). This effect will be discussed in greater detail in Chapter 4 which considers SBS in the presence of feedback. By using this Brillouin oscillator, a Stokes

signal wave is generated with a very narrow spectral linewidth and with a frequency that is at the peak of the Brillouin gain spectrum. The Stokes signal wave is then passed through a polarizer which is rotated such that the transmitted light is polarized parallel to the polarization direction along which the transmitted pump field contains 80% of its power. By slightly misaligning the coupler C2, the Stokes probe power inside the fiber could be varied.

The power of the Stokes probe wave was monitored via reflection from the beamsplitter BS1 with a large area photodetector D2. By measuring the power of the probe beam with the pump beam blocked, and then unblocked, the total gain of the probe due to SBS could be determined. The total gain for the probe wave was measured for two different input pump powers (130 mW and 200 mW inside the fiber) and for two different input probe powers (28 μW and 70 μW inside the fiber). The total gain e^G for a particular pump and probe power is then given by the signal at D2 with the pump unblocked, divided by the signal at D2 with the pump blocked. From this quantity the value of G is determined and the value for the gain factor is given simply by the relation

$$g_o = \frac{0.8GA}{P_l L} \qquad\qquad (3.1)$$

where P_l is the laser power inside the fiber, $A = 1 \times 10^{-11}$ m^2 is the area of the fiber core, $L = 10$ m is the length of the fiber, and the factor of 0.8 in the numerator takes into account the fact that only 80% of the light of transmitted pump wave is polarized parallel to input Stokes field. The

final value for g_o is determined by averaging the four measured values and is given by

$$g_o = (2.5 \pm 0.1) \times 10^{-11} \, \mathrm{m} \, / \, \mathrm{W} \, .$$ (3.2)

This value is close to the theoretically predicted value of 5×10^{-11} m/W for bulk silica.[6]

Section 3.2 Measurement of SBS Threshold

The threshold single-pass gain G_{th} for SBS can be defined as the value of G for which the output Stokes intensity is one percent of the input laser intensity. Using the high-gain ($G \gg 1$) expression for the expectation value for the Stokes intensity [Eq. (2.29)], G_{th} is then given by the following transcendental equation

$$G_{th}^{3/2} \, e^{-G_{th}} = \frac{100\sigma}{\sqrt{\pi}} \, .$$ (3.3)

where σ is the fraction of laser light that is spontaneously scattered into the Stokes field and is given in terms of fundamental parameters by Eq. (2.27). Boyd, et al[9] predict that the threshold single-pass gain for SBS is not a universal value but varies for different materials and for different laser frequencies. The origin of this variation is due to the varying amount of spontaneous Brillouin scattering that initiates the SBS process for different materials. However, since the threshold single-pass gain G_{th} varies approximately with the natural log of the strength σ
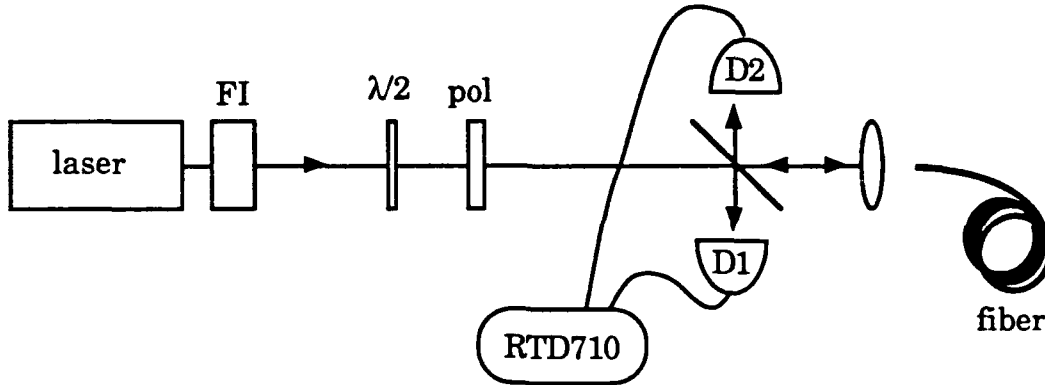
Fig. 3.2 Experimental set-up used to measure the Stokes output power as a function of the laser input power.

of the spontaneous scattering, for most materials the threshold value G_{th} is predicted to be in the range between 20 and 25 in which the interaction region is of a Fresnel number equal to unity, i.e., $L/A \approx 1/\lambda_l$.[10] For optical fibers, the situation can be considerably different. Due to the guiding nature of the fiber, a single-mode interaction is maintained over a much longer length than is generally the case for an interaction region of Fresnel number equal to unity. Thus, the strength σ of the spontaneous scattering can be several orders of magnitude larger than the value which would be expected in a focused geometry, leading to a threshold single-pass gain $G_{th} < 10$ for fiber lengths of several kilometers.

The experimental set-up used to measure the threshold for SBS is shown in Fig. 3.2. The pump beam was coupled into the fiber and, with the pellicle beamsplitter BS1, the input pump power and output Stokes power could be measured with large-area photodetectors D1 and D2, respectively. *The coupling efficiency into the fiber was determined by measuring (at low input powers) the power of the light transmitted though the fiber*, multiplying this value by $e^{\alpha L}$, where α is the absorption

factor for the fiber, and dividing it by the power incident upon the fiber coupler. The signals from detectors D1 and D2 were sent to two separate channels of a Tektronix RTD710 transient digitizer. By setting the total sample interval to 10 sec and by manually rotating the half-wave plate 90° during time interval, the full range of values for Stokes power versus the incident power could then be generated. The measurements were performed for two different lengths of fiber (100 m and 500 m) and at two different laser wavelengths: the single-mode argon operating at 0.5145 μm and a Coherent 669-21 frequency-stabilized single-mode ring dye laser operating at 0.5890 μm. With the single-mode argon-ion laser, up to 400 mW of laser power could be launched into the fiber, and with the dye laser, up to 120 mW could be launched.

Due to the presence of high Brillouin gain inside the fiber, even small reflections from the endfaces of the fiber can result in the formation of a Brillouin oscillator. The characteristics of the Stokes output under these conditions can be dramatically different than would be expected from normal SBS (see Chapter 4).[6,10] In order to prevent the fiber from forming a Brillouin oscillator, the reflections from each end of the fiber were minimized. The back end of the fiber was placed in index matching fluid and the front end was cleaved in such a manner that the Stokes output beam and the specular reflection of the laser from the front end of the fiber were well separated after passing back through the fiber coupler. This procedure insured that the normal to the front endface was not along the axis of the fiber minimizing the amount of Stokes light reflected back into the fiber.
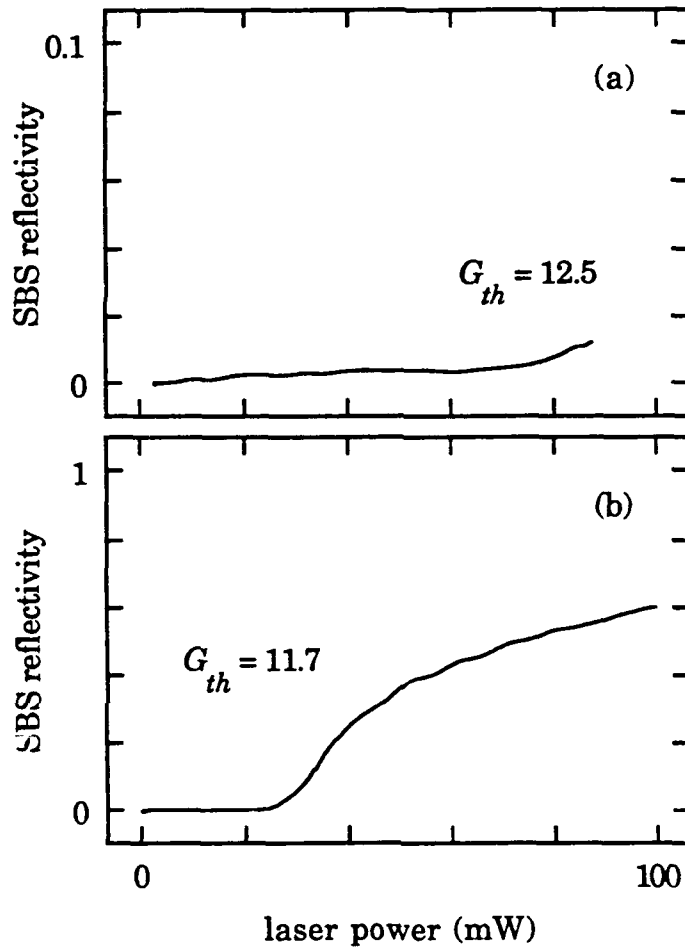
Fig. 3.3 Experimental results for the SBS reflectivity as a function of the input laser power at a wavelength λ_l = 0.5890 µm for the (a) 100-meter-long fiber and the (b) 500-meter-long fiber.
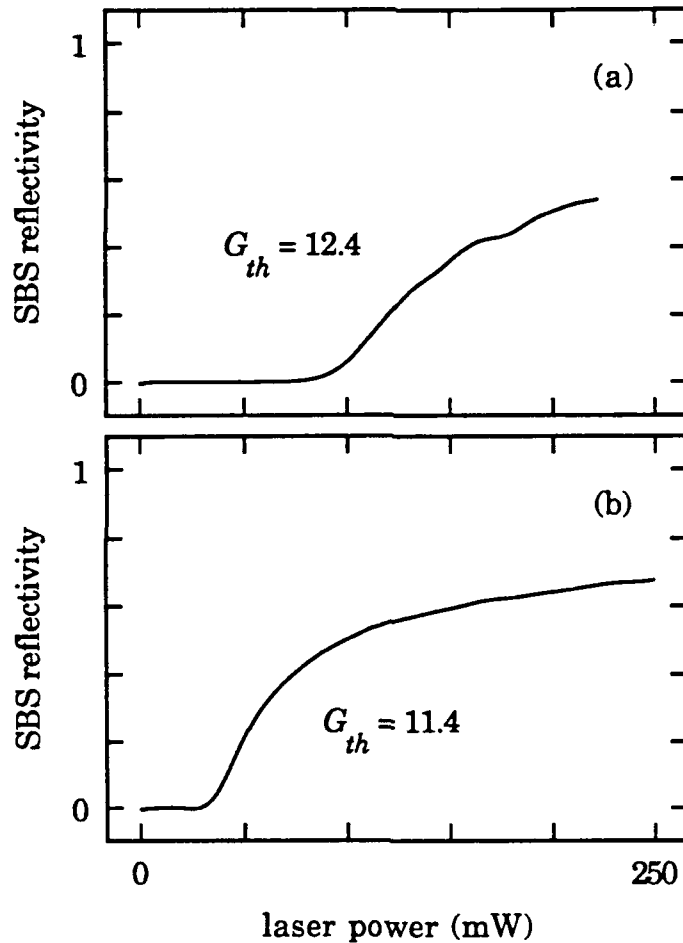
Fig. 3.4 Experimental results for the SBS reflectivity as a function of the input laser power at a wavelength λ_l = 0.5145 µm for the (a) 100 meter-long fiber and the (b) 500 meter-long fiber.

Figures 3.3 and 3.4 are plots of the SBS reflectivity (output Stokes power divided by the input laser power) as a function of the input laser power for the dye laser and the argon laser, respectively. Figures 3.3(a) and 3.4(a) show the results for the case of the 100-m-long fiber and Figs. 3.3(b) and 3.4(b) show the results for the case of the 500-m-long fiber. In all cases the output Stokes light contained approximately 70% of its power in the polarization direction parallel to that of the incident laser.

By assuming that the threshold for SBS occurs when the SBS reflectivity is equal to 1%, and by using the measured value for g_o, an estimate for the threshold single-pass gain for each case can be made with the following expression

$$G_{th} = 0.7 g_o P_{th} L_{eff} / A ,$$ (3.4)

where the factor of 0.7 takes into account the slight depolarization of the laser field inside the fiber, P_{th} is the threshold laser power corresponding to an SBS reflectivity of 1%, and $L_{eff} = (1 - e^{-\alpha L})/\alpha$ is the effective interaction length[1] which takes into account linear optical absorption of the laser and Stokes fields inside the fiber. In the limit where the total absorption pathlength is large ($\alpha L \gg 1$), L_{eff} is simply

	@ 0.5145 μm	@ 0.5890 μm
α	4.38 km^{-1}	3.32 km^{-1}
L_{eff} (100 m)	81 m	85 m
ΓT_t (100 m)	453	360
L_{eff} (500 m)	203 m	269 m
ΓT_t (500 m)	1133	1139

Table 3.1 List of the effective interaction length and the ratio of the transit time to the phonon lifetime for the 100-meter-long and 500-meter-long optical fibers at the two laser wavelengths used in the experiments.

the Beer's length α^{-1}. Table 3.1 lists, for both the laser wavelengths (0.5145 μm and 0.5890 μm), the absorption coefficient α and the effective length L_{eff} for the 100-m and 500-m-long fibers. In calculating the value for ΓT_t, the effective length L_{eff} of the fiber and the experimentally determined value for the Stokes linewidth at 0.5890 μm (see Section 3.4) were assumed. (The value of the linewidth at 0.5145 μm was extrapolated from the ω_l^2 dependence of the linewidth.)

The corresponding values for G_{th} in all four cases are shown in Figs. 3.3 and 3.4. An estimate for the theoretical value of G_{th} can be made using Eq. (3.3) and substituting the appropriate values for σ. The predicted values for G_{th} with the 100-m and 500-m-long fibers is: G_{th} = 12.6 and G_{th} = 11.4, respectively at 0.5890 μm, and G_{th} = 12.1 and G_{th} = 11, respectively at 0.5145 μm. [In determining the magnitude of σ for each case, the values for ΓT_t from Table 3.1 are used.] Thus, the experimentally measured values for the threshold single-pass gain confirms the prediction that the threshold single-pass gain for SBS in an optical fiber can be considerably smaller than the values that would be expected from a geometry with Fresnel number equal to unity.

Section 3.3 Temporal Behavior of the Output Stokes Intensity

The experimental set-up used to observe the temporal behavior of the Stokes output intensity is similar to the set-up shown in Fig. 3.2, except that the large-area detector D2 is replaced by a fast photodiode detector with a uniform frequency response from d.c. to 150 MHz. The output from the photodiode is sent to the transient digitizer and a 5 ns interval between sampling points was used in all cases. As explained in the previous Section, care was taken to insure that the reflections from the ends of the fiber were minimized so that the regime of pure single-beam SBS could be studied. The results shown here are only for case of the wavelength 0.5145 μm, since much higher laser powers could be attained with the argon-ion laser than with the dye laser, and the results for similar laser powers were qualitatively the same in both cases. The temporal evolution of the laser over a 5 μs duration is shown in Fig. 3.5 and shows that the laser intensity is indeed quiet over this time interval.
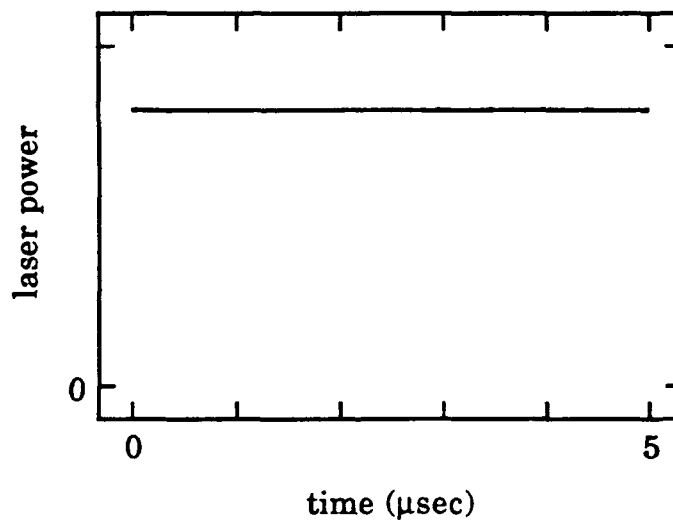
Fig. 3.5 Laser output power is plotted as a function of time.
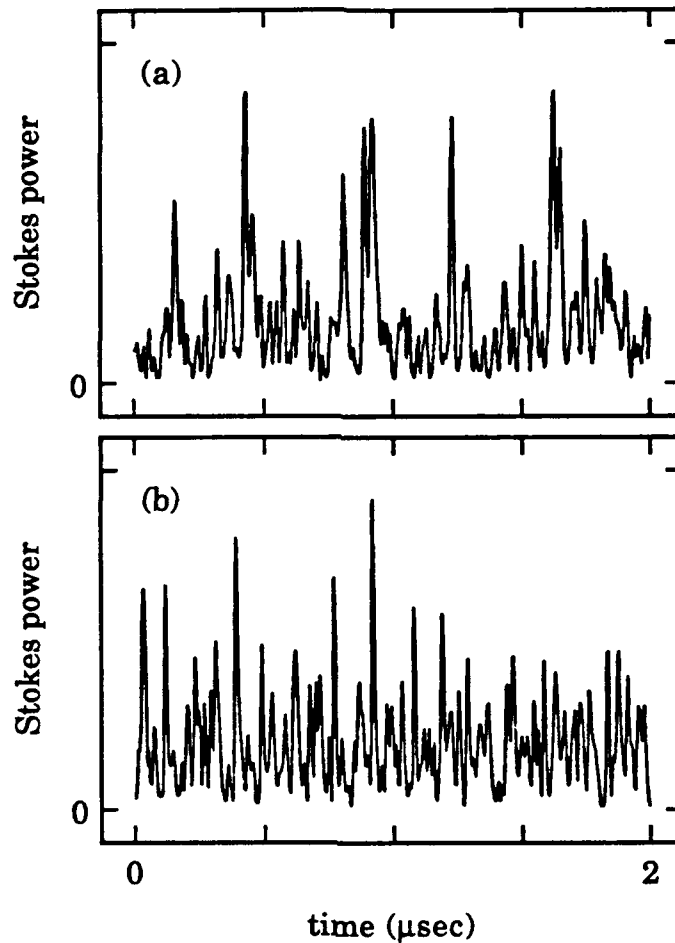
Fig. 3.6 Temporal evolution of Stokes output power for the case of the 100-meter-long fiber for an input laser power of (a) 87 mW and (b) 265 mW.

Figures 3.6 and 3.7 are plots of the temporal evolution of the Stokes power for the 100-meter and 500-meter-long fibers, respectively. Figures 3.6(a) and 3.7(a) show the Stokes output just above threshold, while Figs. 3.6(b) and 3.7(b) show the Stokes output far above threshold. In all cases the Stokes output exhibits the large fluctuations, which is in accordance with theoretical predictions for large values of the product ΓT_t (Section 2.3). The estimated values for ΓT_t for the different fiber lengths and laser wavelengths are listed in Table 3.1.
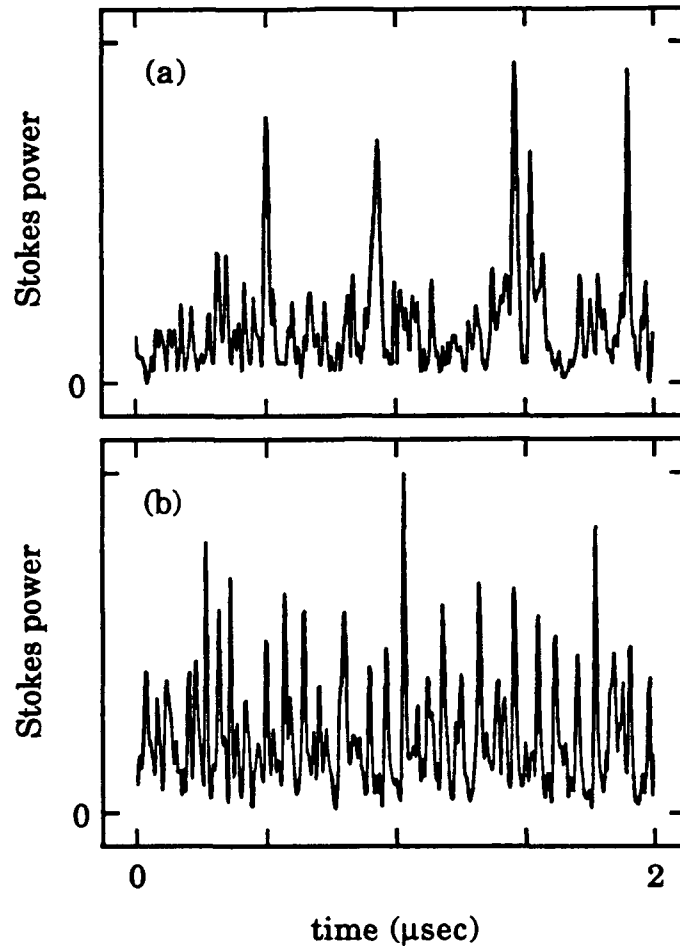
Fig. 3.7 Temporal evolution of Stokes output power for the 500-meter-long fiber an input laser power of (a) 44 mW and (b) 220 mW.

Similar behavior has been observed by Harrison et al.[11] under very similar experimental conditions, but they attribute the source of the fluctuations to the system undergoing deterministic chaos. Their theoretical model assumes that the medium has nonlinear refractive index, and they neglect the stochastic initiation of the SBS process. However, in order for chaotic behavior to occur in their model, the values of the nonlinear-index coefficient and the Brillouin linewidth are required to be several times larger than the measured values.[12] Their

model also predicts that the system undergoes a period-doubling route to chaos as the input laser intensity is increased. In of the none of the experimental data taken by either Harrison *et al.*[12] or myself (in the absence of feedback from the fiber endfaces) was any periodic behavior observed.

Figures 3.8(a) and 3.8(b) are plots of the normalized standard deviation ΔI_s [Eq. (2.22)] of the Stokes intensity as a function of the estimated single-pass gain, G for the 100- and 500-meter-long fibers, respectively. The value of G was estimated from the expression

$$G = 0.7 g_o P_l L / A \qquad (3.5)$$

where the value for L is taken to be the actual length of the fiber. There exists a slight quenching of the fluctuations at higher input powers and in all cases the value of ΔI_s is slightly less than unity. The solid curve represents the result of numerical simulations for the parameters that correspond to the experimental conditions (see Table 3.1) with the inclusion of the depolarization of the Stokes output field. The effect of the depolarization was taken into account by assuming that the statistical nature of the Stokes field is similar to that of a thermal beam. The normalized standard deviation ΔI_{pp} for partially polarized light from a thermal beam is given by the following expression[13]
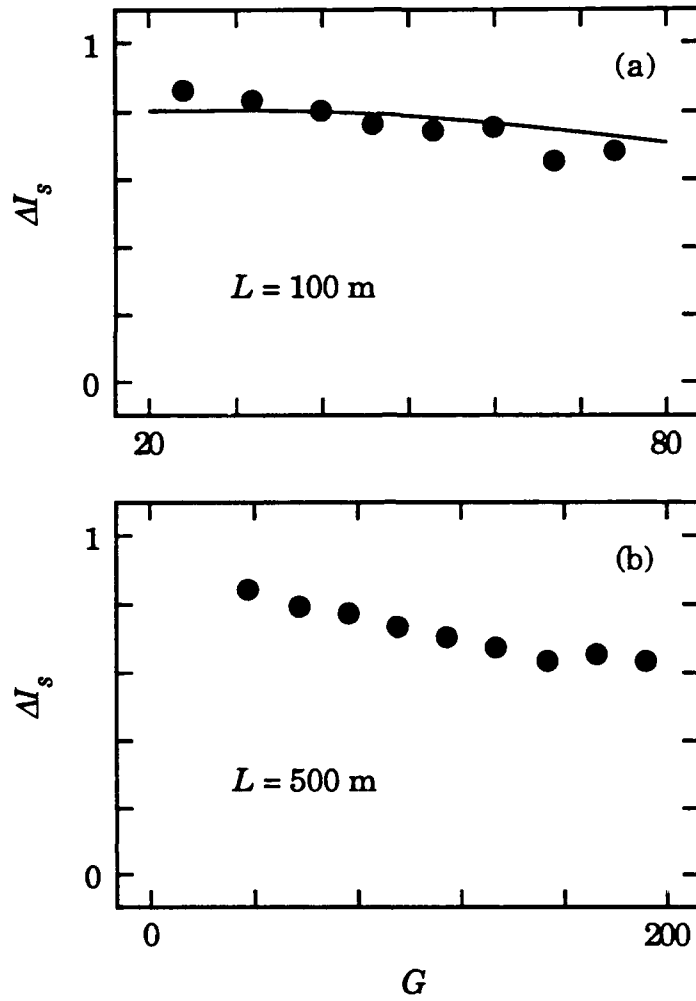
Fig. 3.8   Plot of normalized standard deviation of the experimentally measured Stokes output intensity as a function of the normalized input intensity G for the (a) 100-meter-long fiber and the (b) 500-meter-long fiber.   The solid curve in (a) represents the theoretical prediction.

$$\Delta I_{pp} = \frac{\sqrt{<I_x>^2 + <I_y>^2}}{<I>} \tag{3.6}$$

where I_x and I_y are the intensities of the x and y components of the thermal field, respectively, and $I = I_x + I_y$ is the total intensity.   For the

case in which 70 % of the light is polarized along the x direction, the resulting value for ΔI_{pp} is 0.78. This factor of 0.78 was used to scale the the values of ΔI_s obtained from numerical simulations. The theoretical curve is found to be in reasonable aggreement with experimental data. Obtaining a theoretical curve for the 500 meter-long-fiber would have taken a prohibitive amount of computer time, and thus comparison with theory is not possible in this case.

Section 3.4 Spectrum of Stokes Light

In this Section, the results for the spectrum of the Stokes light measured as a function of the input laser intensity are described. The first measurements of the spontaneous Stokes spectrum in an optical fiber were performed by Thomas, *et al.*[14] At a wavelength of 0.5145 µm and in a pure silica core fiber, they observed the spontaneous spectrum of the light scattered at an angle of 180° to the direction of the laser light
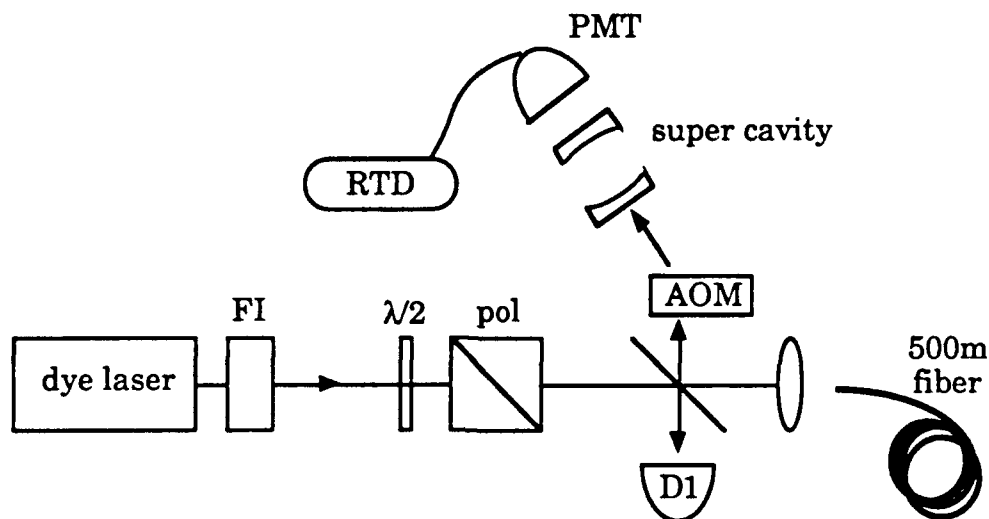
Fig. 3.9 Experimental set-up used for measuring the optical spectrum of the Stokes field.

and measured a value of the Brillouin linewidth equal to 130 MHz. Pump-probe experiments have also been performed to measure the gain spectra for near infrared for fibers of different core profiles and containing various dopants.[15] Various workers have also made careful measurements of the Brillouin frequency shift[4,] and its shift as function of core dopant.[16]

The experimental set-up is shown in Fig. 3.9. For all the spectral measurements, a Coherent 699 frequency-stabilized dye laser was used due to its long term (> 5 s) frequency stability to within 2 MHz. Light from the laser was passed through a Faraday isolator and the laser power to the fiber was varied with the half-wave plate and a polarizer. The Stokes light reflected from the pellicle beamsplitter BS1 was passed through an Isomet acousto-optic modulator model 1205C and the first-order diffracted component was sent into a NRC "super-cavity" scanning Fabry-Perot interferometer. In order to measure the Brillouin frequency shift, the super-cavity model SR-220 was used due to its large free spectral range (100 GHz) and the shift was found to be 35 GHz. In order to perform high resolution measurements on the Brillouin spectral line itself, the longer-length super-cavity (SR-120) was utilized. The model SR-120 possesses a free spectral range of 6 GHz and a finesse greater than 10^4. The scanning rate of the super-cavity was kept at 25 Hz. The acoustic-optic modulator (AOM) served two purposes in the experiment: by modulating the rf signal to the AOM with a frequency generator, sidebands to the carrier frequency could be imposed on the light entering the interferometer which allowed for frequency

calibration of the interferometer; and the AOM isolated the interferometer from the fiber. As the interferometer was scanned, the transmitted light was detected by a cooled Thorn EMI 50 III photomultiplier (PMT). The signal from the PMT was then sent to the RTD710. To achieve well defined spectra, particularly for small Stokes signals, the RTD710 was set to average 128 data, each corresponding to a scan of the super cavity. This averaged data was then read into an PDP-11 microcomputer through an IEEE-4888 interface. The spectrum of the
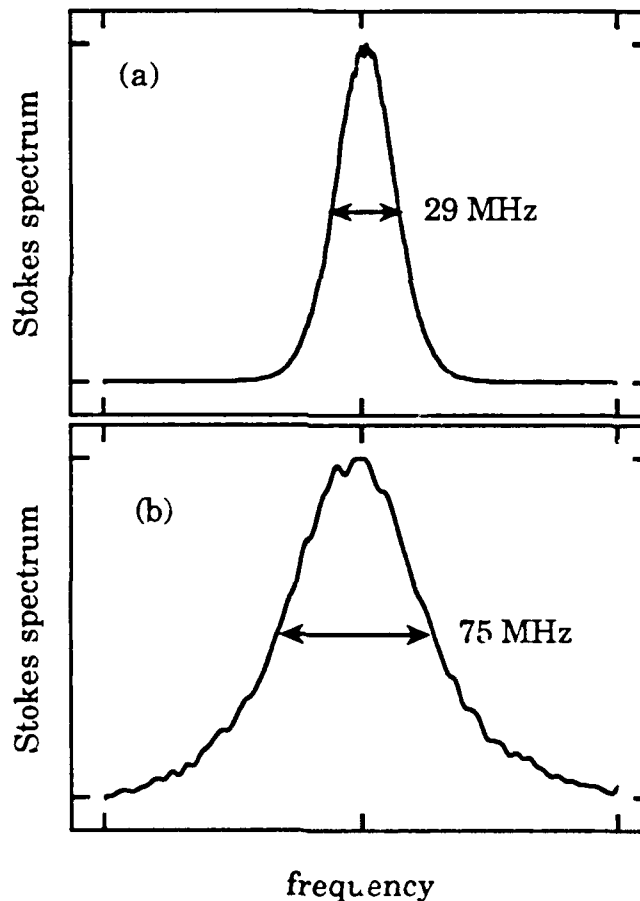
Fig. 3.10 Output Stokes spectrum for an input laser power of (a) 66 mW and (b) 5.8 mW.

Stokes light depends sensitively on the presence of feedback from both the endfaces of the fiber. Thus, as discussed in Section 3.2, reflections from the fiber endfaces were minimized, and the 500-meter-long fiber was used for all the spectral data shown here due to its larger absorption pathlength (Brillouin oscillation is more difficult to achieve with a larger absorption pathlength).

Figures 3.10(a) and 3.10(b) are the Stokes spectra for high (66 mW) and for low (5.8 mW) pump powers, respectively. The gain narrowing at the higher laser power is evident. Figure 3.11 is a plot of the normalized FWHM of the Stokes spectrum as a function of the normalized input intensity G as calculated using Eq. (3.4). The experimental data is given by the solid circles while the solid line denotes the theoretical prediction for the linewidth. The spontaneous linewidth is assumed to be 135 MHz
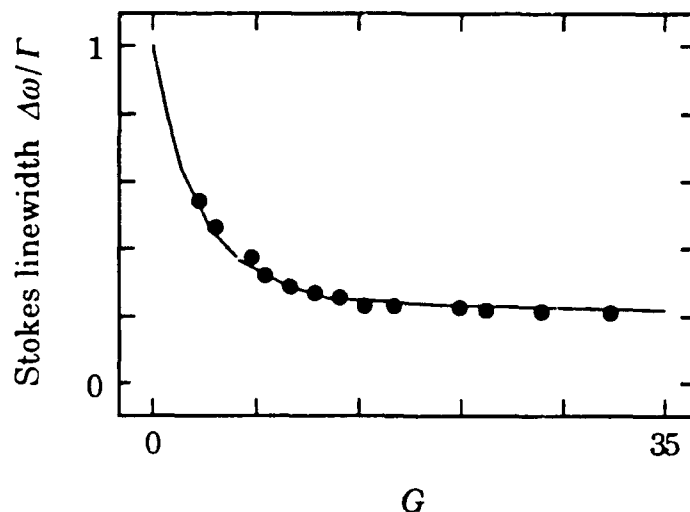
Fig. 3.11 Experimentally measured linewidth of the output Stokes spectrum (solid circles) plotted as a function of the single-pass gain, G. The solid line is the theoretical prediction.

and the single-pass gain G is estimated from the measured value of the gain factor g_o [Eq. (3.2)] and the laser power inside the front end of the fiber. The theoretical prediction for the linewidth for small values of G is given by the FWHM of the lineshape given by Eq. (2.33) and for larger values of G is given by the FWHM of the power spectrum of the numerically integrated times series of the Stokes field. The agreement between theory and experiment is seen to be very good.

1. W. Kaiser and M. Maier, "Stimulated Rayleigh, Brillouin and Raman spectroscopy," in *Laser Handbook*, Vol. 2, edited by F. T. Arecchi and E. O. Schulz-Dubois (North Holland, Amsterdam, 1972).

2. R. Y. Chiao, C. H. Townes, and B. P. Stoicheff, "Stimulated Brillouin scattering and coherent generation of intense hypersonic waves," Phys. Rev. Lett. **12**, 592 (1964).

3. E. P. Ippen and R. H. Stolen, "Stimulated Brillouin scattering in optical fibers," Appl. Phys. Lett. **21**, 539 (1972).

4. N. Usesugi, M. Ikeda, and Y. Sasaki, "Maximum Single frequency input power in along optical fiber determined by stimulated Brillouin scattering," Electron. Lett. **17**, 379 (1981); D. Cotter, "Observation of stimulated Brillouin scattering in low-loss silica fiber at 1.3 μm," Electron. Lett. **18**, 495 (1982).

5. E. A. Kuzin, M. P. Petrov, and B. E. Davydenko, "Phase conjugation in an optical fiber," Opt. and Quant. Electron. **17**, 393 (1985).

6. E. M. Dianov, A. Ya. Karasik, A. V. Lutchnikov, and A. N. Pilipetskii, "Saturation effects at backward-stimulated scattering in the single-mode regime of interaction," Opt. and Quant. Electron. **21**, 381 (1989).

7. V. Bespalov, A. A. Betin, G. A. Pasmanik, and A. A. Shilov, "Observation of transient field oscillations in the radiation of stimulated Mandel'shtam-Brillouin scattering," JETP Lett. **31**, 631 (1980).

8. R. G. Smith, "Optical power handling of low optical fibers as determined by stimulated Raman and Brillouin scattering," Appl. Opt. **11**, 2489 (1972).

9. R. W. Boyd, K. Rzazewski, and P. Narum, "Noise initiation of stimulated Brillouin scattering," to be published (1990).

10. I. Bar-Joseph, A. A. Friesem, E. Lichtman, and R. G. Waarts, "Steady and relaxation oscillations of stimulated Brillouin scattering in single-mode fibers," J. Opt. Soc. Am. B **2**, 1606 (1985).

11. R. G. Harrison, J. S. Uppal, A. Johnstone, and J. V. Moloney, "Evidence of chaotic stimulated Brillouin scattering in optical fibers," Phys. Rev. Lett. **65**, 167 (1990).

12. G. P. Agrawal, *Nonlinear Fiber Optics*, (Academic, San Diego, 1989).

13. R. Loudon, *The Quantum Theory of Light*, (Clarendon Press, Oxford, 1983) Chap 3.

14. P. J. Thomas, N. L. Rowell, H. M. van Driel, and G. I. Stegeman, "Normal acoustic modes and Brillouin scattering in an optical fiber," Phys. Rev. B **19**, 4986 (1979).

15. N. Shibata, R. G. Waarts, and R. P. Braun, "Brillouin-gain spectra for single-mode fibers having pure-silica, GeO_2-doped, and P_2O_5-doped cores," Opt. Lett. **12**, 269 (1987).

16. J. Stone and A. R. Chraplyvy, "Spontaneous Brillouin noise in long-distance high-bandwidth optical-fiber transmission," Electron. Lett. **19**, 275 (1983).

Chapter 4
Stimulated Brillouin Scattering in the Presence of External Feedback

As mentioned in Chapters 2 and 3, an optical system that exhibits gain can serve as an amplifier for the thermal or quantum noise which is inherent in the system. However, as has been shown for the laser, when gain is accompanied by feedback from an optical cavity, the behavior of the system can become dramatically modified. When the gain of the system exceeds the losses of the cavity, the system undergoes a transition from stochastic behavior to one that can be treated in a deterministic fashion. This transition can be understood as the occurrence of an absolute instability in the system. For the case of a laser, an inversion is established within a collection of atoms or molecules, and through the process of stimulated emission, one or more modes of the cavity oscillate. Since gain can also be achieved through nonlinear optical processes (e.g., stimulated Raman scattering, SBS, four-wave mixing), parametric oscillators can be created my introducing feedback to the wave which experiences gain. However, in general, the energy which provides the gain for a parametric oscillator is stored in the pump wave, not in the interacting medium.

Due to the extremely high gain that can be achieved in SBS, several workers have constructed Brillouin oscillators[1] using only a small amount of feedback. Only recently have theoretical studies been undertaken to treat the SBS process in the presence of feedback. Baumgartel *et al.*[2] and Bar-Joseph *et al.*[3] showed that the output intensity of the Stokes wave from a Brillouin oscillator could become temporally unstable and exhibit steady oscillations. Dianov *et al.*[4] studied SBS in the presence of feedback using the full stochastic differential equations and found that the Stokes output intensity loses its stochastic nature at sufficiently high input intensity. However, in both cases[2,3] they studied the temporal behavior of the Stokes output only for short times after the turn-on of the laser field.

In this Chapter, the behavior of SBS in the presence of feedback is investigated. In Section 4.1, the threshold for Brillouin oscillation is determined, and even for the case in which the feedback is weak, the threshold can still be considerably lower than the threshold for usual SBS. The spectrum of the Stokes light is calculated and is found to undergo extreme narrowing at the threshold for Brillouin oscillation. In Section 4.2 results are presented that show the temporal behavior of the Stokes intensity when the system is above the Brillouin-oscillation threshold. The evolution of the output Stokes intensity is found to be deterministic in which both stable or oscillatory behavior occurs. Experimental studies of SBS in an optical fiber with weak feedback are described in Section 4.3. Brillouin oscillation can occur at a threshold considerably lower than at the threshold for normal SBS. The spectrum

is observed to undergo a extreme narrowing and becomes much narrower than what would be expected from the gain-narrowed linewidth associated with usual SBS. In Section 4.4 experimental observations of the temporal evolution of the Stokes output intensity are shown. The behavior is of a deterministic nature in which the Stokes intensity is found to drift between a wide range of oscillatory behavior and a nonfluctuating stable output.

4.1 Spectrum and Threshold of SBS with External Feedback

Most of the theoretical groundwork required to treat SBS in the presence of reflecting boundaries is formulated in Chapter 2, and all that is needed is to provide the appropriate boundary conditions to describe the cavity conditions. The geometry is shown in Fig. 4.1, where r_1 and r_2 are the amplitude reflectivities of the boundaries at $z = 0$ and $z = L$, respectively. The reflecting boundary at $z = L$ leads to a laser field that is counterpropagating in the $-z$ direction. Under these conditions, the generation of a field component at the anti-Stokes sidemode to the laser
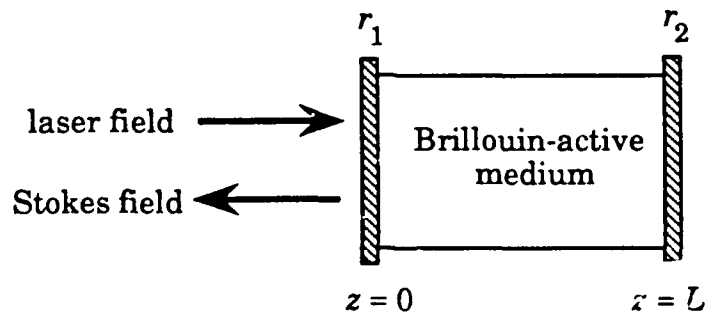
Fig. 4 1 Schematic illustration of the geometry for SBS in the presence of reflecting boundaries where r_1 and r_2 are the amplitude reflectivities.

frequency is possible due to a four-wave mixing process between the Stokes field and forward- and backward-traveling laser fields.[5] However, in this treatment the generation of the anti-Stokes field is ignored. This assumption is valid as long as the intensity of the backward-traveling laser field is weak, or as long as the length of the Brillouin-active medium is sufficiently large that the total phase-mismatch associated with the four-wave mixing process (i.e., $\Delta k L = 2n\Omega L/c$) is much greater than unity. This process is discussed in greater detail in Chapter 5.

The spectrum of the Stokes field is derived using the equations for the Stokes field [Eq. (2.13b)] and the acoustic density [Eq. (2.14)] in the limit of an undepleted laser field. The details of the derivation are given in Appendix 4.1, and the power spectrum $< F_s^{b*}(0,\delta)F_s^b(0,\delta) >$ of the backward-traveling Stokes field is found to be equal to

$$ < F_s^{b*}(0,\delta)F_s^b(0,\delta) > = \frac{4\pi k_B T}{n v A} \frac{[1+|r_2|^2(e^{|\pounds|^2 G_b}-1)]e^{|\pounds|^2 G_f}-1}{\left|1-r_1 r_2 e^{[i(2\delta T_t+\phi)+\frac{1}{2}\pounds(G_f+G_b)]}\right|^2}, \quad (4.1) $$

where $G_{f,b}$ is the single-pass gain due to the forward- (backward-) travelling laser fields inside the cavity, ϕ is the relative detuning of the nearest longitudinal mode of the cavity from the center of the Brillouin spectral line (e.g., $\phi = \pm\pi$ corresponds to the situation in which the peak of the spontaneous Brillouin spectrum lies exactly between two cavity modes), $\pounds = (1 - i2\delta/\Gamma)^{-1}$ and $g = \pounds g_o$. In the limit where $r_1, r_2 \to 0$, the

spectrum reduces to the gain-narrowed spectrum associated with usual SBS. The threshold for Brillouin-oscillation, which is equivalent to the threshold for absolute instability, occurs when the denominator of the right-hand-side of Eq. (4.1) vanishes. By setting both the real and the imaginary parts of the term within the absolute-value brackets equal to zero, we find that the threshold intensities and the oscillation frequency are given by the expressions

$$G_f^{th} + G_b^{th} = -2\ln(r_1 r_2) - \frac{2\phi^2 \ln(r_1 r_2)}{\left[\Gamma T_t - \ln(r_1 r_2)\right]^2} \tag{4.2a}$$

and

$$\frac{\delta_{th}}{\Gamma} = -\frac{\phi}{2\left[\Gamma T_t - \ln(r_1 r_2)\right]} . \tag{4.2b}$$

For the case in which a forward-traveling laser field with a normalized intensity equal to G is incident on the cavity and the feedback is weak ($r_1 r_2 < 10^{-2}$), the left-hand-side of Eq. (4.2a) can be approximated by G_{th}. If the cavity is also assumed to be sufficiently long that many modes of the cavity lie beneath the Brillouin gain curve ($\Gamma T_t \gg 10$), then the oscillation frequency occurs roughly at the peak of the Brillouin line ($\delta_{th} \sim 0$). The threshold laser intensity is then given by

$$G_{th} = -2\ln(r_1 r_2) . \tag{4.3}$$

Thus, even for small values of the reflectivity product (e.g., $|r_1 r_2|^2 = 10^{-4}$), the threshold for Brillouin oscillation ($G_{th} \approx 9$) can be considerably smaller than the threshold value for usual single-beam SBS.

When the term within the absolute-value brackets in the expression for the Stokes spectrum [Eq. 4.1)] becomes small, the output spectrum can become much narrower than either the gain-narrowed spectrum or the cavity lineshape. The origin of this extreme spectral narrowing is that the new modes of the cavity in the presence of Stokes gain resemble a cavity whose effective reflectivity product is enhanced by the factor $\exp[\pounds(G_f + G_b)/2]$ over its empty cavity value of $r_1 r_2$. Thus, even in the limit of very small feedback ($r_1 r_2 \ll 1$), a reasonable amount of gain is sufficient to lead to a considerable narrowing of the Stokes spectrum. Figure 4.2 shows plots of the Stokes spectrum for various values of G for the cases $\Gamma T_t = 5$ and $\Gamma T_t = 100$. In both cases, the values of the reflectivities are taken to be $|r_1|^2 = |r_2|^2 = 0.04$ and the peak of the spontaneous spectrum is assumed to lie at a cavity resonance such that $\phi = 0$. The spontaneous Brillouin spectrum is also shown for comparison. For a value of $G = 3$, the spectrum for both values of ΓT_t possess nearly the same linewidth, but for $\Gamma T_t = 100$ the effect of the cavity on the lineshape is more pronounced due to the oscillations at the cavity-mode frequencies. For a value of G close to the threshold for Brillouin oscillation ($G_{th} = 6.43$), the spectrum for $\Gamma T_t = 5$ has narrowed considerably, but the narrowing is even more dramatic for the case $\Gamma T_t = 100$. At the threshold for oscillation, the spectrum is perfectly monochromatic which suggests that regardless of the stochastic
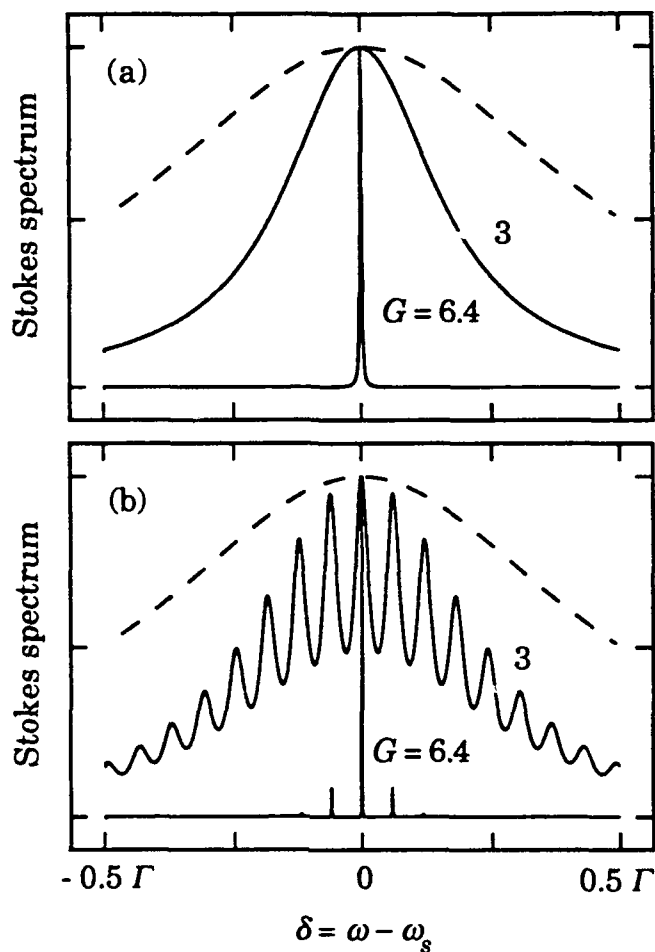
Fig. 4.2 Plots of the Stokes spectrum in the presence of feedback ($|r_1|^2 = |r_1|^2 = 0.04$) for two different values of G for the case of a relatively short medium with $\Gamma T_t = 5$ (a) and a long medium with $\Gamma T_t = 100$ (b). The dashed curve in each case represents the spontaneous Brillouin spectrum.

initiation of the SBS process, the output from a Brillouin oscillator can assume a deterministic nature.

4.2 Temporal Evolution of Stokes Output with Feedback

In order to determine the temporal behavior of the Stokes field for input intensities above the threshold for Brillouin oscillation, the full

stochastic differential equations for the laser field, Stokes field [Eq. (2.14)] and the density [Eq. (2.15)] are numerically integrated with the appropriate boundary conditions. For all the numerical simulations presented in this Section, the reflectivity of the boundary at $z = L$ is assumed to be small, in which case the intensity of the backward-traveling laser field is relatively weak. Under these conditions, the forward-traveling Stokes field will not experience significant gain, thus the Brillouin interaction between the Stokes field and the backward-traveling laser field may be ignored. This effect is modeled by injecting the Stokes field at $z = 0$ back into the medium at $z = L$ with a one transit-time delay and scaled by the reflectivities of the mirrors, such that

$$E_s(L,t) = r_1 r_2 E_s(0, t - T_t) . \qquad (4.4)$$

The validity of this scheme has been tested by comparing the results for several cases with those results obtained in which interaction between the backward-traveling laser and the forward-traveling Stokes field is included. The behavior of the Stokes output field at $z = 0$ is found to be the same for both schemes as long as the value of the product $|r_2|^2 G$ remains approximately less than 3.

Figures 4.3 and 4.4 show the temporal evolution of the Stokes intensity for various values of G for the cases $\Gamma T_t = 5$ and 100, respectively. In all cases, the output is shown for the case in which the transients associated with the turn-on of the laser field are no longer present. For an input laser intensity ($G = 4$) below the threshold value

for Brillouin oscillation, the Stokes intensity fluctuates in a stochastic fashion and remains at a small value for both cases of $\Gamma T_t = 5$ [Fig. 4.3(a)] and $\Gamma T_t = 100$ [Fig. 4.4(a)]. For a value of $G = 8$, which is just above the threshold for Brillouin oscillation, the Stokes output undergoes a transition to an extremely stable state for the case $\Gamma T_t = 5$ [Fig. 4.3(b)] with an SBS reflectvity greater than 15%. However, for $\Gamma T_t = 100$ (Fig 4.4b), the output intensity self-pulses with a period equal to the round-trip time $(2T_t)$ of the cavity. This temporally unstable deterministic behavior corresponds to the behavior predicted by Bar-Joseph et al.[3] through a stability analysis of the Stokes intensity. At still higher input intensities $(G = 15)$, output intensity for the case $\Gamma T_t = 5$
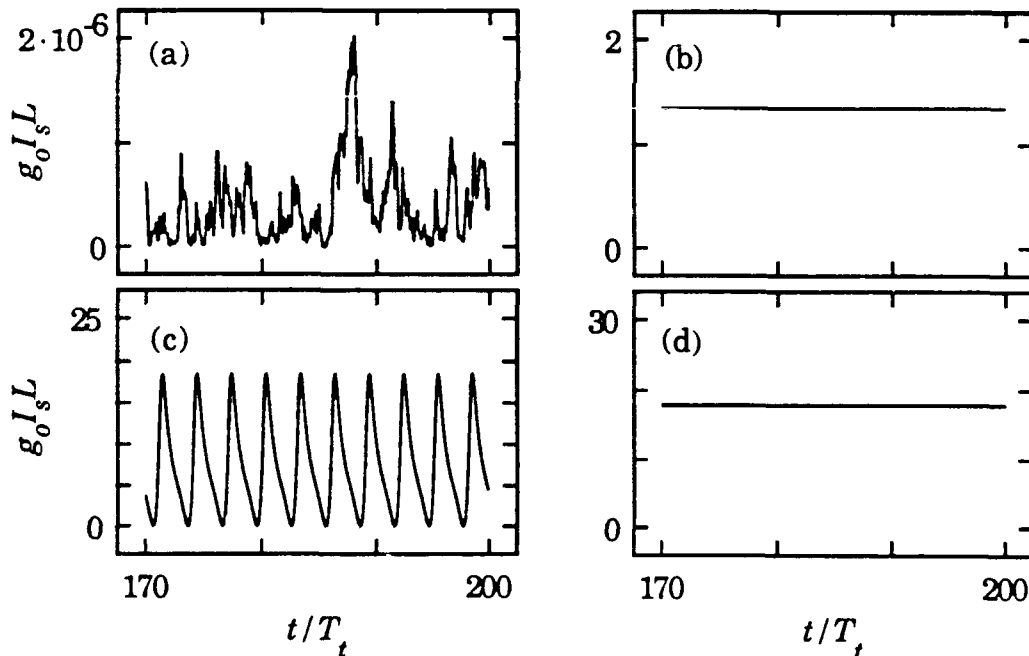
Fig. 4.3 Plots of Stokes output intensity, normalized by $(g_o L)^{-1}$, as a function of time for the case $\Gamma T_t = 5$, $|r_1|^2 = |r_2|^2 = 0.04$, and for (a) $G = 4$, (b) $G = 8$, (c) $G = 15$, and (d) $G = 25$. Above the threshold for Brillouin oscillation $(G_{th} = 6.4)$, a region of oscillatory behavior (b) is found to exist between stable regimes (a),(c).
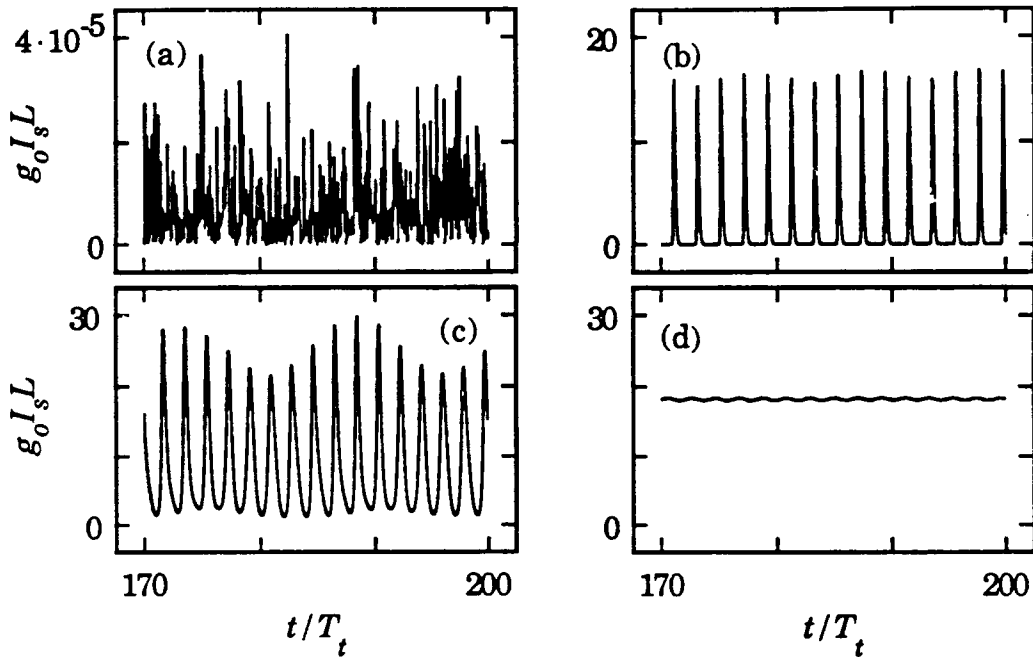
Fig. 4.4 Same as in Fig. 4.3 except $\Gamma T_t = 100$. Above the threshold for Brillouin oscillation, stable output is predicted only at high values of G.

[Fig. 4.3(c)] also becomes temporally unstable, and begins to oscillate with a period roughly equal to $3T_t$. For the case $\Gamma T_t = 100$ [Fig. 4.4(c)] the Stokes intensity still self-pulses at a basic period of $2T_t$, but it also contains a periodic envelope whose period is approximately equal to $15T_t$. As the intensity is increased, the period of this envelope shortens until eventually at an input intensity of $G = 25$ [Fig. 4.4(d)], the output becomes stable and remains stable for increasing laser intensity. The output also becomes stable once again for the case $\Gamma T_t = 5$ and $G = 25$ [Fig. 4.3(d)].

4.3 Experimental Measurements of the Threshold for Brillouin Oscillation and the Stokes Output Spectrum

As shown in Section 4.1, the threshold for SBS can be lower than the threshold for usual single-beam SBS. The experimental set-up for

measuring the backscattered Stokes power as a function of input laser power is the same as that shown Fig. 3.2. No index matching fluid was used and the fiber ends were cleaved such that a fraction (~4%) of the light within the fiber was reflected back into the fiber by the glass-fiber interface. Figures 4.5 and 4.6 are plots of the SBS reflectivity as a function of the input laser power for the dye laser (λ_l = 0.5890 μm) and the argon-ion laser (λ_l = 0.5145 μm), respectively. Figures 4.5(a) and 4.6(a) show the results for the case of the 100-meter-long fiber and Figs 4.5(b) and 4.6(b) show the results for the case of the 500-meter-long fiber. In all cases the output Stokes light contained approximately 70% of its power in the polarization direction parallel to that of the laser. As described in Section 3.2, an estimate can be made for the experimentally measured single-pass gain at threshold by utilizi σ the following expression

$$G_{th} = 0.7 g_o P_{th} L_{eff} / A \ . \tag{4.4}$$

The threshold power P_{th} is the laser power at which the SBS reflectivity reaches 1%. The corresponding values of G_{th} for all four cases are shown in Figs. 4.5 and 4.6. For the 100-meter-long fiber, the values for G_{th} in the presence of feedback are measurably lower than the values measured without feedback [see Figs. 3.3(a) and 3.4(a)] which suggests that feedback from the ends of the fiber could be playing a role in the dynamics of the Stokes light. However, for the 500-meter-long fiber, the reflectivity curves [Figs. 4.5(b) and 4.6(b)] are virtually identical to the

curves measured in the absence of feedback [Figs. 3.3(b) and 3.4(b)], which leads to the same values of G_{th}. Thus, the threshold data for the 500-meter-long fiber does not show evidence for the occurrence of Brillouin oscillation. The effect of the absorption of the Stokes field can be included in the theoretical prediction for the value of G_{th}, by adding the round-trip absorption pathlength ($2\alpha L = 0.88$ for the 100-meter-long fiber, and $2\alpha L = 4.38$ for the 500-meter-long fiber) to the right-hand-side of
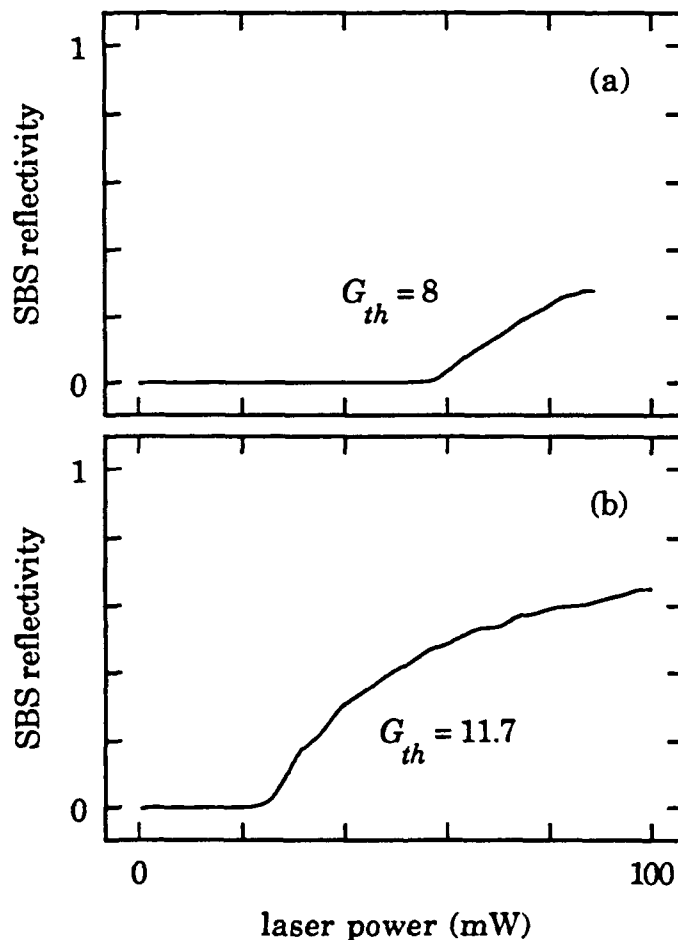
Fig. 4.5 Experimental results for the SBS reflectvity in the presence of feedback plotted as a function of the input laser power at a wavelength $\lambda_l = 0.5890$ μm for the (a) 100-meter-long fiber and for the (b) 500-meter-long fiber.
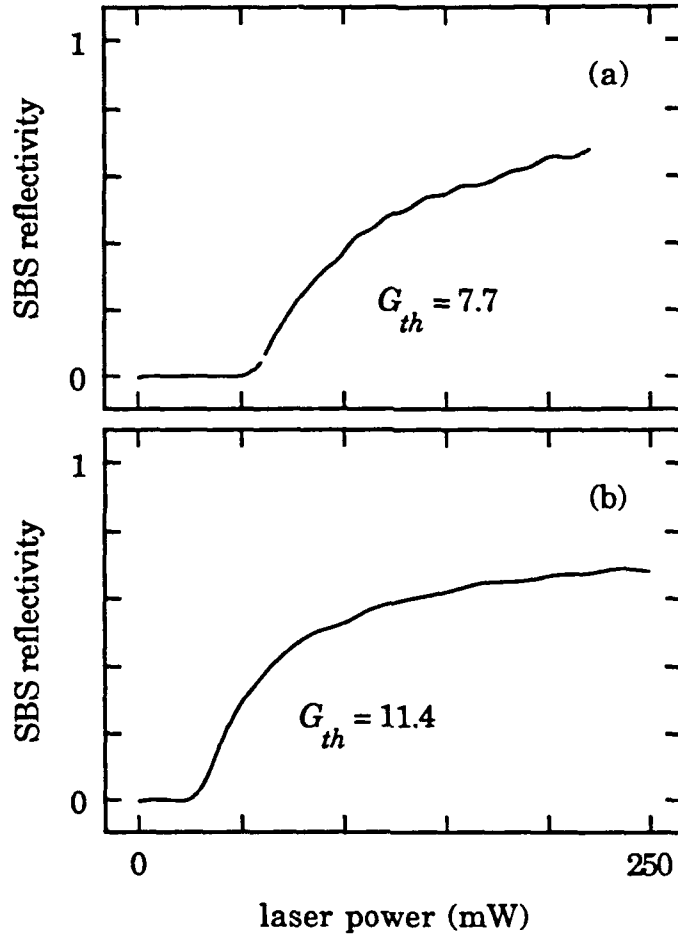
Fig. 4.6 Experimental results for the SBS reflectvity in the presence of feedback plotted as a function of the input laser power at a wavelength $\lambda_l = 0.5145$ µm for the (a) 100-meter-long fiber and the (b) 500-meter-long fiber.

Eq. (4.3). Thus, the predictions for the values of threshold value of G are equal to 7.3 and 10.8 for the 100-and 500-meter-long fibers, respectively. The predicted values of G_{th} agree reasonably well with the experimentally observed values.

The spectrum of the Stokes light was measured with the same experimental configuration as the one shown in Fig. 3.10, except that both fiber lengths (100- and 500-meter-long) were used. Figure 4.7(a) is a

plot of the Stokes spectrum for a input laser power of 36 mW at the front-end of the 100-meter-long fiber. This value of the laser power corresponds to a value of $G = 7.1$. The measured spectral width of 41 MHz is approximately equal to the gain-narrowed linewidth that was measured in the absence of feedback from the fiber endfaces. However, at slightly higher input laser powers the spectrum suddenly collapses with a width equal to that of the laser spectrum. Figure 4.7(b) is a plot of
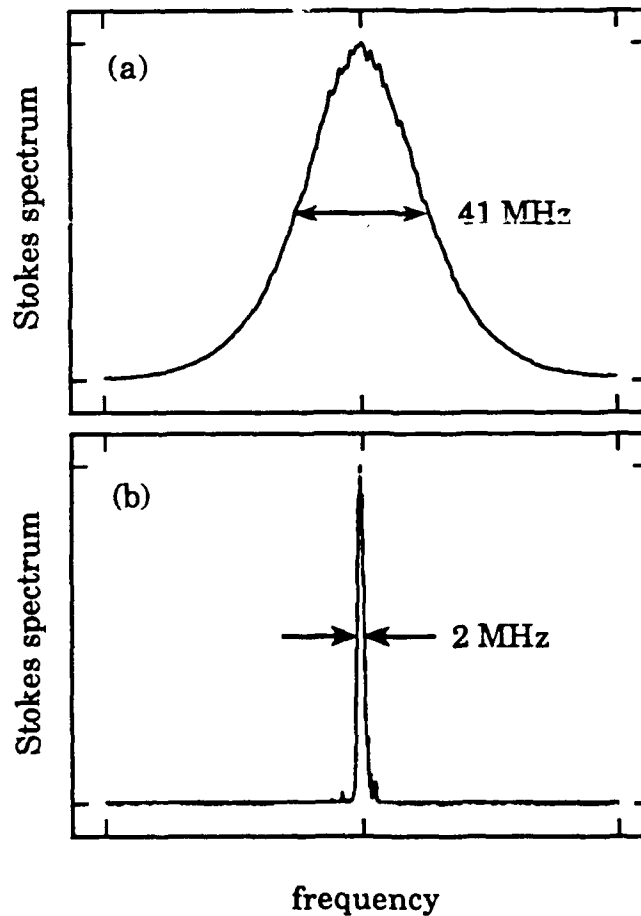
Fig. 4.7 Spectrum of the Stokes light for the 100-meter-long fiber (a) just below the threshold for Brillouin oscillation ($P_l = 36$ mW) and (b) just above the threshold for Brillouin oscillation ($P_l = 48$ mW).

the Stokes spectrum for a laser power equal to 48 mW ($G = 9$) which is just above the threshold for Brillouin oscillation. The spectrum for the case of the 500-meter-long fiber displayed similar behavior.

4.4 Experimental Results for the Temporal Evolution of Stokes Output Power in the Presence of Feedback

The experimental set-up employed to monitor the temporal evolution of the Stokes output power in the presence of feedback is the same as the one discussed in Section 3.3. The argon-ion laser ($\lambda_l = 0.5145$ μm) was used because it can deliver much higher laser powers than those possible with the dye laser. However, for the range of input powers accessible with the dye laser, behavior similar to that of the argon-ion laser was obtained. Also, for all the cases shown here the 100-meter-long fiber was utilized since the absorption pathlength was relatively small ($\alpha L = 0.44$) which made it a more ideal configuration with which to study Brillouin oscillation. As predicted in the Section 4.2, the temporal evolution of the Stokes output above the threshold for Brillouin oscillation takes on a deterministic nature. However, for a fixed input laser power, the output exhibited transitions between different forms of periodic pulsations and intervals of stable output consisting of almost no flucutations. The duration of a particular class of behavior lasted no more than 1 msec, and the transitions occurred in a time equal to roughly 5 μsec.

The period of the pulsations that was most commonly observed was equal to the round-trip time ($2T_t = 1$ μsec) through the fiber. Figure
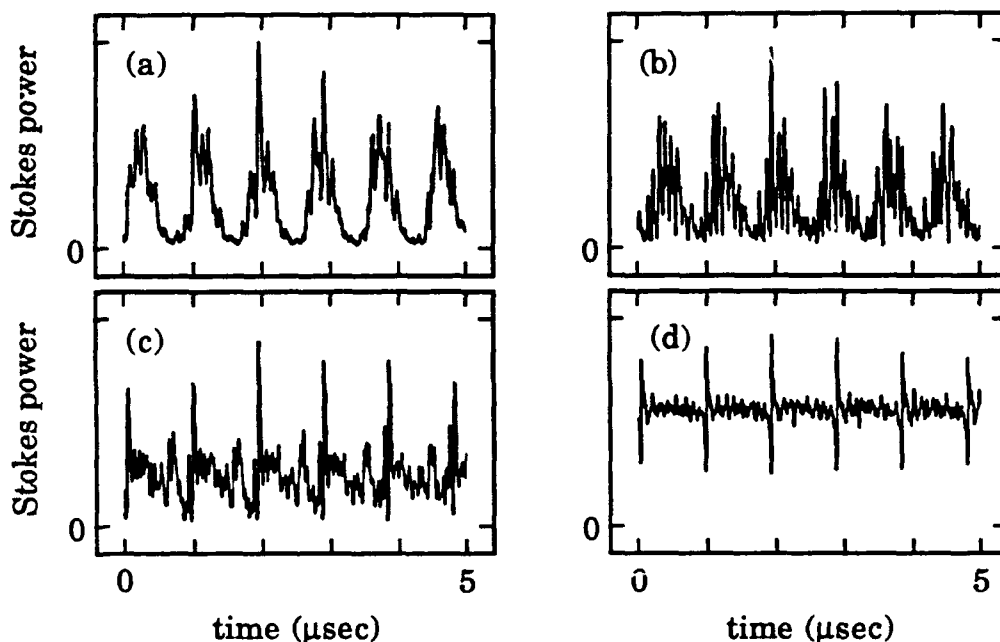
Fig. 4.8 Plots of the temporal evolution of the Stokes output power for input laser powers of (a) P_l = 56 mW, (b) P_l = 79 mW, (c) P_l = 82 mW, and (d) P_l = 202 mW. In all cases the basic period of the self-pulsing is equal to the round-trip time (1 μsec) of the fiber.

4.8 shows several examples of the observed oscillations with a 1 μsec period for various input laser powers. Generally, oscillations with this periodicity were easier to achieve at laser powers close to Brillouin oscillation threshold power (~ 50 mW) than at the higher powers. Oscillations at higher harmonics of the fundamental oscillation frequency ($1/2T_l$) were also observed. Figure 4.9(a)-4.9(e) shows temporal evolution of Stokes output power for the cases in which it exhibits oscillations at the second, third, fourth, fifth, and sixth harmonic of the fundamental oscillation frequency, respectively. In Fig. 4.9(f), the Stokes output is seen to be relatively stable as would be expected from theoretical simulations shown in Section 4.2.
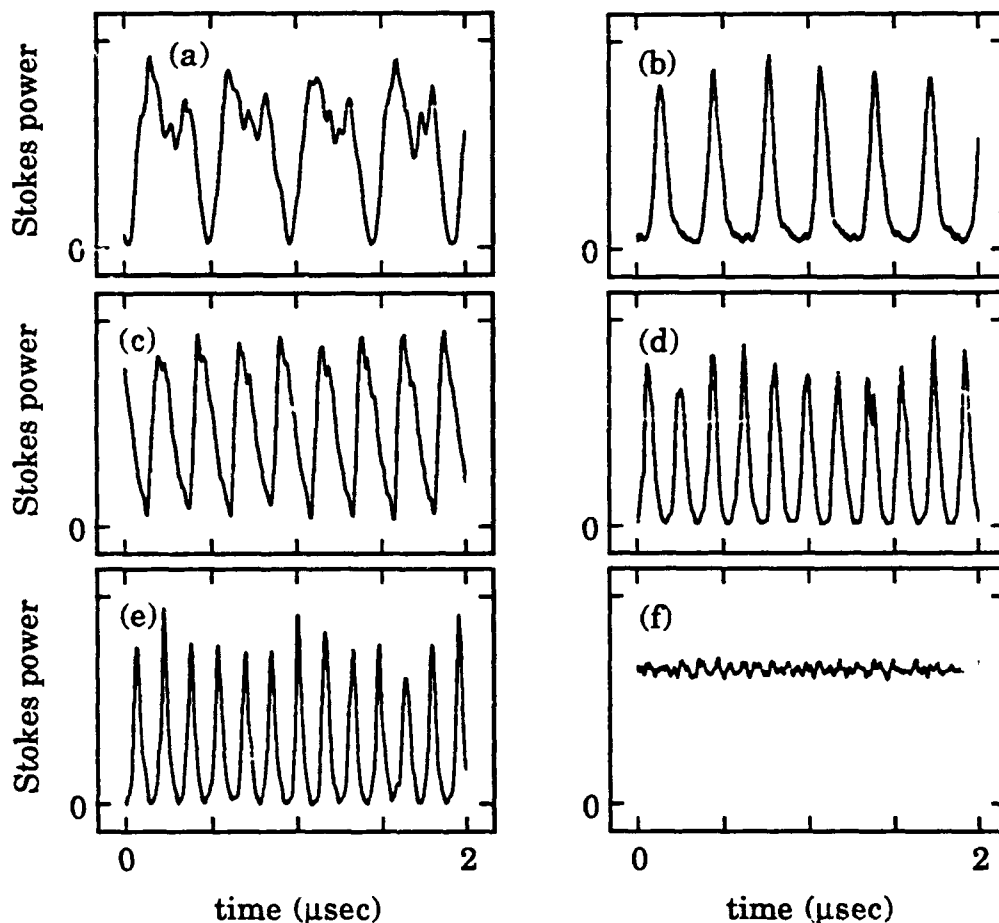
Fig. 4.9 Plots of the temporal evolution of the Stokes output power for input laser powers of (a) P_l = 130 mW, (b) P_l = 96 mW, (c) P_l = 76 mW, (d) P_l = 250 mW, (e) P_l = 100 mW, and (f) P_l = 250 mW. Plots (a)-(e) show evidence of second, third, fourth, fifth, and sixth harmonics, respectively, of the fundamental oscillation frequency $(1/2T_t)$ Plot (f) demonstrates stable Stokes output.

At present, the theoretical model presented here does not predict constant transitions between different types of periodic behavior, nor does it predict the appearance of oscillatory behavior at harmonics of the fundamental oscillation frequency $(1/2T_t)$. However, since the spectrum of the emitted Stokes light is nearly as narrow that of the laser, I believe

that laser bandwidth effects may be playing a role in the complicated dynamics that are observed. Attempts have been made to include laser bandwidth effects by assuming a phase diffusion model[6] for the laser; however, the result of these simulations have not yielded results which could explain either the transitory behavior or the observation of higher harmonics. Another mechanism which may contribute to the observed behavior are fluctuations in the optical pathlength of the fiber due to changes in the ambient temperature. This effect could lead to a relatively slow modification of the mode structure of the Brillouin oscillator within a time interval of a few milliseconds.

In summary, the theoretical model described in this Chapter has been able to confirm most of the experimental observations such as the threshold for Brillouin oscillation and the extreme narrowing of the Stokes spectrum. The numerical simulations have also shown qualitative, but not quantitative, agreement with the experiment in that the temporal evolution of the Stokes intensity displays deterministic behavior including nonfluctuating output and temporal instabilities.

Appendix 4.1 Spectrum of Stokes light with feedback

The geometry under consideration is shown in Fig. 4.1. The spectrum of the Stokes light emitted from the cavity is treated in the limit in which neither the backward-traveling Stokes field E_s^f nor the forward-traveling Stokes field are sufficiently large to deplete the forward-traveling laser field E_f or the backward-traveling laser field E_b,

respectively. Equations (2.13b) and (2.14) are used to describe the propagation of the Stokes fields inside the cavity such that

$$\frac{\partial E_s^b}{\partial z} - \frac{n}{c}\frac{\partial E_s^b}{\partial t} = -i\kappa\rho_b E_f \tag{A4.1a}$$

$$\frac{\partial \rho_b}{\partial t} + \frac{\Gamma}{2}\rho_b = i\Lambda\, E_s^{b^*} E_f + f_2^* \tag{A4.1b}$$

$$\frac{\partial E_s^f}{\partial z} + \frac{n}{c}\frac{\partial E_s^f}{\partial t} = i\kappa\rho_f E_b \tag{A4.1c}$$

and

$$\frac{\partial \rho_f}{\partial t} + \frac{\Gamma}{2}\rho_f = i\Lambda\, E_s^{f^*} E_b + f_1^* \;, \tag{A4.1d}$$

where ρ_b and ρ_f are the amplitudes of the acoustic density associated with the backward- and the forward traveling Stokes fields, respectively, and f_1 and f_2 are uncorrelated noise terms which possess the same Gaussian noise properties as those associated with the noise term $f(z,t)$ described in Section 2.1. The equations for the temporal Fourier transforms of the backward-traveling Stokes field $F_s^b(z,\delta)$ and the forward-traveling Stokes field $F_s^f(z,\delta)$ can be derived from Eq. A4.1(a)-(d) and are given by

$$\frac{dF_s^b}{dz} = \left[\frac{in\delta}{c} - \frac{g}{2}I_f\right]F_s^b - i\mu_b\, h_2^* \tag{A4.2a}$$

and

$$\frac{dF_s^f}{dz} = \left[\frac{-in\delta}{c} + \frac{g}{2}I_b\right]F_s^f + i\mu_f h_1^* \qquad \text{(A4.2b)}$$

where $g = \pounds g_o$, $\pounds = (1 - i2\delta/\Gamma)^{-1}$, $\mu_{f,b} = 2\pounds\kappa E_{b,f}/\Gamma$, $I_{f,b}$ is the intensity of the forward- (backward-) traveling laser field, and h_1 and h_2 are the Fourier transforms of f_1 and f_2, respectively. Since no Stokes field is injected into the cavity, the homogeneous solutions to Eq. (A4.2) vanish. The particular solutions to Eq. (A4.2) are

$$F_s^b(z,\delta) = C_b(z,\delta)e^{\left(\frac{in\delta}{c} + \frac{g}{2}I_f\right)(L-z)} \qquad \text{(A4.3a)}$$

and

$$F_s^f(z,\delta) = C_f(z,\delta)e^{\left(\frac{in\delta}{c} + \frac{g}{2}I_b\right)z} , \qquad \text{(A4.3b)}$$

where C_b and C_f are given by

$$C_b(z,\delta) = C_b(L,\delta) - \frac{i2\kappa\pounds E_f}{\Gamma}\int_L^z dz' \, h_2^*(z')e^{(in\delta/c - gI_f/2)(L-z')} \qquad \text{(A4.4a)}$$

and

$$C_f(z,\delta) = C_f(0,\delta) + \frac{i2\kappa\pounds E_b}{\Gamma}\int_0^z dz' \, h_1^*(z')e^{(in\delta/c - gI_b/2)z'} . \qquad \text{(A4.4b)}$$

The boundary conditions for the total Stokes field leads to the following relations between the Stokes amplitudes

$$F_s^b(L,\delta) = r_2 F_s^f(L,\delta)e^{ik_sL} \qquad\qquad\qquad \text{(A4.5a)}$$

and

$$F_s^f(0,\delta) = r_1 F_s^b(0,\delta)e^{ik_sL} \ . \qquad\qquad\qquad \text{(A4.5b)}$$

The power spectrum of the Stokes field at $z = 0$ is

$$< F_s^{b*}(0,\delta)F_s^b(0,\delta) > \ = \ < C_b^*(0,\delta)C_b(0,\delta) > e^{|\pounds|^2 G_f} \ , \qquad \text{(A4.6)}$$

where $G_f = g_o I_f L$. The expression for $C_b(0,\delta)$ is found by applying the boundary conditions [Eq. (4.5)] to Eqs. (4.3) and (4.4). The resulting expression is then substituted into Eq. (4.6) to yield the power spectrum

$$< F_s^{b*}(0,\delta)F_s^b(0,\delta) > \ = \ \frac{4\pi k_B T}{nvA} \frac{[1+|r_2|^2(e^{|\pounds|^2 G_b}-1)]e^{|\pounds|^2 G_f}-1}{\left|1-r_1 r_2 e^{[i(2\delta T_t+\phi)+\frac{1}{2}\pounds(G_f+G_b)]}\right|^2} \qquad \text{(A4.7)}$$

where $G_b = g_o I_b L$ and $\phi = (\omega_s - 2\pi v_c)T_t$ represents the relative detuning of the Stokes frequency from the nearest cavity-mode frequency v_c (i.e., $\pi < \phi \leq \pi$).

1. K. O. Hill, B. S. Kawasaki, and D. C. Johnson, Appl. Phys. Lett. **30**, 162 (1977); D. R. Ponikvar and S. Ezekiel, "Stabilized single-frequency stimulated Brillouin fiber ring laser," Opt. Lett. **6**, 398 (1981).

2. K. Baumgartel, U. Motschmann, and K. Sauer, "Self-pulsing at stimulated scattering processes," Opt. Commun. **51**, 53 (1984).

3. I. Bar-Joseph, A. A. Friesem, E. Lichtman, and R. G. Waarts, "Steady and relaxation oscillations of stimulated Brillouin scattering in single-mode optical fibers," J. Opt. Am. B **2**, 1606 (1985).

4. E. M. Dianov, A. Ya. Karasik, A. V. Lutchnikov, and A. N. Pilipetskii, "Saturation effects at backward-stimulated scattering in the single-mode regime of interaction," Opt. and Quantum Electron. **21**, 381 (1989).

5. B. Ya Zel'dovich and V. V. Shkunov, "Characteristics of stimulated scattering in opposite pump beams," Sov. J. Quantum Electron. **12**, 223 (1982).

6. See for example, S. Stenholm, *Fundamentals of Laser Spectroscopy*, (Wiley, New York, 1984).

Chapter 5
Instabilities and Chaos of Counterpropagating Waves in an Brillouin-Active Medium

Several theoretical investigations have shown that the mutual interaction of two light waves in a nonlinear medium can lead to very complicated behavior, including chaotic fluctuations in the intensities of the transmitted waves. The possibility of instability in the interaction of counterpropagating waves was considered by Silberberg and Bar-Joseph[1] for the case of a nonlinear Kerr medium having a noninstantaneous response. They showed that for sufficiently large input intensities these fluctuations become chaotic. The origin of this instability is the combined action of the gain experienced by the sidemodes to the input fields and the distributed feedback due to scattering from the grating formed by the interference between the two input fields. Khitrova et al.[2] have observed a related instability in sodium vapor. More recently, Gaeta et al.[3] have shown that chaotic temporal fluctuations can occur in the polarizations of waves counterpropagating in a Kerr medium that possess tensor properties, even for the case of a medium with instantaneous response. The threshold for this instability can be much lower than the scalar

instability. Gauthier *et al.*[4] have observed the polarization instability also in sodium vapor.

In Chap. 2 and 4 only the generation of Stokes light was considered. This assumption is valid as long as only a single pump wave is present. In the case of counterpropagating waves, if the medium is sufficiently long then the anti-Stokes field cannot grow due to the large phase mismatch which suppresses the four-wave mixing process leading to anti-Stokes generation.

In this Chapter, the behavior of two laser beams counterpropagating in a Brillouin-active medium is studied. Unlike the case of normal SBS, this interaction leads to coupling of Stokes and anti-Stokes waves through a four-wave mi ing process, which can lead to deterministic fluctuations of the two laser beams. Under certain conditions chaotic fluctuations are predicted.

5.1 Theoretical Development

The total field within the Brillouin-active medium is represented as the sum of the forward- and backward-travelling plane-wave components as

$$\tilde{E}(z,t) = \tfrac{1}{2}E_f(z,t)e^{i(kz-\omega t)} + \tfrac{1}{2}E_b(z,t)e^{i(-kz-\omega t)} + c.c. \qquad (5.1)$$

Unlike the case of normal SBS treated in Chap. 2, both the forward and backward travelling waves may contain contributions at the the Stokes and anti-Stokes frequencies. Since we are interested in the deterministic

dynamical behavior of the two strong fields, only the electrostrictive driving term in Eq. (2.4) for the material density is considered such that

$$\frac{\partial^2 \tilde{\rho}}{\partial t^2} - \Gamma \frac{\partial}{\partial t} \frac{\partial^2 \tilde{\rho}}{\partial z^2} - v^2 \frac{\partial^2 \tilde{\rho}}{\partial z^2} = \frac{-\gamma}{8\pi} \frac{\partial^2}{\partial z^2} \bar{E}^2 \; . \tag{5.2}$$

In evaluating the electrostrictive driving term on the right-hand side of Eq. (5.2), the terms that oscillate at optical frequencies are neglected as well as those terms which lead to an acoustic wave with a wave vector nearly equal to zero. The right-hand side of Eq. (5.2) then reduces to

$$\frac{q^2 \gamma}{16\pi} \left(E_f E_b^* e^{iqz} + c.c. \right) \; , \tag{5.3}$$

where $q = 2k$. The form of Eq. (5.2) can now be simplified by introducing the complex representation

$$\tilde{\rho}(z,t) = \tfrac{1}{2} \rho(z,t) e^{iqz} + c.c. \; , \tag{5.4}$$

by making the slowly varying amplitude approximation for the acoustic field, and by assuming that the acoustic field is strongly absorbed, i.e., that $\Gamma |\partial \rho / \partial t| \gg (2\Omega^2/q) |\partial \rho / \partial z|$, to give

$$\frac{\partial^2 \rho}{\partial t^2} + \Gamma \frac{\partial}{\partial t} \rho + \Omega^2 \rho = \frac{q^2 \gamma}{8\pi} E_f E_b^* \; . \tag{5.5}$$

The expression for the acoustic field amplitude [Eq (5.4)] is substituted into the polarization given by Eq. (2.13). Both the polarization and the

field amplitudes [Eq. (5.1)] are then substituted into the driven wave equation (2.12) and the SVEA is made which yields the following coupled-amplitude equations

$$\frac{\partial E_f}{\partial z} + \frac{n}{c}\frac{\partial E_f}{\partial t} = i\kappa\rho E_b \qquad (5.6a)$$

and

$$\frac{\partial E_b}{\partial z} - \frac{n}{c}\frac{\partial E_b}{\partial t} = -i\kappa\rho^* E_f \ . \qquad (5.6b)$$

Equations (5.5) and (5.6) have been derived previously but were used to treat the case in which E_b was generated by reflection of the transmitted field E_f.[5] The case treated here is one in which both E_f and E_b are applied externally. As shown below, complex temporal behavior can occur even when there is no external feedback. Equations (5.5) and (5.6) yield the following simple steady-state solution (designated by the superscript zero):

$$\rho^o(z) = \frac{\gamma}{8\pi v^2} E_f^o(z) E_b^{o*}(z) \ , \qquad (5.7a)$$

$$E_f^o(z) = E_f^o(0)e^{i\frac{\Gamma}{2\Omega}g_o I_b z} \ , \qquad (5.7b)$$

and

$$E_b^o(z) = E_b^o(L)e^{i\frac{\Gamma}{2\Omega}g_o I_f(L-z)} \ , \qquad (5.7c)$$

where $I_f = (nc/8\pi)|E_f(0)|^2$ and $I_b = (nc/8\pi)|E_b(L)|^2$ are the input intensities of each wave. One can see from Eqs. (5.7) that in the steady-state the fields do not exchange energy but that the phase velocity of propagation of each wave is affected by the intensity of the other wave. The nonlinear contribution to the phase shift is proportional to the product of the line-center gain factor g_o with the ratio Γ/Ω of the Brillouin linewidth to the Brillouin frequency shift. Since g_o is itself proportional to Γ^{-1} [see Eq. (2.17)], we note that the nonlinear phase shift is actually independent of Γ.

5.2 Linear Stability Analysis

To determine the stability characteristics of the steady-state solution [Eq. (5.7)], the amplitudes of the forward and backward waves are perturbed such that

$$E_f(z) = E_f^o(z) + f_s(z)e^{\lambda t} + f_a(z)e^{\lambda^* t} \qquad (5.8a)$$

and

$$E_b(z) = E_b^o(z) + b_s(z)e^{\lambda t} + b_a(z)e^{\lambda^* t} , \qquad (5.8b)$$

where the second and third terms in each equation represent small perturbations to the steady-state solution. If $\mathrm{Re}(\lambda) > 0$, the steady-state solution will be temporally unstable to the growth of these perturbations. The linearized equations for the perturbations amplitudes are derived by inserting these expressions for the electric fields into Eqs. (5.5) and (5.6):

$$\frac{df_s}{dz} = (-\lambda n / c + \frac{g}{2} I_b^o) f_s + i \frac{\Gamma}{\Omega} g_o \left(\frac{cn}{16\pi} E_f^o E_b^{o*} \right) b_s + g \left(\frac{cn}{16\pi} E_f^o E_b^o \right) b_a^* , \quad (5.9a)$$

$$\frac{db_s}{dz} = (\lambda n / c - \frac{g}{2} I_f^o) b_s - i \frac{\Gamma}{\Omega} g_o \left(\frac{cn}{16\pi} E_f^{o*} E_b^o \right) f_s - g \left(\frac{cn}{16\pi} E_f^o E_b^o \right) f_a^* , \quad (5.9b)$$

$$\frac{df_a^*}{dz} = -(\lambda n / c + \frac{g}{2} I_b^o) f_a^* - i \frac{\Gamma}{\Omega} g_o \left(\frac{cn}{16\pi} E_f^{o*} E_b^o \right) b_a^* - g \left(\frac{cn}{16\pi} E_f^{o*} E_b^{o*} \right) b_s , \quad (5.9c)$$

and

$$\frac{db_a^*}{dz} = (\lambda n / c + \frac{g}{2} I_f^o) b_a^* + i \frac{\Gamma}{\Omega} g_o \left(\frac{cn}{16\pi} E_f^o E_b^{o*} \right) f_a^* + g \left(\frac{cn}{16\pi} E_f^{o*} E_b^{o*} \right) f_s , \quad (5.9d)$$

where

$$g = g_o \frac{i\Gamma\Omega}{\lambda^2 + \Gamma\lambda + \Omega^2} . \quad (5.9e)$$

To understand the nature of the coupling described by these equations, we assume $\text{Im}(\lambda) > 0$. The complex amplitudes f_s and b_s can then be interpreted to be the amplitudes of the forward- and backward-traveling Stokes fields, respectively, and the complex amplitudes f_a and b_a can be interpreted to be the amplitudes of the forward- and backward-traveling anti-Stokes fields, respectively. Then, for example, Eq. (5.9a) describes the spatial evolution of the forward-traveling Stokes wave. The first term on the right-hand side describes the change in the propagation vector that is associated with λ and with the normal SBS gain (proportional to g) owing to the presence of the backward pump wave [see Fig. 5.1(a)]. The backward pump wave scatters from the

retreating acoustic field created by its interference with the forward-Stokes wave. The gain coefficient is resonantly enhanced when $Im(\lambda)$ (i.e., the frequency difference between the pump and Stokes fields) is equal to the Brillouin frequency Ω. The second term in Eq. (5.9a) [see Fig. 5.1(b)] can be interpreted as the scattering of the backward-Stokes wave from the refractive-index variation associated with the standing-wave pattern created by the interference of the counterpropagating pump waves. This term describes distributed feedback of the same type as that discussed by Silberberg and Bar-Joseph. The third term describes the four-wave mixing process arising from the scattering of the backward pump wave from the retreating acoustic wave driven by the interference between the forward pump wave and the backward anti-Stokes wave [see Fig. 5.1(c)]. The other equations [(5.9b)-(5.9d)] can be interpreted in an analogous fashion. For each equation the second term vanishes for the case of a sharp Brillouin line, $\Gamma/\Omega \to 0$, which is the limit in which SBS is usually studied. In this limit the system of four coupled equations decouples into two systems of two coupled equations; each system describes a four-wave mixing process.[6]

The linearized equations [Eqs. (5.9)] are solved with pump wave amplitudes given by Eqs. (5.7b) and (5.7c) by seeking solutions for the perturbations that vary as $e^{\alpha z}$. The general solution for f_s, b_s, f_a, and b_a is then found in terms of linear combinations of such solutions for each of the four eigenvalues of α. The particular solution is found by applying the boundary conditions $f_s(0) = b_s(L) = f_a(0) = b_a(L) = 0$. Because the steady-state solution is unstable for $Re(\lambda) > 0$, the threshold for instability
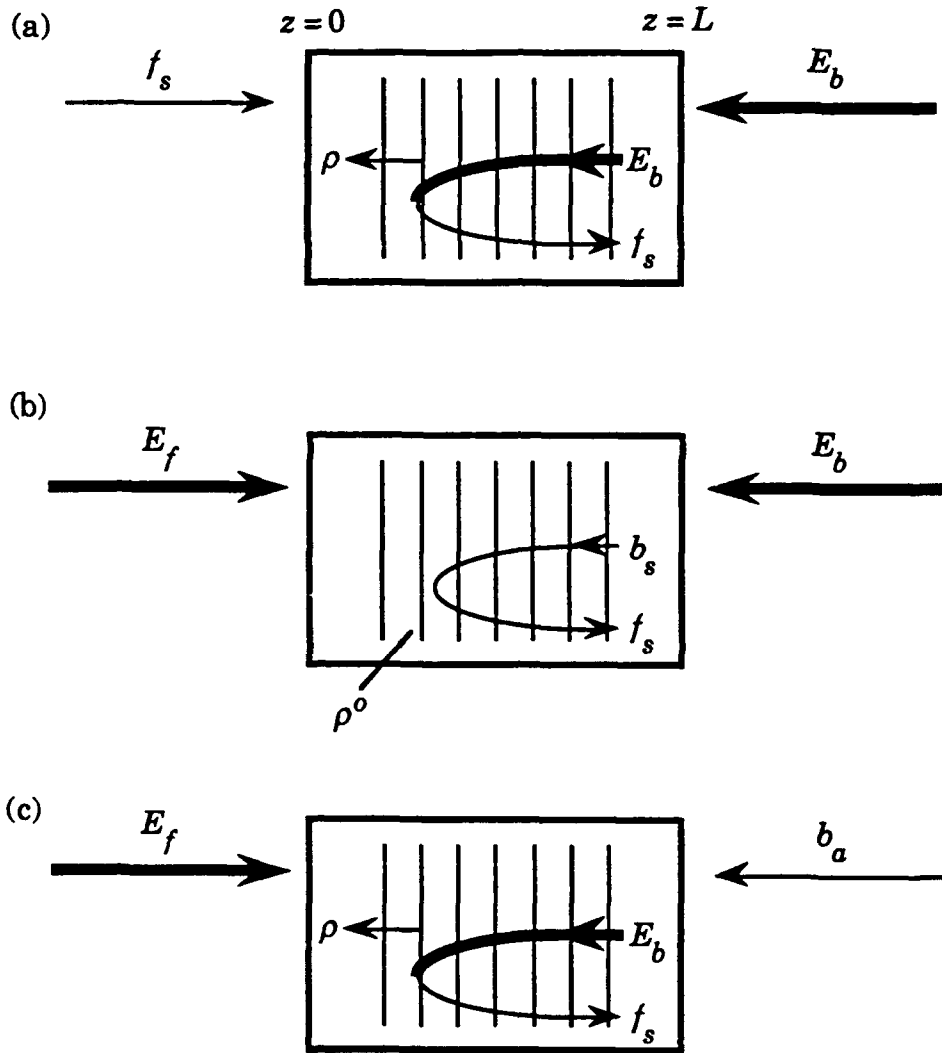
Fig. 5.1 Schematic diagrams that illustrate the three contributions to the forward-traveling Stokes field f_s given by Eq. (5.9a).

is determined by setting $Re(\lambda) = 0$. More than one solution to the linearized equations can be found even under these conditions, and the different solutions correspond to different longitudinal modes of the system and to different oscillation frequencies $Im(\lambda)$. The instability threshold for the system is the lowest intensity that yields a solution to the coupled linearized equations with $Re(\lambda) = 0$ for any value of $Im(\lambda)$.

Typical results of the stability analysis are shown in Fig. 5.2 for the case of a Brillouin medium with $\Gamma/\Omega = 0.03$. In Fig. 5.2(a) the normalized forward input intensity at threshold for the Brillouin instability is plotted as function of the ratio of the input intensities for several different values of the normalized length of the medium. In each case the system is unstable in the region above the curve. Figure
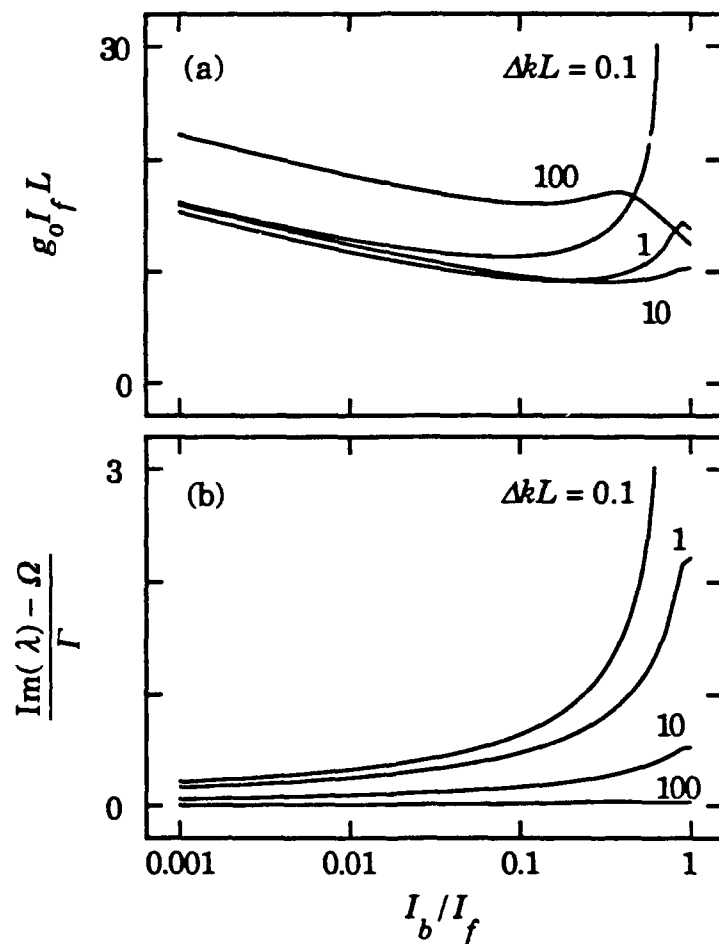

Fig. 5.2 Forward input intensity at (a) the threshold for instability and (b) the frequency of oscillation, each plotted as a function of the backward-to-forward input intensities for $\Gamma/\Omega = 0.03$ and for various values of the normalized length of the medium $\Delta k L$.

5.2(b) shows the normalized oscillation frequency $\text{Im}(\lambda)$ at threshold. The oscillation frequency is close to the Brillouin frequency for each case shown. The quantity $\Delta k L = 2n\Omega L/c$, which here is called the normalized length of the medium, is therefore approximately equal to the single-pass phase mismatch of the nearly degenerate four-wave mixing process.[7] The threshold input intensity increases rapidly for a short medium ($\Delta k L = 0.1$) with balanced pumping ($I_b/I_f = 1$). This increase occurs because for balanced pumping the Stokes gain is nearly
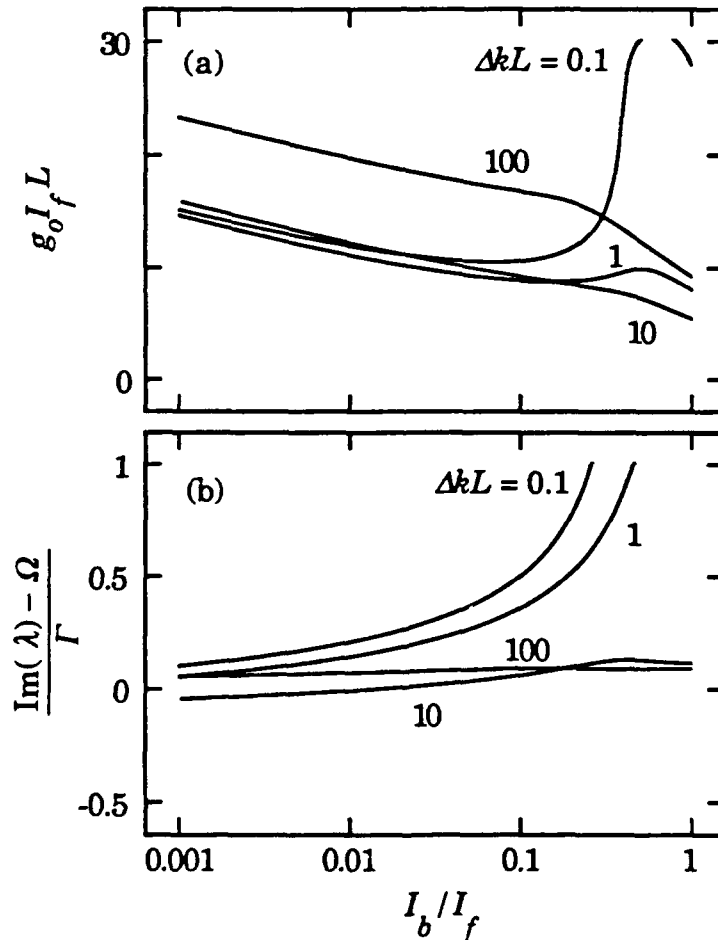

Fig. 5.3 Same as in Fig. 5.2 but for the case of a much larger Brillouin linewidth such that $\Gamma/\Omega = 0.3$.

equal to the Stokes loss, and for a short medium the coupling between the waves is sufficiently strong to prevent either wave from growing.[6,8,9] For comparison, we have plotted the results of the stability analysis for the case of a medium with a much larger Brillouin linewidth such that $\Gamma/\Omega = 0.3$ (Fig. 5.3). Although these two cases are quite similar in their behavior near the threshold for instability, the temporal behavior of the two cases will be shown to be considerably different.

The Brillouin instability predicted above is an example of a absolute instability in that perturbation to the steady-state solution grows exponentially in time and thus will develop from an arbitrarily small initial perturbation. The process of SBS is the exponential spatial growth of an input Stokes wave and hence is a convective instability. Even if no Stokes wave is applied externally, an input Stokes (and anti-Stokes) wave is created by spontaneous Brillouin scattering. The threshold for SBS excited by a single laser beam and seeded by spontaneous Brillouin scattering is described by the condition that the single-pass gain $G_f = g_o I_f L$ is approximately equal 25. From Figs. 5.2 and 5.3 the threshold for the Brillouin instability is seen to be lower than the threshold for single beam SBS for most of the cases that are considered; hence the dynamic Brillouin instability will occur but SBS will not. However, the threshold for instability predicted in Figs. 5.2 and 5.3 is higher than that of single-beam SBS for the case of a short medium with balanced pumping and for the case of long medium with imbalanced pumping. To determine whether SBS or the dynamic instability will occur in these two cases, a more detailed consideration of

the initiation of SBS by spontaneous Brillouin scattering on the present calculation must be performed. For the case of highly imbalanced pumping, the situation is similar to that of SBS with a single pump beam, and a threshold for SBS is simply $g_o I L = 25$, where I is the intensity of the stronger pump beam. Therefore, since the dynamic instability treated here has a higher threshold, it is probably not experimentally observable for this case. For the case of a short medium ($\Delta k L \ll 1$) with balanced pumping, the situation is quite different. Here, as mentioned above, the coupling between the Stokes wave (which in the absence of coupling, experiences gain) and the anti-Stokes wave (which in the absence of coupling, experiences loss) is so large that that the coupled solution experiences little net gain, and as a result, even the usual SBS process is suppressed by the presence of the counterpropagating pump waves.[6] To see that even the normal SBS process is suppressed by the presence of the counterpropagating wave, the simple limiting case is considered in which Γ/Ω approaches 0 and the Stokes and anti-Stokes waves are tuned exactly to Brillouin resonance. By solving Eqs. (5.9a) and (5.9d), the transmitted Stokes field strength is found to be related to the input Stokes and anti-Stokes fields when $I_f = I_b$ and in the limit $G_f \gg 1$ by

$$f_s(L) = 2f_s(0) + b_a^*(L) \ . \tag{5.10}$$

Hence, in the presence of counterpropagating pump waves, the Stokes field is amplified only by a factor of approximately 2, although the

amplification in the presence of a single pump wave of the same intensity would be e^{G_f} where G_f was assumed to be large.

Figure 5.4 shows plots of the normalized length of the medium ΔkL versus the normalized intensity G_f [Fig. 5.4(a)] and normalized oscillation frequency $[\text{Im}(\lambda) - \Omega]/\Gamma$ [Fig. 5.2(b)] corresponding to each of the allowed solutions of the linearized perturbation Eqs. 5.10 with
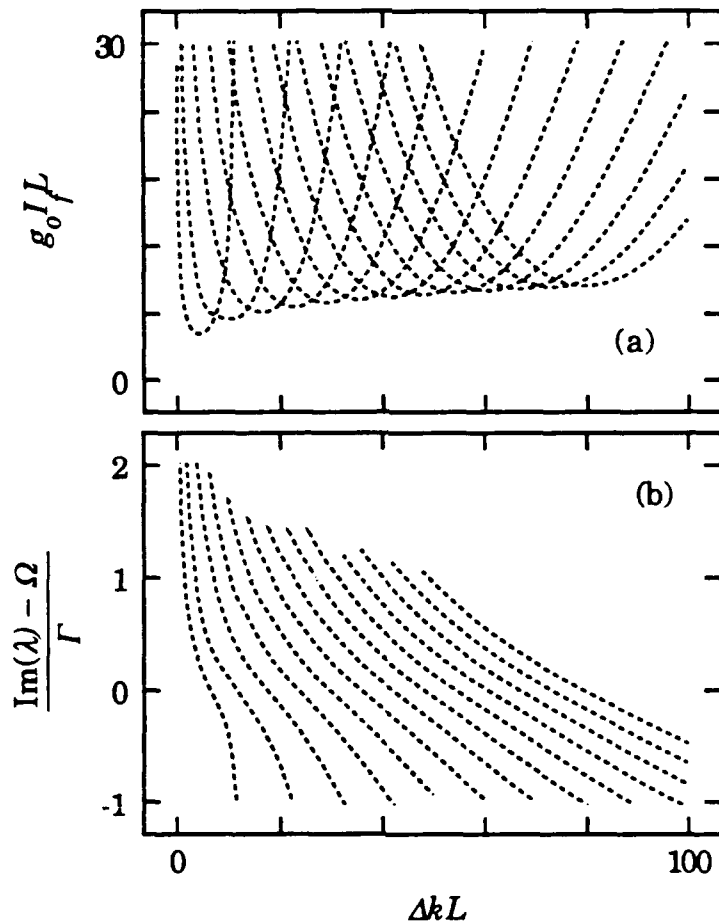

Fig. 5.4 Forward input intensity at (a) the threshold for instability and (b) the frequency of oscillation for each mode of the system for the case of equal input intensities and $\Gamma/\Omega = 0.3$. The solid curve in (a) gives the lowest threshold intensity for any mode, and the solid curves in (b) give the corresponding oscillation frequency.

$Re(\lambda) = 0$. The case of balanced pumping ($I_f = I_b$) and a broad Brillouin line ($\Gamma / \Omega = 0.3$) is assumed. The various U-shaped curves in Fig. 5.4(a) can be interpreted as the threshold for instability for the different longitudinal modes of the system. The solid curve in Fig. 5.4 corresponds to the lowest input intensity that leads to instability for any mode. Local minima in this threshold occur for $\Delta k L$ approximately equal to the integral multiples of π. The solid curves in Fig. 5.4(b) give the oscillation frequency of the mode with the lowest threshold. This frequency is approximately equal to the Brillouin frequency except for the case of a short medium, in which case the lowest-frequency mode of the system has an eigenfrequency much greater than the Brillouin frequency.

Silberberg and Bar-Joseph[1] have shown that the origin of the instability of counterpropagating waves in a Kerr medium with noninstantaneous response is the combined action of gain experienced by the sidemodes of the pump frequency and distributed feedback. Distributed feedback[10] results from the scattering of light at the sidemode frequencies from the grating induced by the interference between the two pump waves. However, this gain distributed feedback mechanism does not appear to be the origin of the instability for the case of a Brillouin-active medium. The Brillouin instability occurs even in the limit of a medium with a sharp Brillouin linewidth, although as mentioned above there is no distributed feedback structure in this limit. The Brillouin instability appears to be more closely related to the infinite reflectivity that is predicted to occur for certain values of the pump

intensity in phase conjugation by four-wave mixing. We can establish this connection most simply by considering the limit $\Gamma/\Omega \to 0$, in which case the linearized perturbation equations [Eqs. (5.9)] decouple into two sets of equations. Each set describes a four-wave mixing process. These equations are identical to those describing Brillouin-enhanced four-wave mixing, and the Brillouin instability is a consequence of the infinite reflectivity that can occur in phase conjugation by Brillouin-enhanced four-wave mixing.[7] Infinite reflectivity is also predicted for phase conjugation by degenerate four-wave mixing in a Kerr medium,[11] and it might be thought that this infinite reflectivity is related to the instabilities that can occur with counterpropagating beams in a Kerr medium.[1] However, in the scalar limit such instabilities occur only for the case of a medium with noninstantaneous response, whereas the infinite reflectivity is predicted for any value of the response time. Infinite reflectivity in degenerate four-wave mixing does not necessarily imply instabilities in counterpropagating waves for the following reason: when the angle between the pump and probe waves in the phase conjugation geometry is sufficiently small, additional nearly phase-matched contributions to the nonlinear polarization, known as cross-coupled waves, become important.[12] These additional contribution prevent the development of the instability unless the medium has noninstantaneous response. Curiously (and importantly), the cross-coupled waves do not contribute for the case of a Brillouin-active medium with $\Gamma/\Omega \ll 1$ because these additional contributions are not Brillouin resonant. Moreover, polarization instabilities in

oscillates at the Brillouin frequency. However, for the higher input intensity $G_f = 8$, the output oscillates periodically with a fundamental frequency equal to to one half the Brillouin frequency. For still higher intensities ($G_f = 16$), the output intensity oscillates with a fundamental frequency equal to one quarter of the Brillouin frequency. At the highest intensity shown ($G_f = 30$), the output intensity oscillates in a chaotic fashion.
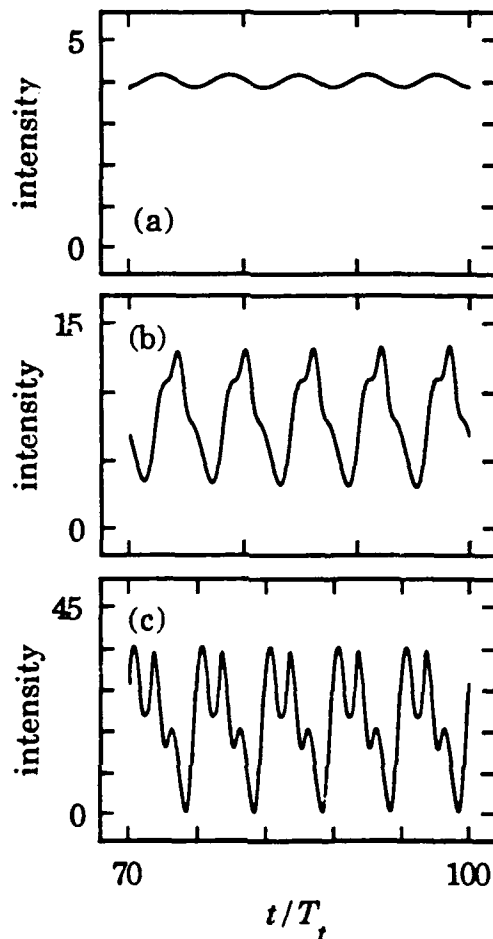

Fig. 5.5 Temporal evolution of the transmitted intensity of the forward-traveling wave normalized by $(g_o L)^{-1}$ for three different values of the input intensity [(a) $G_f = 8$, (b) $G_f = 16$, and (c) $G_f = 40$] for the case $\Delta k L = 2$, $\Gamma/\Omega = 0.03$, and $I_f = I_b$.
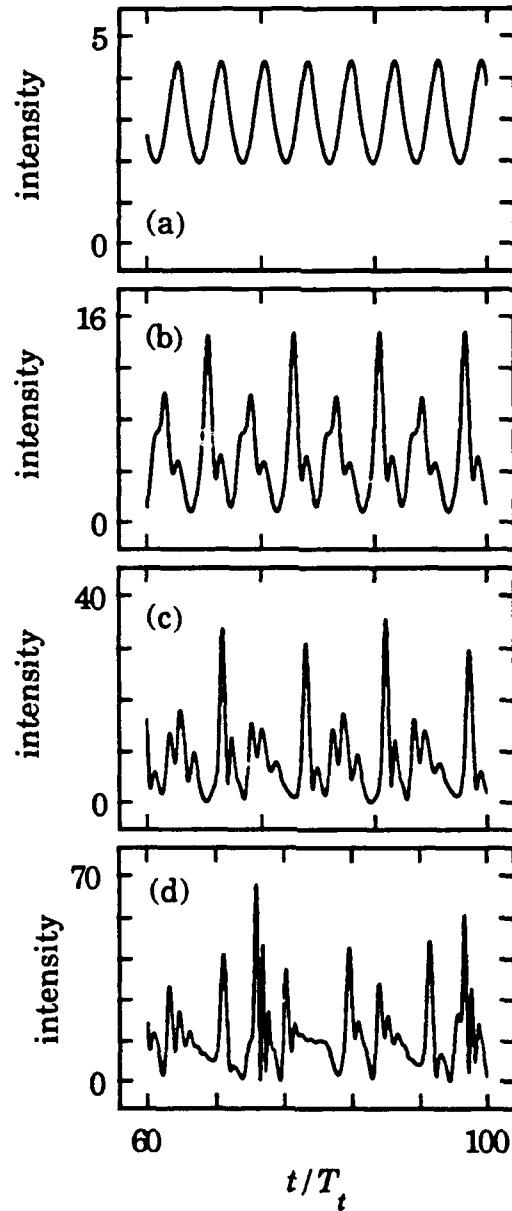
Fig. 5.6 Temporal evolution of the transmitted intensity of the forward-traveling wave normalized by $(g_o L)^{-1}$ for the case $\Delta k L = 2$, $\Gamma / \Omega = 0.3$, and equal input intensities. As the input intensities are increased, the system becomes chaotic following the periodic-doubling route. For input intensities such that (a) $G_f = 6$, the output oscillates at the Brillouin frequency. For input intensities equal to (b) $G_f = 10$ and $G_f = 16$ the out put oscillates with a fundamental frequency equal to one half and one quarter, respectively, of the Brillouin frequency. For $G_f = 30$ the temporal evolution is chaotic.

The dynamical behavior can also be illustrated by means of phase-space trajectories. Figure 5.7 are plots for various values of G_f of the real part versus the imaginary part of the complex electric amplitude of the forward-traveling wave at its output from the interaction region. As for the case shown in Fig. 5.6, the ratio of the two input intensities is unity, $\Delta kL = 2$, and $\Gamma/\Omega = 0.3$. For the case of low input intensities ($G_f = 4$), the system is seen to be stable, and the trajectory reduces to that of a single point. Slightly above the threshold for instability ($G_f = 6$), the output

Fig. 5.7 Phase-space trajectories of the complex field amplitude of the transmitted traveling wave normalized by $(g_o L)^{-1/2}$ for four different values of the input intensities [(a) $G_f = 4$, (b) $G_f = 6$, (c) $G_f = 16$, and (d) $G_f = 30$] for the case of $\Gamma/\Omega = 0.3$, $\Delta kL = 2$, and $I_f = I_b$.
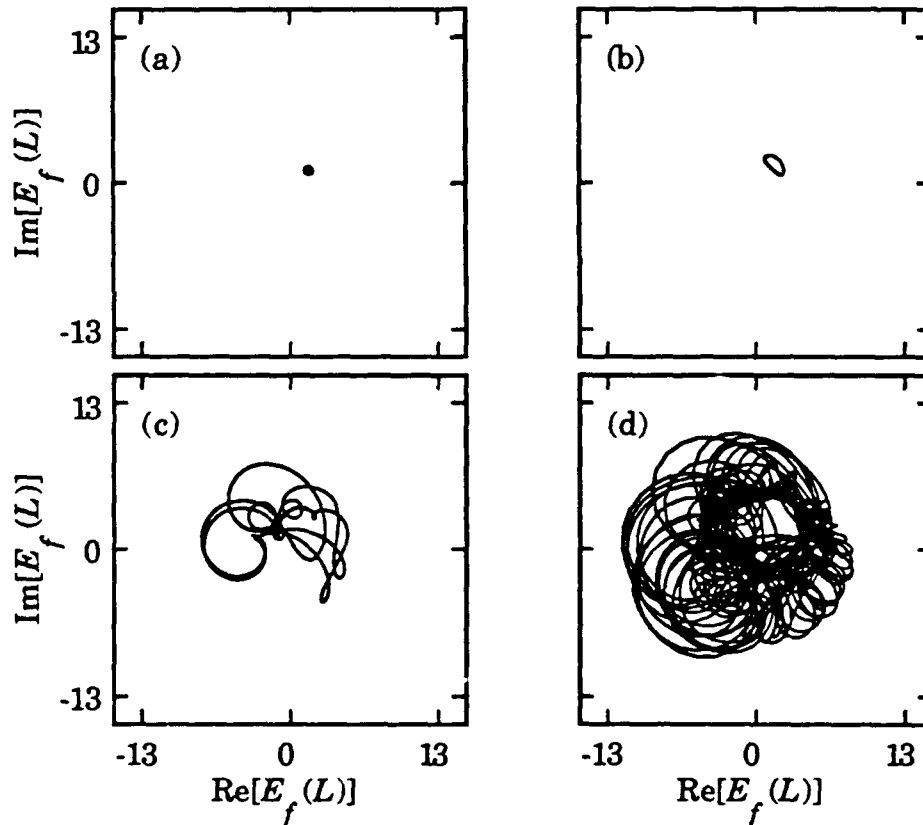
fields oscillate sinusoidally about their steady-state values, and the phase-space trajectory takes the form of a closed loop. For still higher input intensities (G_f = 16), the trajectory is still periodic but with a period equal to twice the fundamental Brillouin period (i.e., the evolution is period 2), and the phase-space trajectory takes on a more complicated form. Finally, for the case G_f = 30, the system evolves chaotically. Analysis using the method of Grassberger and Procaccia[13] shows that this trajectory is chaotic with a fractal dimension of 2.2.

Figure 5.8 shows the phase-space trajectories for the case of a narrow Brillouin resonance with Γ/Ω = 0.03 and an interaction pathlength such that ΔkL = 72. These parameters correspond to those of our experimental investigation discussed in the following Section. The threshold for instability for this case, as determined by the stability analysis, occurs for G_f = 12.6. For the case of an input intensity corresponding to G_f = 10, the trajectory reduces to a single point. For intensities above the instability threshold, the trajectory takes on the form of a nearly circular orbit corresponding to an output wave consisting of a component at the laser frequency and of a Stokes sideband. Note that the amplitude of the Stokes sideband increases with increasing input laser intensity.
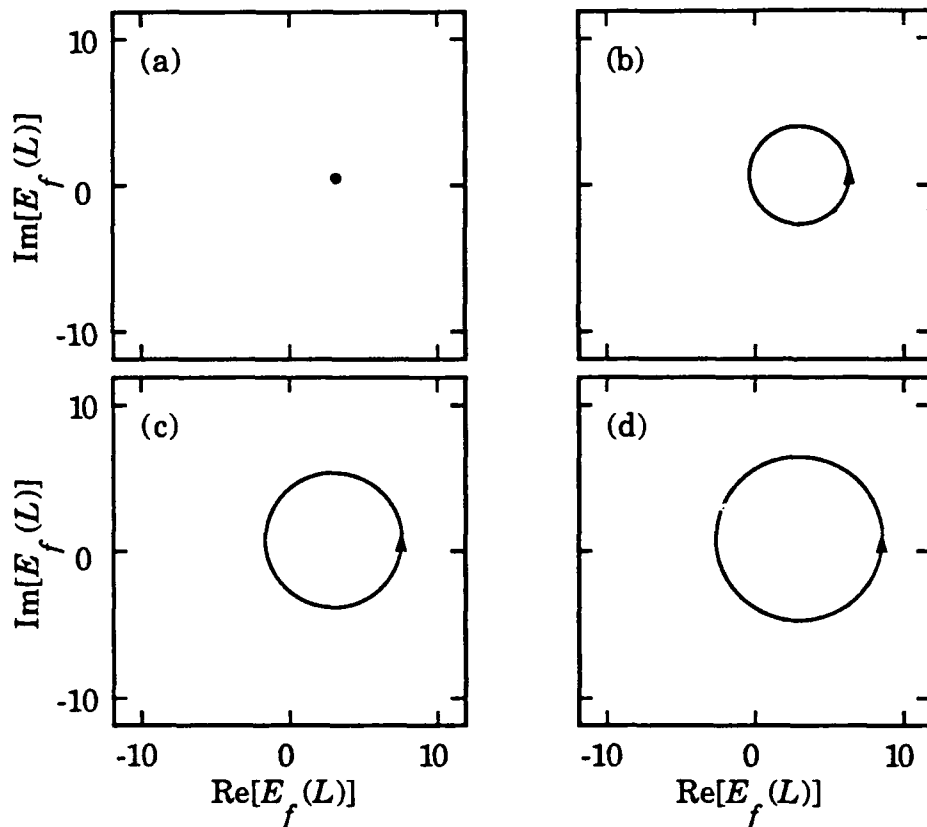
Fig. 5.8 Phase-space trajectory of the complex field amplitude of the transmitted forward-traveling wave for four different values of the input intensities [(a) $G_f = 10$, (b) $G_f = 20$, (c) $G_f = 30$, and (d) $G_f = 40$] for the case of $\Gamma / \Omega = 0.03$, $\Delta kL = 72$, and $I_f = I_b$.

5.4 Experimental Results

The experimental investigation of the stability of counterpropagating laser beams was conducted using a frequency-doubled Nd:YAG laser that operated in a single transverse and a single longitudinal mode. The laser produced a smooth output pulse of 22-nsec duration (FWHM intensity) containing as much as 30 mJ of energy. the output beam was collimated with a diameter of 1 mm (FWHM intensity) was split into two beams that were directed counterpropagating into a
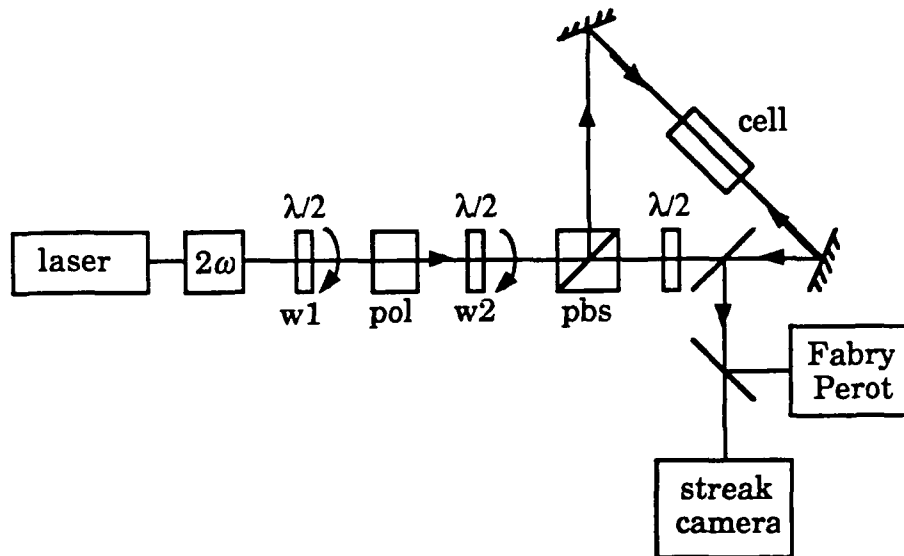
Fig 5.9 Experimental arrangement used to study counterpropagating light waves in a cell containing carbon disulfide: w1, w2, half-wave plates; pbs, polarizing beamsplitter.

15-cm-long cell containing carbon disulfide. The intensities of the two beams could be adjusted independently by using polarizing optics, as shown in Fig. 5.9.

The threshold for instability relative to that for normal, single-beam SBS was determined by means of the following procedure. One of the beams is blocked (i.e., the backward-traveling beam) and the intensity of the other (forward) beam is slowly increased until the threshold for SBS is reached. The occurrence of SBS is signaled by the generation of backscattered Stokes radiation which is detected using a Fabry-Perot. The measured threshold intensity for single-beam SBS was found to be $I_{SBS}^{th} = 42$ MW/cm^2. The backward beam is then unblocked, and the intensities of the two beams are gradually decreased (at a fixed intensity ratio) until the Stokes component no longer appears in the
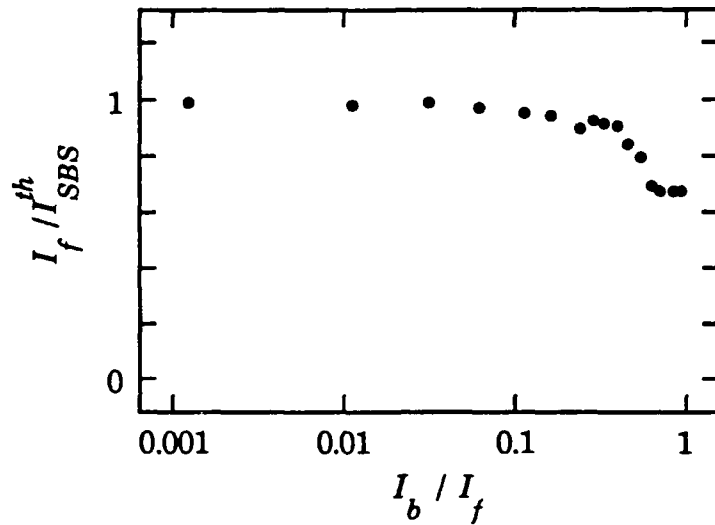
Fig. 5.10 Experimental measurement of the threshold for instability relative to the threshold for single-beam SBS plotted as a function of the ratio of intensities of the backward and forward waves.

output. The intensity of the forward-going beam at which this occurs gives the instability threshold relative to that of SBS. The results of these measurements are shown in Fig. 5.10. These results show that for the case equal input intensities the threshold for instability is approximately 67% that for single-beam SBS. These results also show that the presence of the counterpropagating beam whose intensity is even 10% of the that of the pump wave is sufficient to lead to a measurable reduction of the threshold for instability.

The temporal evolution of the intensity of the light leaving the interaction region was measured with a streak camera having a resolution of 2 psec. Experimental results for the case of equal input intensities are shown in Fig. 5.11. In Fig. 5.11(a) the input intensity of each beam is equal to $0.66I_{SBS}^{th}$, which is just below threshold for instability. Figures 5.11(b) and (c) show the time evolution for input
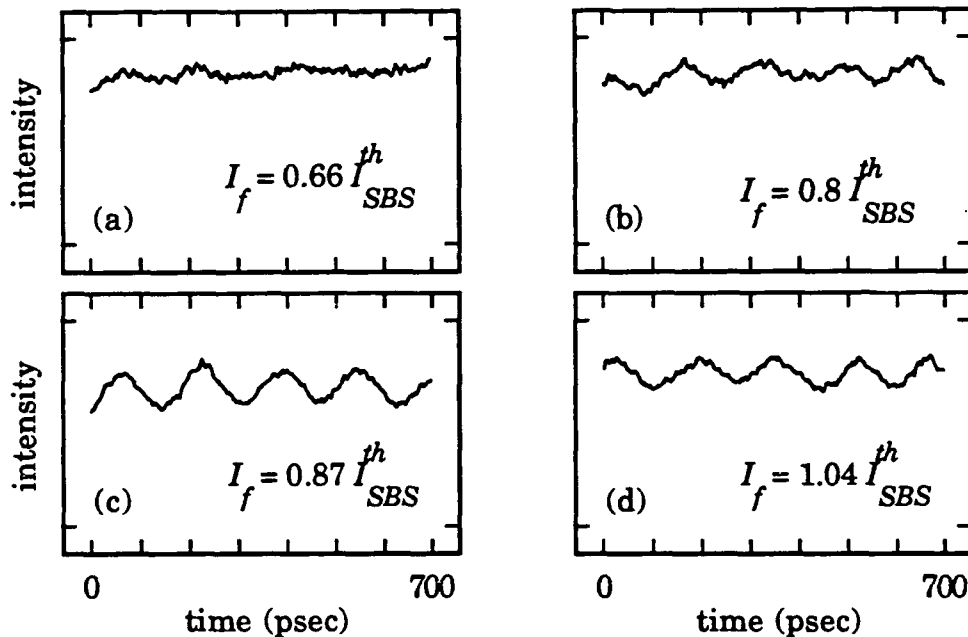
Fig. 5.11 Experimental data showing showing the temporal evolution of the transmitted intensity of the forward-traveling wave for the case of equal input intensities $(I_f = I_b)$. Just below the threshold for instability (a), the output remains stable. For the remaining three cases (b)-(d) the output oscillates at the Brillouin frequency (7.7 GHz). Note in (b) and (c) the input intensities are below the threshold for single-beam SBS.

intensities equal to $0.8I_{SBS}^{th}$ and $0.87I_{SBS}^{th}$, respectively. These input intensities are above the threshold for instability but well below the threshold for single-beam SBS. Hence the oscillation seen in the experimental data provide evidence for the instability predicted in Section 5.2. In Fig. 5.11(d) the input intensity is equal to $1.04I_{SBS}^{th}$. The frequency of the observed oscillations is in all cases equal to within our measurement accuracy to the value[14] 7.7 GHz, which is the Brillouin frequency of carbon disulfide at 0.53 µm. Using the Fabry-Perot

interferometer, the spectral content of the radiation leaving the interaction region was examined. For all cases in which the instability occurred, radiation was observed only at the laser and the first Stokes frequencies. These results (that the Stokes intensity greatly exceeds that of the anti-Stokes) agree with the predictions of the theory in Section 5.3.

The far-field emission pattern of the transmitted light was also examined. We find that under conditions of dynamical instability part of the Stokes radiation is emitted in the form of a hexagon surrounding the transmitted laser beam as shown in Fig. 5.12. The angle between the pump wave and this part of the Stokes radiation is 3×10^{-3} rad. We find that the hexagonal emission occurs for $I_f \approx I_b$ and for I_f/I_{SBS}^{th} in the range 0.8 to 1.05. The origin of this could be related to the transverse spatial instabilities predicted for Kerr media[15] and atomic systems.[16] A spatial instability of similar nature has been observed by Grynberg et al.[17]

Fig. 5.12 Hexagonal far-field emission pattern of the Stokes emission. The central portion of the transmitted beam has been blocked.

1. Y. Silberberg and I. Bar-Joseph, "Instabilities, self-oscillations, and chaos in a simple nonlinear interaction," Phys. Rev. Lett. **48**, 1541 (1982).

2. G. Khitrova, J. F. Valley, and H. M .Gibbs, "Gain-feedback approach to instabilities in sodium vapor," Phys. Rev. Lett. **60**, 1126 (1988).

3. A. L. Gaeta, R. W. Boyd, J. R. Ackerhalt, and P. W. Milonni, "Instabilities and chaos in the polarizations of counterpropagating light fields," Phys. Rev. Lett. **58**, 2432 (1987).

4. D. J. Gauthier, M. S. Malcuit, and R. W. Boyd, "Polarization instabilities of counterpropagating laser beams in sodium vapor," Phys. Rev. Lett. **61**, 1827 (1988).

5. C. J. Randall and J. R. Albritton, "Chaotic nonlinear stimulated Brillouin scattering," Phys. Rev. Lett. **52**, 1887 (1984).

6. B. Ya Zel'dovich and V. V. Shkunov, "Characteristics of stimulated scattering in opposite pump beams," Sov. J. Quantum Electron. **12**, 223 (1982).

7. P. Narum, and R. W. Boyd, "Non frequency-shifted phase conjugation by Brillouin-enhanced four-wave mixing," IEEE J. Quantum Electron. **QE-22**, 1211 (1987).

8. N. Bloembergen, *Nonlinear Optics* (Benjamin, New York, 1965), pp. 115.

9. R. W. Boyd, M. G. Raymer, P. Narum, and D. J. Harter, "Four-wave parametric interactions in a strongly-driven two-level system," Phys. Rev. A **24**, 411 (1981).

10. H. Kolgenik and C. V. Shank, "Coupled-wave theory of distributed feedback lasers," J. Appl. Phys. **43**, 2327 (1972).

11. A. Yariv and D. M. Pepper, "Amplified reflection, phase conjugation, and oscillation in degenerate four-wave mixing," Opt. Lett. **1**, 16 (1977).

12. J. H. Marburger, in *Optical Phase Conjugation*, R. A. Fisher, ed. (Academic, New York, 1983) Chap. 4.

13. P. Grassberger and I. Procaccia, "Estimation of the Kolmogorov entropy from a chaotic signal," Phys. Rev. Lett. **50**, 346 (1983).

14. M. Skeldon, Ph. D. Thesis, "Optical Phase Conjugation Enhanced by the Brillouin Interaction," (University of Rochester, Rochester, N. Y., 1987).

15. W. J. Firth and C. Pare, "Transverse modulational instabilities for counterpropagating beams in Kerr media," Opt. Lett. **13**, 1096 (1988); G. G. Luther

and C. J. McKinstrie, "Transverse modulational instability of colinear waves," J. Opt. Soc. Am. B **7**, 1125 (1990).

16. G. Grynberg and J. Paye, "Spatial instability for a standing wave in a nonlinear medium," Europhys. Lett. **8**, 29 (1989).

17. G. Grynberg, E. LeBihan, P. Verkerk, P. Simoneau, J. R. R. Leite, D. Bloch, S. Le Boiteux, and M. Ducloy, Opt. Commun. **67**, 363 (1988).

Chapter 6
Conclusions

In this Thesis, the results of theoretical and experimental investigations of SBS under a variety of conditions have been presented. Stimulated Brillouin scattering has proven to be a versatile nonlinear optical process with which to study both stochastic and deterministic behavior.

In Chapter 2, a treatment of normal SBS with a single pump wave is described in which the spontaneous initiation of the process is included. The amount of laser light that is scattered spontaneously is derived by assuming that the density of the medium is driven by thermal fluctuations (represented by a delta-correlated fluctuating force). Thus, the full stochastic nonlinear differential equations are used to examine the statistical properties of SBS. In the limit of an undepleted laser field, an analytic solution to the output Stokes field is derived, whose intensity is predicted to exhibit 100% fluctuations and whose spectrum is gain-narrowed. The dynamical behavior of the Stokes light is explored in the depletion region by numerically integrating the stochastic differential equations. The ratio of the transit time of the light through the medium to the phonon lifetime (i.e., ΓT_t) is shown to strongly determine temporal behavior of the Stokes output intensity. For smaller values of ΓT_t, the

the Stokes output intensity. For smaller values of ΓT_t, the fluctuations in the Stokes intensity become suppressed above the SBS threshold. However, dispersive looking features appear in the intensity that are the result of phase jumps in the Stokes field which propagate through the medium and reverse the flow of energy between the Stokes field and the laser field. These phase-waves are analogous to those predicted for superfluorescence and stimulated Raman scattering. For larger values of ΓT_t, large fluctuations in the Stokes intensity persist until the value of the single-pass gain G is larger than the value of ΓT_t. This is also the condition for the appearance of phase-waves in the Stokes output. Thus, the condition for the suppression of Stokes fluctuations cannot be considered as equivalent to the condition of strong depletion of the laser field.

In Chapter 3, the results of experiments in both 100- and 500-meter-long single-mode optical fibers are discussed, and many of the predictions of the theoretical model introduced in Chap. 2 are verified. The value of the SBS gain factor g_o was measured and is found to be equal to 2.5×10^{-11} m/W. Since the effective value of the Fresnel number for a guided-wave geometry can be much larger than the value that is possible in a focused geometry, the respective threshold single-pass gain for SBS can be much lower. Experimental measurements of the threshold result in values as low as $G_{th} = 11.4$ for the 500-meter-long fiber. The temporal evolution of the Stokes intensity is found to exhibit large fluctuations which is in good agreement with theory. Phase waves were not observed since the intensities that could be reached in the

experiment were insufficiently high to suppress the stochastic intensity fluctuations. The output spectrum of the Stokes light is observed to narrow as a function of increasing input laser power. For the largest value of the input power, the gain-narrowing saturated such that at the highest input laser powers, the linewidth of the Stokes spectrum was roughly one fifth of the spontaneous Brillouin linewidth of 155 MHz. These results also agree closely with the theoretical analysis.

Theoretical and experimental studies of SBS in the presence of feedback are described in Chap. 4. As a result of the extremely high gain that is achievable with SBS, a very small amount of feedback leads to a Stokes output whose behavior is entirely different in character from the stochastic behavior observed in Chapters 2 and 3. With the appropriate boundary conditions, theoretical analysis of the stochastic differential SBS equations demonstrates that the system exhibits a transition from stochastic behavior to deterministic behavior. The resulting threshold for this Brillouin oscillation can be much lower, and the output spectrum is dramatically narrower than for the case of usual single-beam SBS. In the Brillouin oscillation regime, the temporal behavior of the Stokes wave can show stable output with no fluctuations as well as temporal instabilities which lead to periodic behavior. The input laser intensity G and the parameter ΓT_t determine into which regime the system settles. Experiments were performed in an optical fiber in which the ends were cleaved such that a small fraction of the light was fed back into the fiber. The threshold input intensity for Brillouin oscillation is measured to be as low as $G_{th} = 7.7$ for the 100 meter-long fiber. The

Stokes spectrum is observed to be as narrow as that of the incident laser. The Stokes output power displays a wide range of behavior in the regime of Brillouin oscillation, not all of which could be explained by the theoretical model. Both stable output and oscillations at twice the transit time through the fiber are observed. However, for a fixed input intensity, the Stokes output drifts between different types of behavior, which includes oscillations at sub-harmonics of the transit time. The origin of the behavior can perhaps be ascribed to the fact that the frequency stability of the input laser field was insufficient to allow the system to reach a stationary state, or to fluctuations in the length of the fiber due to environmental factors.

In Chapter 5 a study is made of SBS with counterpropagating equal-frequency laser beams in a Brillouin-active material. Theoretical analysis demonstrates that the transmitted beams can become temporally unstable and can show deterministic chaos. The threshold for this instability can be as much as five times below the threshold for usual single-beam SBS. The important parameters that determine the threshold input intensities for the temporal instability are the effective phase-mismatch $\Delta k L$ associated with the four-wave mixing process between the Stokes and anti-Stokes waves and the ratio between the two input laser intensities. For values of $\Delta k L$ less than 100 and for ratios of the backward-to forward input intensity in the range $10^{-3} < I_b/I_f < 10^3$, the threshold for instability is found in almost all cases to be less than usual SBS threshold. Although the ratio of the Brillouin linewidth to the Brillouin frequency shift Γ/Ω plays a small part in determining the

determining the temporal behavior of the output waves above the threshold for instability. For small values of Γ/Ω (< 0.2), the output intensity is predicted to show oscillations at the Brillouin frequency. However, for larger values of this ratio, the output intensity is observed to exhibit a period-doubling route to chaos as the total input intensity is increased. Results of an experiment performed in carbon disulfide with a frequency-doubled, pulsed Nd:YAG laser provide evidence for the existence the temporal instability. The threshold intensity for the instability was found to be 33% lower than the threshold for usual SBS. The transmitted field was observed to oscillate at the Brillouin frequency, which is in agreement with the theoretical predictions. The reason that chaos is not observed experimentally is due to the large phase-mismatch ($\Delta k L = 72$) and to the small value of the Brillouin linewidth to the Brillouin frequency ($\Gamma/\Omega = 0.01$) associated with the experimental conditions. Kulagin and Pasmanik[1] have recently suggested that ultra-pure freon would be a suitable candidate as a Brillouin-active material with which to observe Brillouin chaos since it has a reasonably large value of Γ/Ω (~ 0.25 at 1.06 μm).

---

1. O. Kulagin and G. A. Pasmanik, private communication (1990).